



Lawrence Berkeley Laboratory

UNIVERSITY OF CALIFORNIA

RECEIVED
LAWRENCE
BERKELEY LABORATORY

Materials & Molecular Research Division

SEP 3 1986

LIBRARY AND
DOCUMENTS SECTION

STUDIES OF MICROMORPHOLOGY AND CURRENT EFFICIENCY OF
ZINC ELECTRODEPOSITED FROM FLOWING CHLORIDE ELECTROLYTES

L. Mc Vay*, R.H. Muller, and C.W. Tobias
(*M.S. Thesis)

May 1986

TWO-WEEK LOAN COPY

*This is a Library Circulating Copy
which may be borrowed for two weeks.*



LBL-21492
c.2

LEGAL NOTICE

This book was prepared as an account of work sponsored by an agency of the United States Government. Neither the United States Government nor any agency thereof, nor any of their employees, makes any warranty, express or implied, or assumes any legal liability or responsibility for the accuracy, completeness, or usefulness of any information, apparatus, product, or process disclosed, or represents that its use would not infringe privately owned rights. Reference herein to any specific commercial product, process, or service by trade name, trademark, manufacturer, or otherwise, does not necessarily constitute or imply its endorsement, recommendation, or favoring by the United States Government or any agency thereof. The views and opinions of authors expressed herein do not necessarily state or reflect those of the United States Government or any agency thereof.

STUDIES OF MICROMORPHOLOGY AND CURRENT EFFICIENCY
OF ZINC ELECTRODEPOSITED FROM FLOWING CHLORIDE ELECTROLYTES

Laura Mc Vay
(M.S. Thesis)

with

Rolf H. Muller and Charles W. Tobias

Department of Chemical Engineering
Materials and Molecular Research Division
Lawrence Berkeley Laboratory
University of California
Berkeley, California 94720

May, 1986

This work was supported by the Assistant Secretary of
Conservation and Renewable Energy, Office of Energy Storage
and Distribution of the U.S. Department of Energy,
under Contract No. DE-AC03-76SF00098 with the
Lawrence Berkeley Laboratory.

TABLE OF CONTENTS

Abstract v

Acknowledgments vii

I. Introduction 1

 1. Zinc Chemistry 1

 2. Zinc Uses and Production 2

 3. Zinc in Rechargeable Battery Systems 3

 4. Purpose and Scope of this Study 7

II. Literature Review 13

 1. Recent History of the Electrodeposition Project 13

 2. The Morphology of Electrodeposited Metals 16

 3. The Current Efficiency of Zinc Deposition 23

III. Experimental 34

 1. Experimental Cells 34

 2. Electrodes 34

 3. Electrolytes 35

 4. Analysis and Solutions 36

 5. Equipment 36

IV. Experimental Procedures 44

 1. Electrode Preparation 44

 2. Electrolyte Preparation 44

 3. Preparation of Analysis Solutions 45

 4. Details of Operation 45

V. Results and Discussion 49

 1. The Morphology of Electrodeposited Zinc from
 Acidic Solutions 49

 A. The Structure of the Initial Deposits 49

 B. Effect of Current on the Morphology 50

 C. Effect of Flow Rate on the Morphology 51

 D. Effect of Zinc Concentration on the Morphology 51

 E. Effect of Hydrogen Ion Concentration
 on the Morphology 52

 F. Effect of Impurities on the Morphology 53

 G. Effect of Substrate on the Deposit Morphology 54

 H. The Appearance of Striations 55

 I. The Propagation of Striations 57

 2. Current Efficiency of Electrodeposited Zinc 61

 A. Shape of the Current Efficiency Curves 61

 B. Accuracy of the Current Efficiency Measurements 63

 C. The Effect of Zinc Concentration on the
 Current Efficiency 65

D. The Effect of Hydrogen Ion Concentration on the Current Efficiency	66
E. The Effect of Flow Rate on the Current Efficiency	67
F. The Effect of Substrate on the Current Efficiency	68
G. The Effect of Impurities on the Current Efficiency	69
VI. Summary and Conclusions	105
Appendix 1. Principles of Video Microscopy	110
Appendix 2. Calculation of Current Efficiency	115
References	117

STUDIES OF MICROMORPHOLOGY AND CURRENT EFFICIENCY
OF ZINC ELECTRODEPOSITED FROM FLOWING CHLORIDE ELECTROLYTES

Laura Mc Vay

(M.S. Thesis)

Department of Chemical Engineering
Materials and Molecular Research Division
Lawrence Berkeley Laboratory
University of California
Berkeley, California 94720

May, 1986

ABSTRACT

Results of a study of the micromorphology and current efficiency of zinc electrodeposited from flowing, acidic chloride solutions are reported. The effects of six variables were examined: flow rate, current density, zinc and hydrogen ion concentration, concentrations of nickel, iron and cadmium impurity ions, and the nature of the substrate.

The development of micromorphology was studied in-situ by means of videomicrography and ex-situ by means of scanning electron microscopy. This investigation focused on the formation of grooved deposits, which are found under a wide range of deposition conditions. The major conclusions of this study are: (1) the most important variable determining whether grooved deposits form is the interfacial concentration; (2) large protrusions orient themselves parallel to the flow direction with the orientation starting upstream and progressing downstream;

(3) large protrusions become ridges due to growth of the highest current density portions of the electrode under mass transport control.

The current efficiency was measured using EDTA titration and weight measurements. The fraction of the current taken by zinc deposition increased with zinc concentration, ranging up to 100%, and decreased with pH. The efficiency of zinc deposition was affected by the flow rate and the substrate employed. Impurities lowered the current efficiency.

ACKNOWLEDGMENTS

A degree is an achievement that cannot be accomplished without the support of many people. There have been many role models in my life, and without the help of some people the achievement of this degree would not have been possible. At this time, I would like to give recognition to those people who I feel have made a difference in my life. First of all, I would like to thank my parents, James and Mary Mc Vay, for everything; I cannot even begin to list their gifts. My grandparents, Mary and Harold Harrigan, have also given in a truly Christian manner, and I am eternally grateful to them for their encouragement, love and financial support. Sister Mary Edward Zipf, PhD., has motivated my desire to study science, and may her infectious enthusiasm for science and life stay with her forever. Dr. H.C. Hollein encouraged me to come to Berkeley to continue my studies in Chemical Engineering, and without Dave Downing, Ted Zucconi and all of the other people at Northern Telecom, my interest in electrochemistry would never have been stimulated. Bill Love gave me immeasurable help with microscopy, and Steve Mayer and Mike Armstrong were always patient when I needed help with the computer. Valerie Kelly did the final typing of the manuscript and the final changes. Dave Wallack has given me his love and emotional support. Last of all, but certainly not least, I would like to thank Dr. Muller and Professor Tobias for many stimulating discussions, their time, patience and their financial support.

I. INTRODUCTION

Zinc, an important metal to mankind, has been known since ancient times. It was used by early civilizations in the production of bronze; alloying copper with zinc made the resulting metal harder. Zinc anodes were contained in the first primary battery developed around 1800 by Count Alessandro Volta. Currently, zinc still is the most common battery electrode; this is due to its low cost, \$0.35/lb, and its moderately high negative reduction potential relative to hydrogen.

1. Zinc Chemistry

Zinc is a member of group IIb in the periodic table, along with cadmium and mercury. The elements in this group have 2 s electrons outside a filled d shell (1). These elements are unable to lose electrons from the d shell, so there are no oxidation states higher than 2 for these metals. The univalent state of zinc exists in the form Zn_2^{+2} (2,3,4), but this ion is unstable and no compounds or complexes are formed. Therefore, the only important oxidation state of zinc is the divalent ion. As the zinc ion is an electron pair acceptor, it is considered a Lewis acid.

A large variety of compounds are formed with zinc. Since no compound is formed in which the electrons of the d shell bond to ligands, zinc is not considered a transition element. All of the halides are well known, as are the oxide, sulfate, cyanide, and chlorate compounds. Organozinc compounds were the first organometallic compounds synthesized and as such have greatly contributed to our current

understanding of chemical bonding (1). Zinc is found in human enzymes and is second only to iron in biological importance among the heavy metals (1).

Zinc resembles the transition metals in its ability to form complexes which enhance the solubility of zinc salts in aqueous solutions (5). Complexes form with halides, hydroxides, and ammonia, as well as with other ligands; these complexes are tetrahedrally coordinated (6). A distribution diagram showing the chloride complexes of zinc is given in Fig. 1.1, taken from Mc Breen and Cairns (5).

2. Zinc Uses and Production

Zinc has very important applications in many industries. In galvanized steel, a zinc coating on iron acts as a sacrificial anode to protect iron from corrosion. Zinc is used in the production of bronze and in die castings (7). It is the most common anode in both primary and secondary batteries because of its low reduction potential (8), relatively low equivalent weight and moderate cost.

The most common method of producing high-grade zinc is electrowinning. There are two types of electrowinning processes both employing zinc sulfate solutions: the low-acid low current density (sulfuric acid concentration = 10%, $i = 30 \text{ mA/cm}^2$) and the high-acid high current density process (8) (sulfuric acid 25%, $i = 80 \text{ mA/cm}^2$). A diagram of the steps involved in the electrowinning process is shown in Fig. 1.2.

The feed to a zinc electrowinning process is zinc sulfide (sphalerite) concentrates containing about 50% zinc (10). This concentrate is fed to a roaster that converts the sphalerite into acid-soluble oxides

of the constituent metals, after which the concentrates are leached (10); first, with spent zinc sulfate electrolyte, then with hot sulfuric acid. The sulfuric acid leaching is usually performed in several steps, using progressively greater concentrations of acid.

The solutions are then treated to remove impurities that are detrimental to zinc electrowinning. Iron is first precipitated as a sodium jarosite ($\text{NaFe}_3(\text{SO}_4)_2(\text{OH})_6$). Other impurities are removed by cementation, (treatment by zinc dust) usually in two steps. Copper and cadmium are cemented at low temperatures, and cobalt and germanium are cemented onto zinc dust at 90°C.

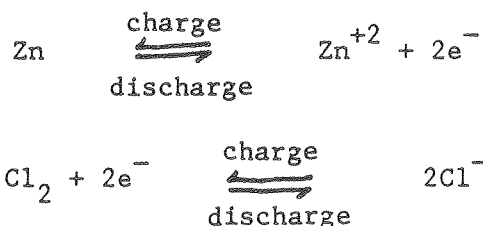
The typical solution feed to an electrowinning cell contains about 65 g/l zinc (10). The cell is operated at about 38°C to limit hydrogen evolution. Zinc is deposited on aluminum substrates for about 48 hours, using a current density range of 30 to 80 mA/cm². The current efficiency for an electrowinning process is about 90%. The deposition process is very sensitive to the presence of impurities that catalyze hydrogen formation; codeposition of metals such as cadmium, germanium and antimony can result in drastically lowered current efficiencies. The requirements for zinc electrowinning are summarized in Table 1.1.

3. Zinc in Rechargeable Battery Systems

Ever since the Volta pile, zinc has been the most common electrode in primary battery systems. For a review of primary batteries involving zinc electrodes, see (5). Only the rechargeable zinc/chlorine and zinc/bromine batteries will be discussed in this section.

The zinc/chlorine and zinc/bromine batteries have been under intensive development during the past 10-15 years. The materials are cheap and readily accessible. The zinc/halide batteries have high theoretical energy densities and the cell voltages are high: 2.32 V for the chlorine (12) and 1.85 V for the bromine battery (12). In addition, the reactions are fast at ambient temperatures. Potential applications for these batteries include electric vehicles and load leveling for power plants (11,13).

The zinc/chlorine battery, shown in Fig. 1.3, consists of an electrolytic cell, a refrigeration system to form and store chlorine hydrate, and a flow system to circulate the electrolyte. The half reactions are:



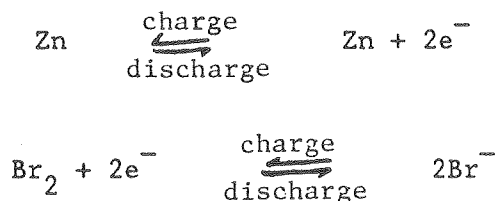
The chlorine is stored as a hydrate, $\text{Cl}_2 \cdot \text{H}_2\text{O}$, a solid with a melting point of 6°C , to prevent hazards associated with the storage of hydrochloric acid/chlorine mixtures, and to eliminate the need to compress the chlorine gas. When the cell is discharged, the chlorine hydrate is heated and it decomposes. This decomposition provides the material for the cathodic reaction.

The cell includes a porous graphite chlorine electrode and a dense graphite zinc electrode. During charging, the zinc is deposited on the dense graphite electrode and chlorine is evolved on the porous graphite electrode. The electrolyte circulates and is cooled to 6°C in the

refrigeration compartment where the chlorine hydrate is formed and collected. During discharge, the zinc is oxidized on the dense graphite electrode, and the chlorine gas is reduced on the porous graphite electrode. The overall energy efficiency achieved by this device at practical rates of charge/discharge is 65% (11).

There are several unique features of the zinc/chlorine battery. No separator is employed, which means that the chlorine can migrate to the zinc electrode. The cell can operate at ambient temperatures without loss of efficiency. The electrolyte is flowing, which ensures a constant, fresh supply of reactant. The flow patterns in this battery were studied by Jorne (14).

A schematic of the zinc/bromine battery is shown in Fig. 1.4. It consists of a battery stack and storage compartments. This battery operates at ambient temperature. The half reactions are:



The bromine in solution is complexed by a complexing agent such as quaternary ammonium bromide (11). The complex is stored in the storage compartment and not allowed to flow freely with the electrolyte. During charging, zinc is plated on the graphite-loaded polymer electrodes, and bromine produced at the anode, forms a complex. The resulting brominated complex flows to the storage tank, where the insoluble complex is separated from the electrolyte by gravity. On discharge, the complexed phase flows freely, and bromine is reduced to bromide from the complex.

The zinc that was plated during the charging cycle is oxidized (dissolved) during the discharge cycle. 50-60% energy efficiency has been achieved in prototype hardware (15).

Like the zinc/chloride battery, the zinc/bromine battery uses flow to transport the reactants and products. As a result the battery is very adaptable because the storage compartments are separate from the cell stack. The use of graphite-loaded polymer electrodes allows construction of a bipolar battery stack. This type of arrangement eliminates much complicated circuitry, and the battery can be operated as a high-voltage/low-current system.

Various problems are associated with both batteries. Scaleup and activation of the graphite electrodes are difficulties and are currently under investigation. The low energy efficiency is of concern; modeling efforts have shown that reduction of halogens at the zinc electrode during the charging process is the major source of inefficiency (16). To prevent the reduction of halogens at the zinc electrode, one would normally put in a separator. The use of separators presents another difficulty, since these break down quickly under the strongly acidic conditions that exist in zinc/halide batteries. In addition, employing a separator increases the ohmic resistance of the battery. Dendritic growths can cause shorts, reducing the cycle life of the cells. These growths are commonly controlled in electroplating by the use of organic leveling agents. However, these chemicals cannot be used in batteries because they break down after a period of time, and they also increase the overvoltage for metal deposition.

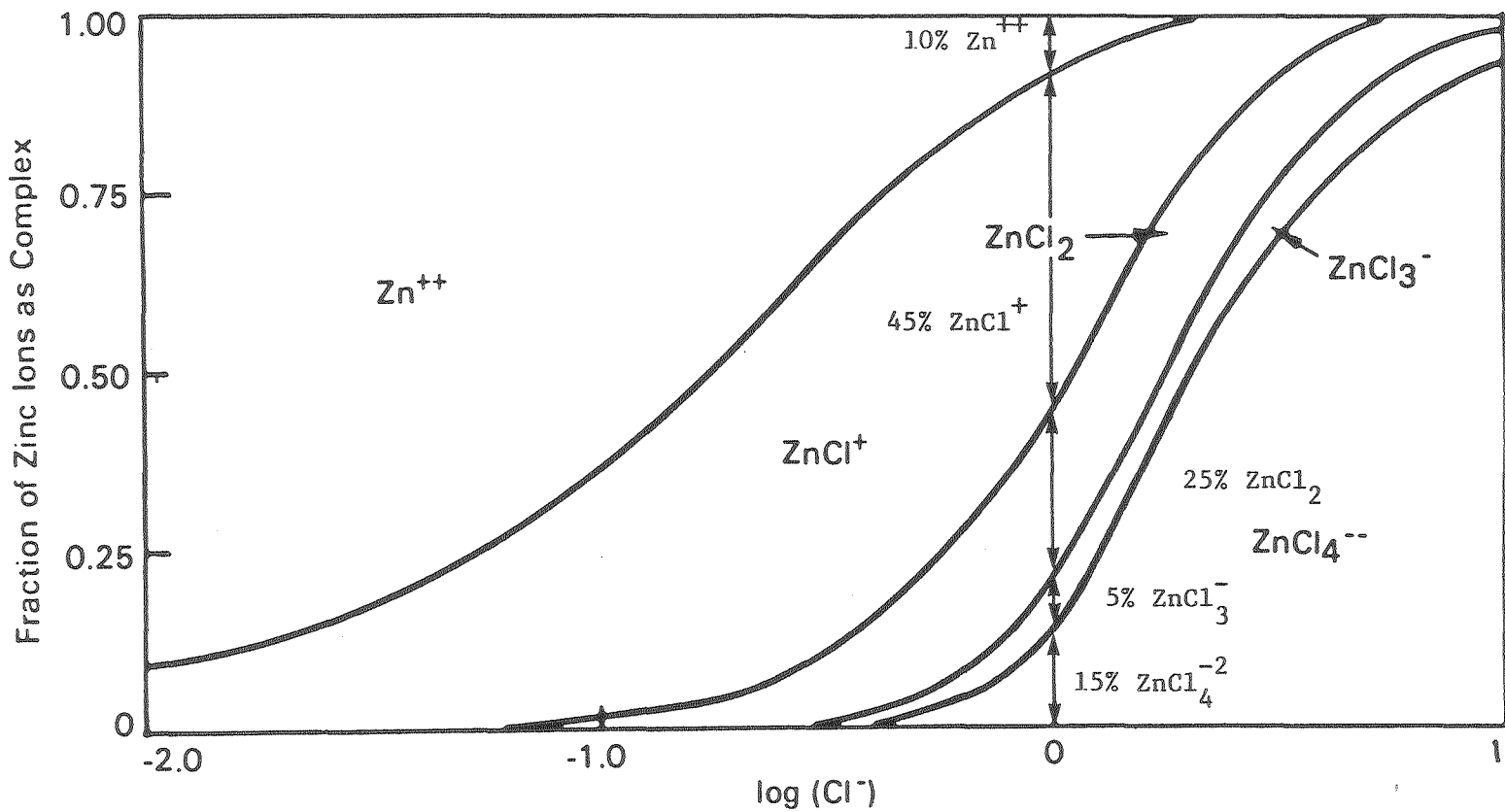
4. Purpose and Scope of this Study

The purpose of investigations on the electrodeposition of zinc in this laboratory has been to understand and control the factors that determine the macromorphology of deposits. Of particular interest are the effects of process parameters on the morphology in the range typically used in chloride and bromide batteries. By varying the current density, flow rate and concentration, control of the deposit morphology may be achieved without using additives. Properties of the deposits are characterized using scanning electron microscopy and photomicrography. Observations are made under various conditions of zinc concentration, current density, flow rate, and hydrogen ion concentration.

A particularly vexing problem in the deposition of zinc from flowing solutions is the formation of striations, which, as shown in Fig. 1.5, are ridges or grooves in the deposit oriented parallel to the direction of flow. In this investigation we attempted to further define the conditions under which striations form and the steps involved in the formation of striae. We have sought to define the mechanisms of origin and propagation and to further speculate on the reasons for the appearance of striations. By determining the current efficiency for zinc deposition, we evaluate the effect of hydrogen evolution on striation formation. Certain authors have proposed that the appearance of striations is directly related to the appearance and codeposition of hydrogen (17). Hydrogen gas evolution is the thermodynamically favored reaction, but is kinetically limited.

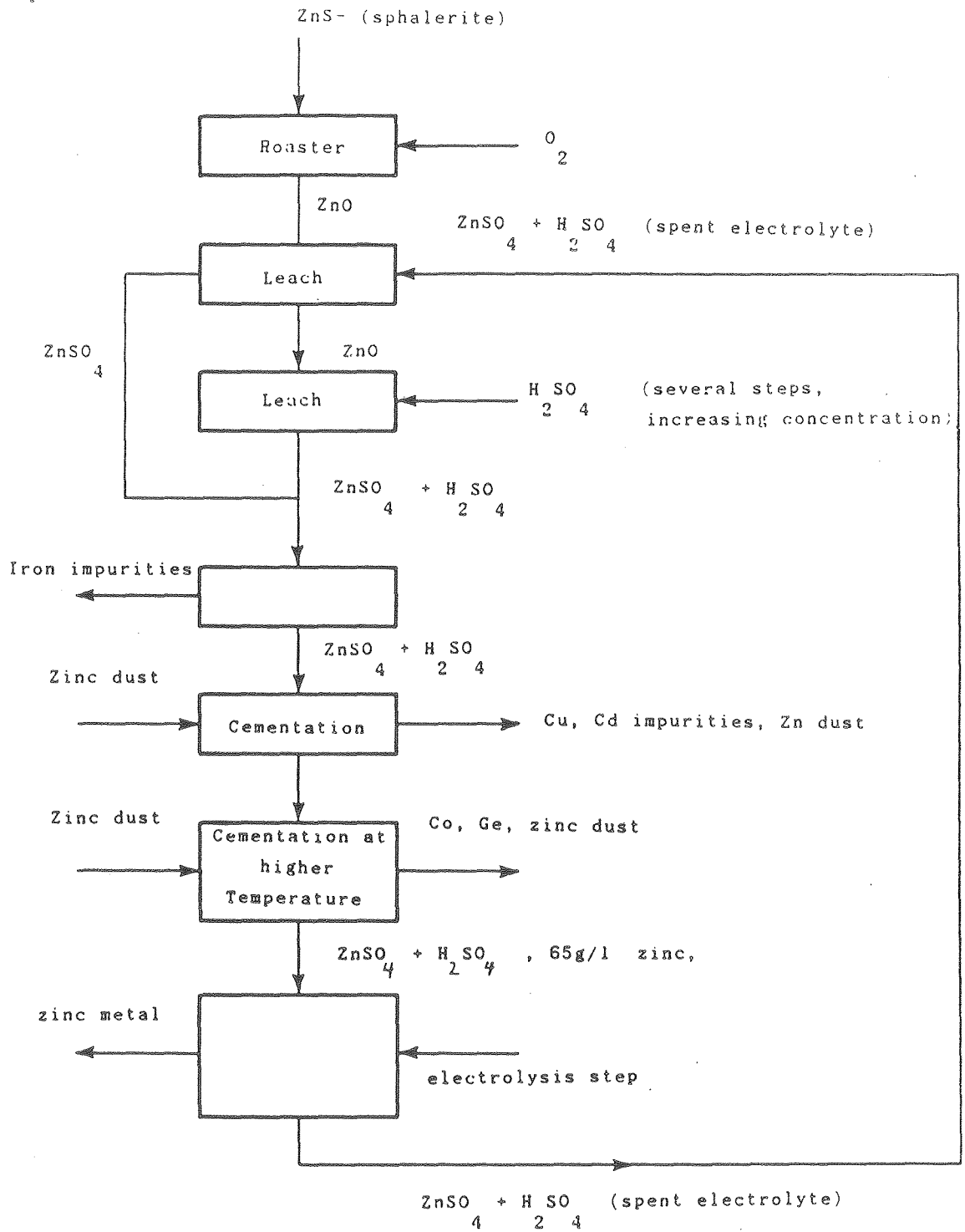
Table 1.1. Requirements for Zinc Electrowinning

Solution	ZnSO ₄
Entering Solution Concentration (Zinc)	65-200 g/l
Entering Solution Concentration (Sulfuric Acid)	100-200 g/l
Anode	Pb or Pb-Ag alloy
Cathode	Al
Current Density	30-80 mA/cm ²
Voltage	3-3.7 V
Temperature	38°C (average)
Time of Electrolysis	8-72 hours
Current Efficiency	90%
Spent Electrolyte Concentration (Zinc)	40-60 g/l



XBL 838-11146

Figure 1.1- Distribution diagram of ZnCl₂ system
(from J. Faltemier's thesis)



XBL 865-1792

Figure 1.2- Flow diagram for a typical zinc electrowinning process

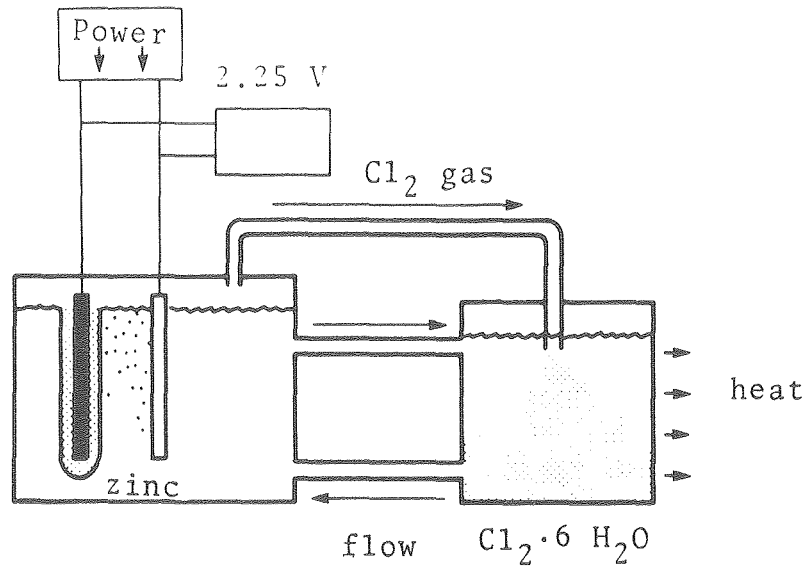
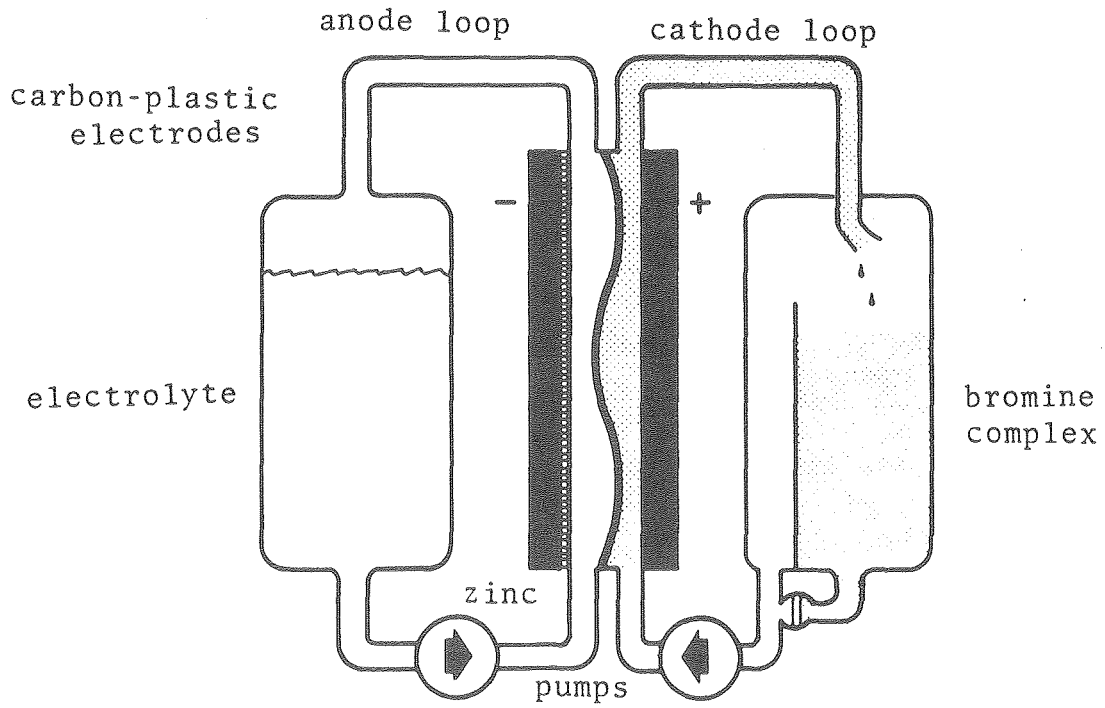


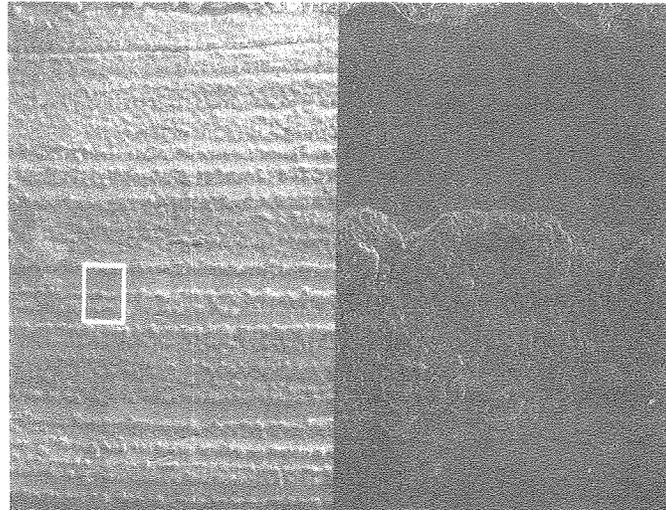
Figure 1.3- Zinc/chlorine battery (11)



XBL 865-1791

Figure 1.4- Zinc/bromine battery (11)

Figure 1.5 - **Striated electrode**



x 10

1M ZnCl_2 + 3M KCl pH=5.2

45 mA/cm² Re = 5000

20 minutes of deposition

= 505 μm

Platinum substrate

II. LITERATURE REVIEW

1. Recent History of the Electrodeposition Project

The macromorphology of metal deposits has been of great interest in our laboratory for the past 10-12 years. The earlier studies addressed the morphology of copper deposits. Landau (18) and Kindler (19) studied the morphology of copper deposits in a parallel-plate flow cell in 3 regimes of current density: at the limiting current density, below the limiting current density, and using pulsed-current deposition. The conclusions from this study were: (1) The mass transfer conditions at the time of deposition strongly influence the type of deposit obtained. (2) Changes in current density and interfacial electrolyte concentration influence the morphology; these changes in morphology should be predictable. (3) Pulsed current can eliminate the need for organic leveling agents.

Carlson (20) studied the effect of individual protrusions on the deposition of copper, under various conditions of flow rate, overpotential, and current. It was shown that the wake is reflected in the deposit and, as shown in Fig. 2.1, there are both areas of enhanced growth and areas with no increased deposition around a protrusion.

The first studies on zinc deposition in our laboratory were carried out by Dr. Milan Jaksic (21). He observed the general progress of zinc deposition and formation of striations under various conditions using primarily a rotating disk electrode. Jaksic showed that striations develop from a series of nodules, as shown in Fig. 2.2. He attributed

the appearance of striae to the formation of Taylor vortices in the grooves of the deposit.

Faltemier (13,22) studied various problems related to the deposition of zinc from acidic solutions. In the limiting-current study, done in collaboration with Rajhenbah (22), the diffusion coefficient at 25°C was found to be 0.98×10^{-5} cm²/sec for dilute solutions of zinc chloride and 0.78×10^{-5} cm²/sec for dilute solutions of zinc sulfate. These diffusion coefficients decreased greatly with increasing concentration; this decrease was attributed to greater structuring in the solution.

Faltemier (13) also deposited zinc at different currents and flow rates on platinum and observed the progression of striae using motion picture macrophotography. He found that zinc first deposits smoothly on the surface, and then after several minutes, protrusions appear and join with other nodules downstream to produce striae. Striations formed more rapidly at higher flow rates, and were deeper at low flow rates. With pulsed current deposition the formation of striae could be eliminated. At low current density levels, wakes forming behind the largest protrusions provided enhanced mass transfer in the downstream direction, and therefore there was a higher local current density in the wake of a large protrusion.

Tsuda (23) studied the development of macromorphology on a rotating disk and the effect of lead impurities on the deposition of zinc. Deposition was performed under galvanostatic conditions using a platinum substrate. Some experiments were conducted using pulsed current deposition. It was found that the amplification of surface roughness

proceeded in several steps. First, nucleation occurred, and the small protrusions grew. Then, the nuclei coalesced into larger protrusions. The larger protrusions grew preferentially, and consumed the smaller protrusions. The connection of protrusions to form striations was hypothesized to occur because of enhanced crystal growth in the wakes of protrusions. It was found that the presence of lead ions enhanced the successive coalescence and preferential growth of protrusions. The role of hydrogen ions was found to be negligible with respect to the growth of protrusions.

Anderson (24) examined the role of nucleation in the development of striations and also determined kinetic parameters for the zinc chloride system. He deposited zinc from 1M zinc chloride solution at various hydrogen ion concentrations onto several substrates: glassy carbon, graphite-loaded polymer, synthetic graphite, and platinum. The exchange-current density was determined to be on the order of 1 mA/cm². Nodule densities generally increased with current density and ranged from 200-1000 nodules/(mm²-mV). The potential transient was found to attain a maximum during the first few milliseconds of the experiment, and the magnitude of this transient was inversely related to the number of nucleation sites available. The substrate activities, based on the number of nucleation sites available and the nodule density, toward zinc deposition ranked in decreasing order are: Union Carbide synthetic graphite, platinum, Gould synthetic graphite, graphite-loaded polymer, and glassy carbon.

2. The Morphology of Electrodeposited Metals

The morphology of electrodeposited metals is important in all electroplating applications. For rechargeable batteries, dendrite formation causes a shortened cycle life. In the manufacture of printed-circuit boards, failure to evenly plate drilled connections on the boards causes the boards to be defective. Additives in plating baths affect the properties of the electrodeposit. Formation of powdery deposits in electroforming renders the metal useless without further processing. Clearly, it is desirable to learn about and to control the morphology of an electrodeposited metal.

A major study of electrodeposited growth layers was accomplished by Wranglen (25), who used photomicrographic techniques to record the progress of deposition of several metals on different substrates. Two types of dendrites were observed: two-dimensional, which looked like ferns, and three-dimensional, which were treelike. These two types of dendrites are shown in Fig. 2.3. The dendritic growth was determined more by the preferred growth directions of the lattice than by streamlines. Cadmium, chemically similar to zinc, grew primarily three-dimensional dendrites composed of hexagonal plates. Two types of hexagonal plates were observed. At low current densities, the dendrites were thick and branched away from the electrode, and at high current densities, the dendrites were thinner and branched toward the electrode.

The growth of layers was also studied by Wranglen (25). Growth occurs by the lateral extension of layers. At low current densities, growth occurred by the extension of layers from the center of the surface outward, and a new layer was not started until the old layer

reached the edge of the electrode. At high current densities, growth started at the edges and corners of the electrode and several growth layers developed simultaneously. Several types of growth centers were observed, and some of these are shown in Fig. 2.5. Anodic dissolution was also observed to occur by layers.

The effect of electrolyte flow on the morphology of zinc from alkaline solutions was studied by Naybour (26), who recorded the morphology of electrodeposited zinc under a variety of current densities and flow rates. Three types of morphology were observed: plate-like, bulbous, and dendritic. It was found that a phase diagram could be constructed for the various morphologies; this is shown in Fig. 2.6. The transition current density between bulbous and dendritic growth was a function of the Reynolds' number (Re) to the 1.1 power for $Re > 2000$ and proportional to $(Re)^{0.7}$ for $Re < 2000$. The transition current density between flat and bulbous morphology was a function of Re . Levich (27) states that the limiting current is approximately proportional to the 0.8-0.9 power of the fluid velocity for turbulent flow and to the 0.3-0.5 power of the fluid velocity for laminar flow. According to Naybour (26), the transition between the bulbous and dendritic morphologies is the locus of the limiting currents as a function of Re . The maximum protuberance height was measured, and the ratio of protrusion height to deposit thickness was found to increase with current density at a constant Reynolds number. This ratio appeared to decrease with increasing Reynolds number. In some experiments, the bulbous deposits were oriented in the direction of flow.

The effect of small protrusions on mass transport to a rotating-disk electrode was studied by Rogers and Taylor (28), who studied the deposition of nickel from a Watts-type plating solution. They observed spiral patterns on their rotating disks when depositing under mass transport control, which indicated to them that conditions for deposition were not uniform over the disk. Their results indicated that striations were traces of the wakes behind small, microscopic protrusions, such as burrs or gas bubbles, on the disk. Smaller protrusions gave better defined striations. There was no evidence of vortex formation or boundary-layer separation in the wakes; the Reynolds number indicated completely laminar flow.

The kinetics and mass transfer to the zinc electrode from chloride solutions was studied by Kim and Jorne (29), who used a rotating-disk electrode. The primary focus of this research was to determine exchange-current densities and diffusion coefficients; however, some work was done on the morphology as well. It was found that the morphology depended greatly on the interfacial concentration, expressed by the fraction of the limiting current density. Two regions were observed: (1) at a high fraction of the limiting current, the deposit morphology was determined by the hydrodynamic conditions, and (2) at low fractions of the limiting current, the deposit morphology was more influenced by field effects and by charge transfer overpotential. Striations were hypothesized to form in one of two ways: (1) they are the trajectories of hydrogen bubbles as they move along the surface, and (2) they are formed as a result of secondary flows behind protrusions.

Mc Breen and Gannon (30,31) studied the deposition of zinc on glassy carbon using cyclic voltammetry, potential-step techniques, and scanning electron microscopy. Zinc nucleation could be fitted to a model that assumed instantaneous nucleation and continued growth under kinetic control. The kinetics were much faster in bromide than in chloride solutions. The nodule structure was platelike and consisted of hexagonal plates. The current efficiency for zinc deposition was estimated to be 100%, with no hydrogen evolution.

Diggle, Despic, and Bockris (32) studied the mechanism of dendritic electrocrystallization of silver and zinc from alkaline solutions as a function of overpotential, concentration, and temperature. Dendrites were found to propagate linearly with time; this growth depended on all three variables. The growth of dendrites was mass transfer controlled when the height of the dendrite was less than the diffusion-layer thickness. Growth under mass transport control was characterized by a linear dependence of height with time. When the height of the dendrite exceeded the diffusion-layer thickness, the growth of the dendrite became activation controlled. The growing dendrite was assumed to be monocrystalline with a parabolic tip. The current density on the tip of a growing dendrite is expressed by the equation:

$$i = v (nF)/V$$

where: i = current density

V = molar volume of zinc

n = electrons/molecule reduced

F = Faraday's constant

v = propagation rate of the dendrite

It was proposed that dendrites form from deposition around a screw dislocation, and that there was a narrow range of overpotentials in which the growth of dendrites can occur. Two critical overpotentials relating to dendrite growth were defined: (1) the overpotential needed to deposit around a screw dislocation, and (2) the overpotential for dendrite initiation.

The kinetics of growth of zinc dendrite precursors was studied by Moshtev and Zlatilova (33), who studied zinc deposition on a rotating-disk electrode from zincate solutions. They found that the propagation rate of dendrite precursors was constant within the limits of the diffusion-layer boundary. The propagation kinetics followed the model of Diggle, Despic, and Bockris. Dendrites were assumed to occur as a result of pyramidal growth and screw dislocations. The appearance of dendrites coincided with the appearance of a transition in the slope of an I vs t curve. At the time of this transition, the height of the precursors corresponded to the height of the diffusion layer.

The morphology of zinc from acidic, sulfate solutions was studied by Adcock and co-workers (34), who used x-ray diffraction to characterize the crystal orientation of the deposits. Results were used to specify plant operating conditions. The current efficiencies were in the range of 85-90%. The morphologies had a preferred orientation of (101), and were characterized by closely packed nodules and holes from bubbles such as shown in Fig. 2.7.

Landau (16,35,36) attempted to relate the development of roughness to the stability of the electrodeposited metal. He identified several discrete stages in roughness evolution. First, the surface is covered

with clusters of plated material. Growth in this stage is controlled by atomistic and crystallographic factors. As the overpotential exceeds a critical value, the surface experiences a perturbation that causes the protrusions to grow at a faster rate. This critical overpotential for roughness evolution may be correlated with the degree of reversibility of the reaction. Eventually, some protrusions grow at an appreciably faster rate, and these protrusions branch out and form dendrites. The propagation rate for dendrites is constant once the dendrites have been initiated.

The model proposed by Landau (16,35,36) is based on the realization that roughness evolution on the surface is not unique to electrochemical systems; it is observed in the crystallization of salts and crystallization from the melt. The goal of Landau's research was to tie together the growth rate of a single roughness element to the macroscopic current and potential distribution in the cell. By applying conditions of morphological stability to electrochemical systems, Landau found that all electrochemical deposition is inherently unstable and will eventually lead to roughness evolution. However, there is a pseudo-stable region in which no dendrites will form. The exchange-current density was found to be the dominating factor in determining the system's stability. Equations for the initial growth of dendrites were derived, and it was found that the current density at the dendrite tip was a function of overpotential and the concentration of the electrolyte. The tip radius varied inversely with the overpotential. It was found that at a given current density increasing both the zinc concentration and the flow rate will produce compact deposits.

Selman and co-workers (37,35,17) studied the properties of zinc solutions and the electrodeposition from those solutions using a rotating concentric cylinder cell. Visual observations of the development of striae and other morphological features were made and the growth rates of dendrites was observed. The growth rate of dendrites increased with increasing convection. The morphology was influenced by gas bubbles clinging to the surface and by secondary convection patterns, which are formed by flow around small protrusions. The growth rate of striations decreased and the growth rate of dendrites increased with increasing convection. Several types of morphology were observed. Fishnet structures were stated to be caused by gas bubbles clinging to the surface, which shielded the electrode surface from zinc deposition. Ridges were observed and explained to be the result of gas bubbles clinging to the electrode in the valleys between the nodules. Single nodules were seen, and it was stated that there was alignment in the flow direction and that gas evolution played an important role in this alignment. Examples of ridges and fishnet structures are shown in Fig. 2.8.

Popov and Krstajic (38) studied the mechanism of spongy-deposit formation from zincate solutions. From zincate solutions spongy deposits were formed in the 40-80 mV range of overpotentials, and there was an induction time for spongy-deposit formation. It was concluded that spongy deposit formation on inert substrates was caused by mass transfer limitations on conditions of low nucleation rate. Spongy-deposit formation arose when the limiting current was equal to or less than the exchange-current density.

3. The Current Efficiency of Zinc Deposition

When zinc is deposited from an aqueous, acidic solution the thermodynamically favored reaction is the evolution of hydrogen.



Because this reaction has slow kinetics the deposition of zinc may proceed with high current efficiency.

Most of the previous studies on zinc current efficiency emphasized the role of additives on the current efficiency in the presence of free convection. Reported current efficiencies ranged from 30-100% (39).

Thomas and Fray (39) studied the feasibility of electrowinning at high rates ($> 100 \text{ mA/cm}^2$) from zinc chloride solutions supported by ammonium chloride and containing additives. Although their data are scattered, they found that there was a peak in current efficiency at about 2M zinc concentration. The current efficiency generally decreased with increasing temperature. The range of current efficiencies found was 30-90%; periodic current reversal increased the current efficiency. The optimal composition for electrowinning from zinc chloride was found to be 2-3M zinc concentration, 7 weight % ammonium chloride, 10 mg/l potassium fluoride, and 40-100 g/l high-protein additive. The ideal current density was 200-250 mA/cm^2 ; the current efficiency achieved was 90%.

Thomas and Fray (40) also studied the effects of additives on the current efficiency. They found that the current efficiency for a pure 1M zinc chloride solution was only 50% at 250 mA/cm^2 , and the deposit

was dendritic. With various additives, the morphology type changed from dendritic to block and then to plates as the current efficiency was increased. The highest current efficiency, 89.6%, occurred with the additive Croda K1V, an animal glue.

MacKinnon and co-workers (41,42) studied the electrowinning of zinc chloride using a diaphragm cell with DSA anodes and aluminum cathodes. They evaluated the effects of various metallic impurities and their combinations on the current efficiency in a 0.15M zinc chloride solution supported by hydrochloric acid and tetrabutylammonium chloride. The maximum current efficiency found was greater than 96%. Cadmium and lead were found to codeposit with zinc. Antimony and copper were found to decrease the polarization of the surface. This decrease in polarization resulted in a lower current efficiency. The presence of cobalt and iron caused the deposit to become more basally oriented and the current efficiency to decrease. The presence of germanium decreased the overpotential of zinc deposition, but caused severe dissolution of the deposit and a corresponding loss in current efficiency even at concentrations as low as 0.1 mg/l. The ranking of various impurities in terms of their detrimental effect on zinc electrowinning is as follows:

$Sb > Ge > Cu > Pb > Cd > Ni > Fe > Co$.

There was no observed effect of hydrochloric acid concentration on the current efficiency or on the deposit quality, although other workers (43-45) have noted an improvement in the deposit quality with increasing concentrations of hydrochloric acid.

Begum and coworkers (46) studied the deposition of zinc from zinc chloride solution with glue additions. The current efficiency was found to increase only slightly in the 25-100 g/l zinc chloride concentration range, from 95 to 97%. The current efficiency decreased from 97% to 91% when the current density increased from 25 to 45 mA/cm².

Rogers and Taylor (47), using a rotating-disk electrode, determined the currents for hydrogen evolution and zinc deposition at various potentials and alkaline zinc concentrations ranging from 0.01M to 0.3M. For this range of concentrations, there was no hydrogen current when the current was below the limiting current for zinc deposition. The current efficiency decreased greatly when the limiting current was exceeded.

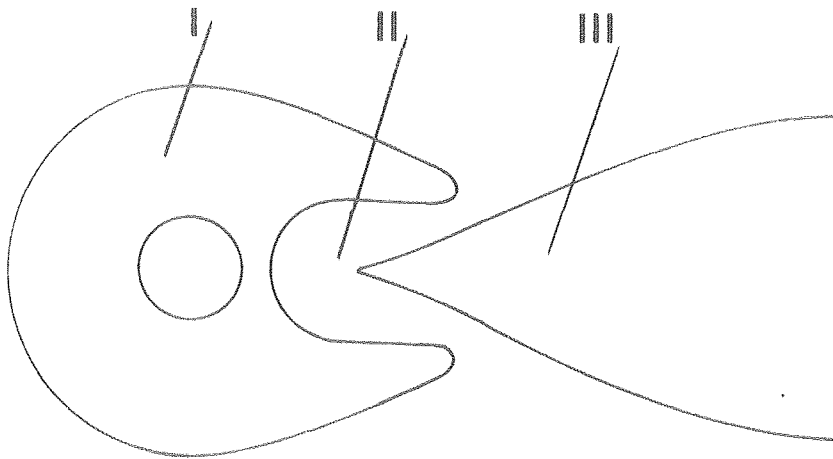
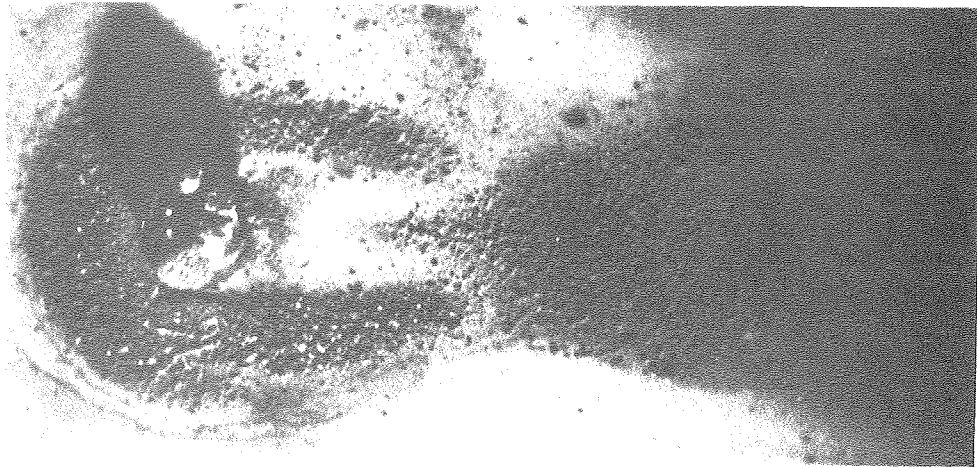
The influence of nitrate ion on the morphology and the current efficiency of zinc deposition from acidic sulfate solutions was studied by Gay and Pergsma (48). The deposits obtained from sulfate solutions with a current efficiency of 92% had a platelike morphology. With the addition of nitrate ion, the efficiency dropped to 45%, and the deposit was dark and spongy. In solutions that contained only nitrate ion, the current efficiency was about 100%, although the deposits were always dark and poorly adhering.

Cadmium is often found in zinc ores and is the main impurity found in zinc compounds. The effect of cadmium on the deposit structure and current efficiency of electrodeposited zinc from acidic sulfate solutions was studied by MacKinnon et al. (42) and Foulkes and co-workers, (49) who found that the addition of cadmium impurities to the electrolyte increased the current efficiency when the cadmium concentration in the electrolyte was over 20 mg/l. The current efficiency increased

because the structure of the deposit was refined and the hydrogen overpotential was increased. The incorporation of cadmium into the zinc deposit did not alter the crystal orientation of the deposit, nor did it alter the mechanism for hydrogen evolution. For cadmium concentrations under 20 mg/l, the zinc plating current efficiency was found to decrease due to a decrease in the hydrogen overpotential. The results of MacKinnon and co-workers agree with the results of Foulkes.

The effect of nickel codeposition on the morphology and current efficiency of zinc deposition from both acidic sulfate baths and alkaline zincate baths was studied by Fratesi and co-workers (50). At sulfuric acid concentrations above 3N, periodic deposition and redissolution occurred until no more zinc was deposited. For deposition from solutions with sulfate concentrations less than 3N, the nickel partial current was found to vary linearly with zinc concentration. It was found that there were deep holes on the surface of deposits obtained from nickel containing solutions. These holes were thought to be centers of hydrogen evolution.

The effect of lead on zinc deposit structures was studied by MacKinnon and co-workers (57), who deposited zinc from acidic sulfate solutions. The current efficiency was found to decrease with increasing current density and lead concentration in the deposit. The maximum current efficiency achieved from a 55 g/l zinc sulfate solution was 97%, obtained at a current density of 80.7 mA/cm².



I - region of high enhancement

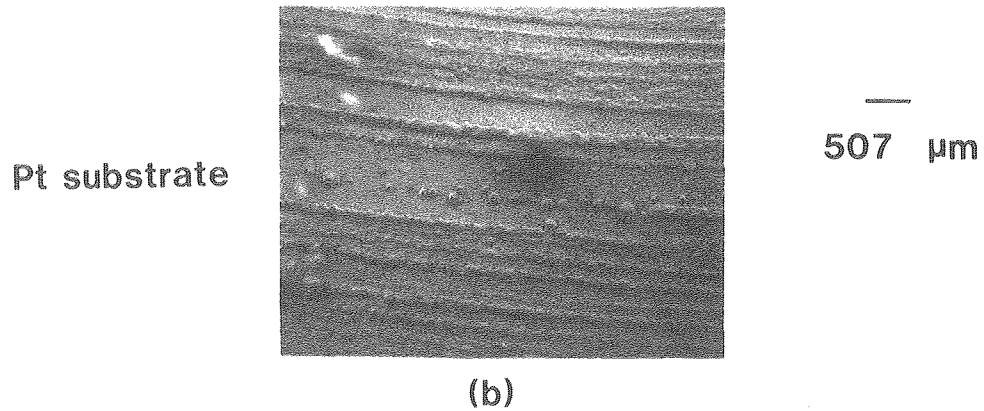
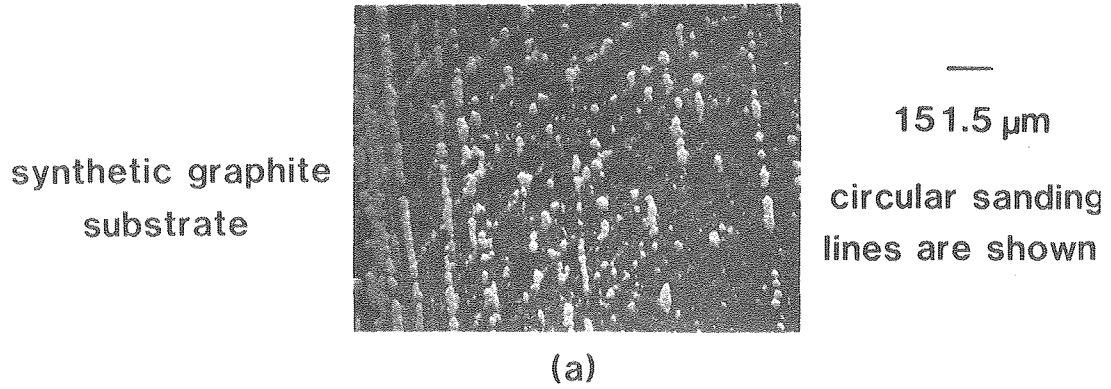
II - region of attenuation

III - region of moderate enhancement

XBB 840-8624

Figure 2.1 - Effect of conducting sphere on localized electrodeposition in the presence of forced convection (from experiments by Carlson and (24))

Figure 2.2 - Striation showing boulders



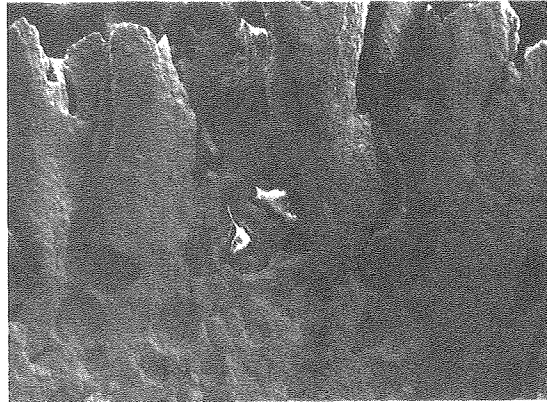
1M ZnCl_2 + 3M KCl

(a) $\text{Re} = 3115$ 10 mA/cm^2 $\text{pH} = 1$ 10 minutes

(b) 30 mA/cm^2 $108 \text{ coulombs/cm}^2$ $\text{pH} = 5.2$

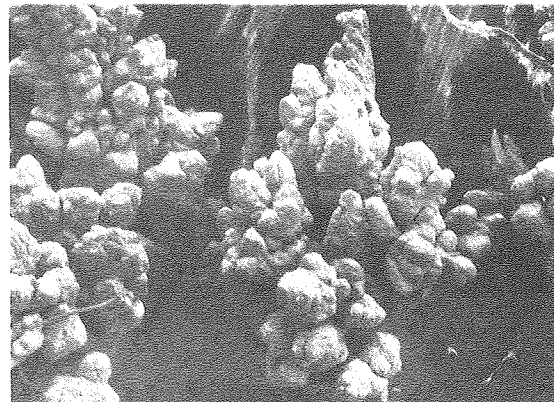
$\text{Re} = 9000$

Figure 2.3 - 2 D and 3 D dendrites



—
246 μm

(a)



—
47.4 μm

(b)

1M ZnCl_2 + 3M KCL pH=1

500 coulombs/ cm^2 passed Re=1022

(a) 25.5 mA/cm^2
(b) 238.2 mA/cm^2

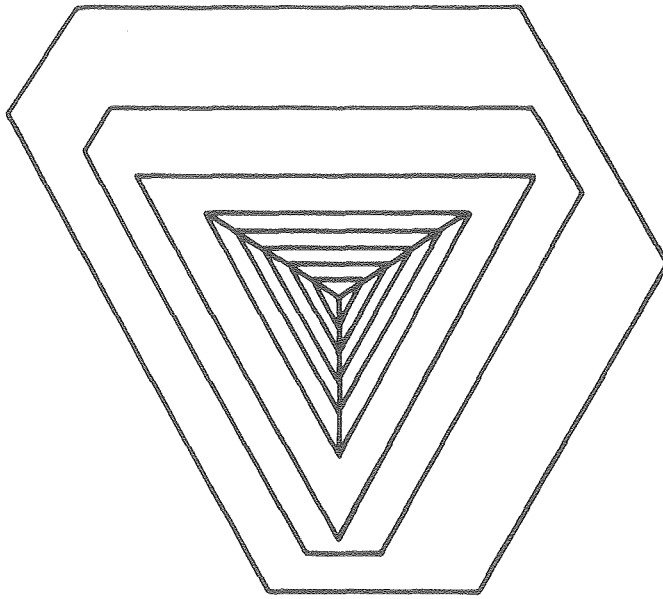
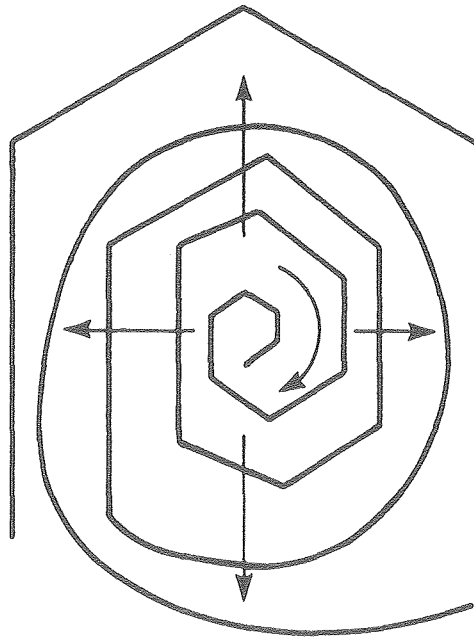
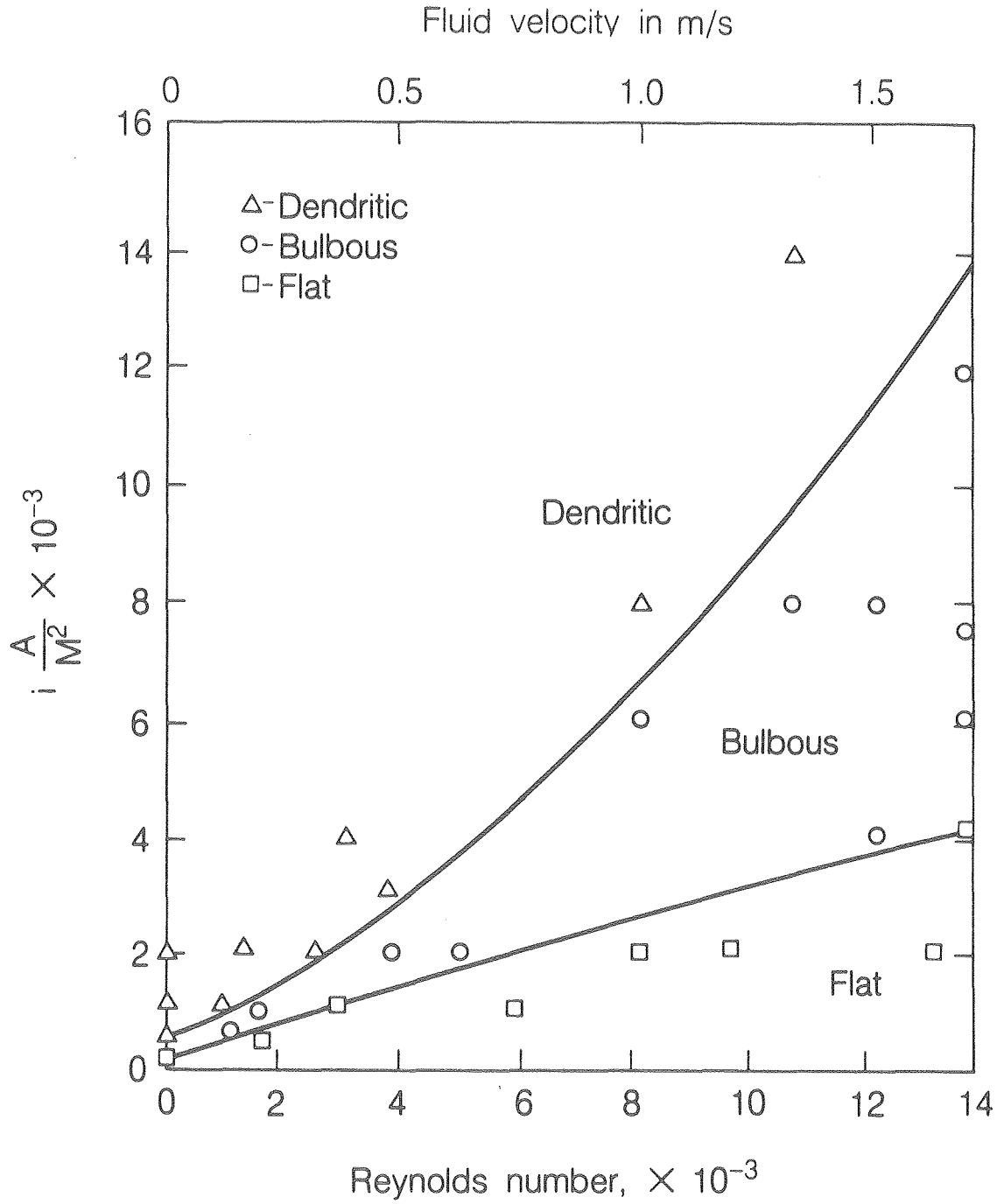


Figure 2.4- Pyramid growth center



XBL 865-1789

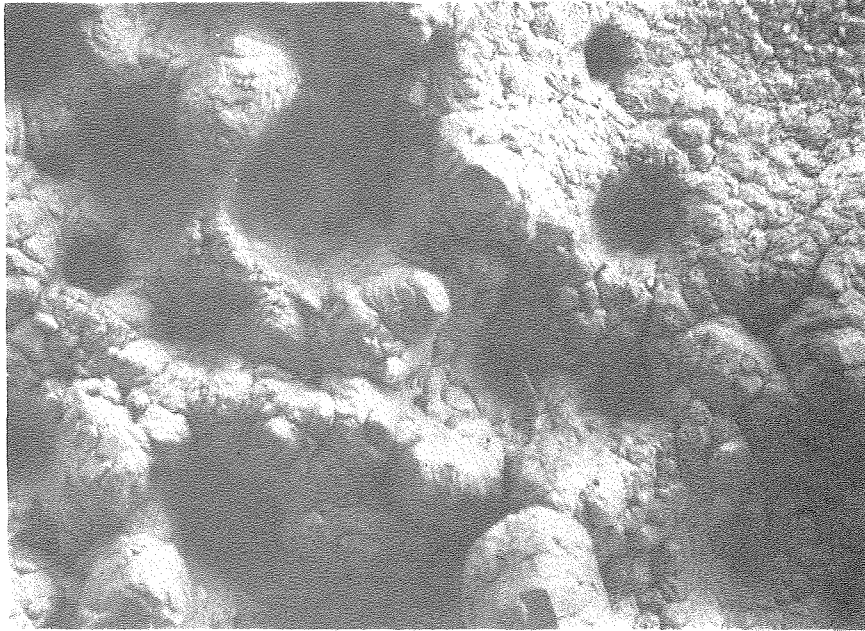
Figure 2.5- Spiral growth center



XBL 865-1790

Figure 2.6-

Phase diagram showing morphologies obtained at different current densities and flow rates (26)



1M ZnCl₂ + 3M KCl pH=1.5

Re=1022

238.2 mA/cm²

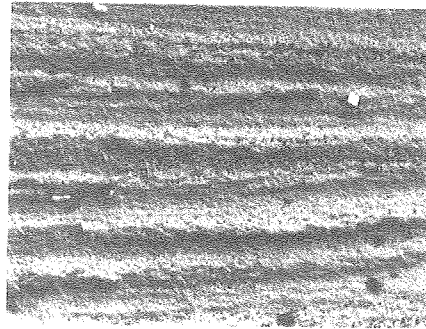
=47.4 μm

XBB 865-3589

Figure 2.7 - Morphology characterized by closely packed nodules and bubble craters

Figure 2.8- Ridges and fishnet structures

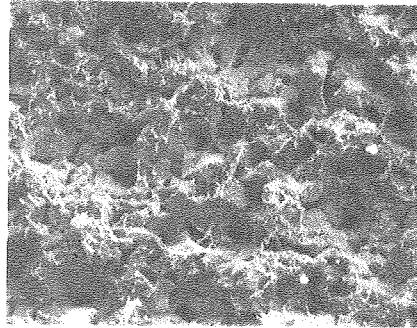
ridges



1cm=200 μ m

(a)

fishnet structure



1cm= 255.6 μ m

(b)

3M $ZnCl_2$ + 3M KCl $Re=4000$

500 coulombs/cm² passed synthetic graphite surface

(a) 47.8 mA/cm² pH=1.4

(b) 95.3 mA/cm² pH=0.6

XBB 865-3591

III. EXPERIMENTAL

1. Experimental Cells

Two experimental cells were used in this study. A channel flow cell, shown in Figs. 3.1 and 3.2, was used for most of the experiments. The rotating disk cell, shown in Fig. 3.3, was used for the impurity effect studies. All experiments were conducted galvanostatically.

The channel-flow cell had a 10 mm \times 6 mm rectangular cross section, and contained removable planar electrodes. A long entrance length assured fully developed flow at the location of the electrode. The cell was constructed of polypropylene and transparent polymethyl methacrylate through which the cathode was photographed. The piping system consisted of polypropylene pipes and valves. The solution capacity of this system was 5 gallons.

The rotating disk system consisted of a 1 liter borosilicate glass beaker through which a 0.64 cm hole was blown to facilitate mounting a large zinc anode facing upward. This assembly, the anode and the solution chamber, was sealed solution-tight using rubber o-rings and electrically connected to the rest of the circuit. The cathode was attached to a rotator and lowered into the solution to achieve electrical contact.

2. Electrodes

The cathodes used in this study, shown in Fig. 3.4, were constructed by attaching a piece of synthetic graphite or platinum to a brass core with silver epoxy resin. The electrodes were then encased in epoxy resin, heat-cured and machined to the desired circular shape. The

channel-cell electrodes were 2 cm in diameter and had an active surface area of 0.5 cm^2 (52). The rotating-disk electrodes were 3 cm in diameter and had an active surface area of 1 cm^2 .

The anode used in the rotating disk system, shown in Fig. 3.5, was a 99.99% zinc disk, with a diameter of 7.5 cm. Attached to the back of the disk, was a steel bolt that was coated with epoxy resin to prevent corrosion.

The anodes for the channel cell, also shown in Fig. 3.5, were pieces of zinc with an exposed surface area of 0.36 cm^2 . Attached to the back of each anode was a silver wire, which provided electrical contact. All sides except the one facing the flow were coated with non conducting resin to insulate them from the electrolyte.

3. Electrolytes

All of the solutions used in this study were prepared from "analytical grade" chemicals using distilled and deionized water. All experiments were performed in zinc chloride with a supporting electrolyte of either hydrochloric acid or potassium chloride. The following chemicals were used:

- (1) Mallinckrodt analytical reagent-grade zinc chloride.
- (2) Mallinckrodt analytical reagent-grade hydrochloric acid.
- (3) Mallinckrodt analytical reagent-grade potassium chloride.
- (4) MCB reagent-grade zinc dust and zinc powder.

4. Analysis Solutions

Most of the deposits from the experiments were dissolved off of the substrate and analyzed by EDTA titration. The chemicals used to analyze for zinc follow.

- (1) Mallinckrodt analytical-grade EDTA powder.
- (2) Baker analyzed reagent-grade Eriochrome Black T (Erio T)
($\text{HO}C_{10}H_6:NC_{10}H_6(OH)(NO_2)SO_3Na$).
- (3) Absolute ethyl alcohol.
- (4) Baker analyzed reagent-grade triethanolamine.

5. Equipment

An overall view of the experimental apparatus is shown in Fig. 3.6. The electrical equipment included the following:

- (1) Princeton Applied Research Model 371 galvanostat with a Model 178 electrometer probe.
- (2) Keithley Model 173A digital multimeter.

All experiments involved flow. The equipment used to generate and measure flow follows.

- (1) Gorman Rupp Industries Model 14110 magnetic drive pump (0.05 Hp)
maximum flow rate = 2000 m³ H₂O/min at 1 atm, 70°F for the channel flow system.
- (2) Gilmont Instruments rotameter (used in the channel flow system).
- (3) Pine ASR2 analytical rotator and speed controller (used in the rotating disk system).

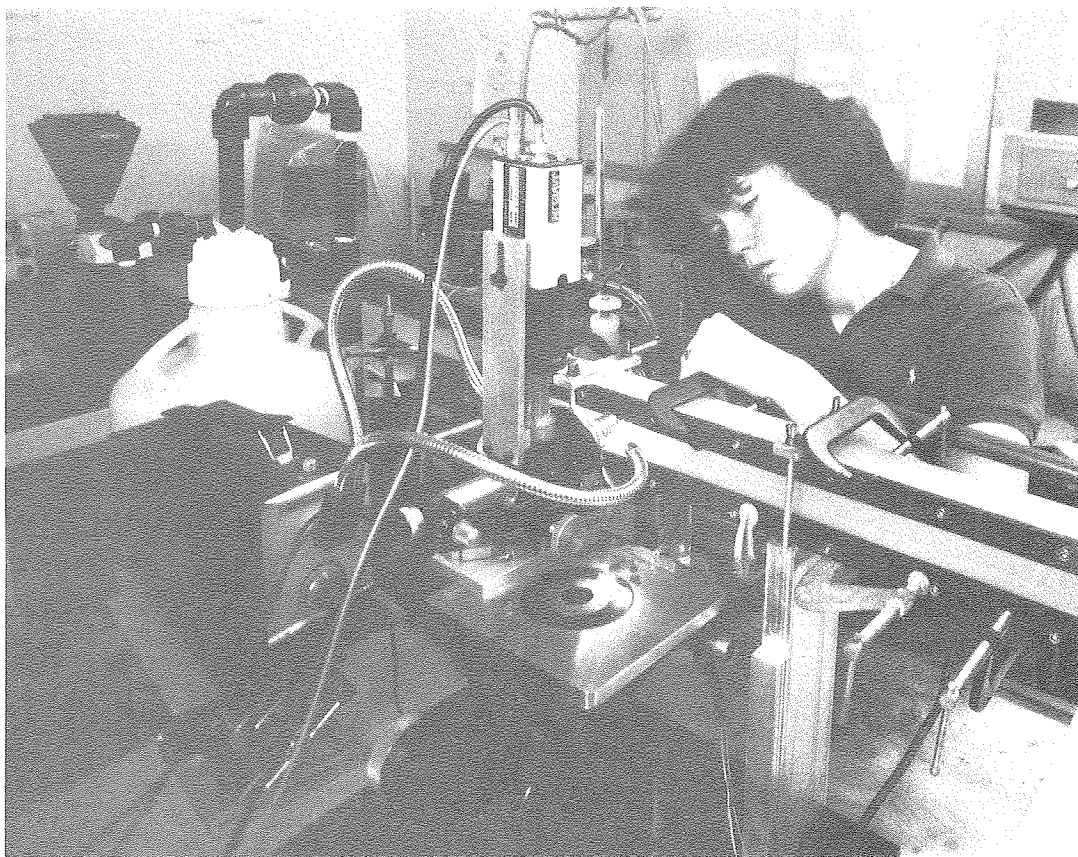
The electrode surface was examined both during and after deposition. The following equipment was used to view the electrode surface.

- (1) AMR Model 1000 scanning electron microscope.
- (2) ISI scanning electron microscope, Model # DS130.
- (3) Microscope constructed in house, consisting of a Bausch and Lomb microscope tube and American Optical stage.
- (4) Leitz 32x ultralong-focusing lens of numerical aperture (N.A.) = 0.3 and working distance of 13 mm,
- (5) Bausch and Lomb 5X hyperplane eyepiece.
- (6) Sony MV-11 microscope adapter.
- (7) Javelin Model JE2062 Metal oxide sensor (mos) black and white camera.
- (8) Sony VO-5800H video recorder.
- (9) Javelin VM-15 video monitor.
- (10) American Optical light source, model number 1177 (150 W).

Items 3-10 were used to observe the surface during deposition.

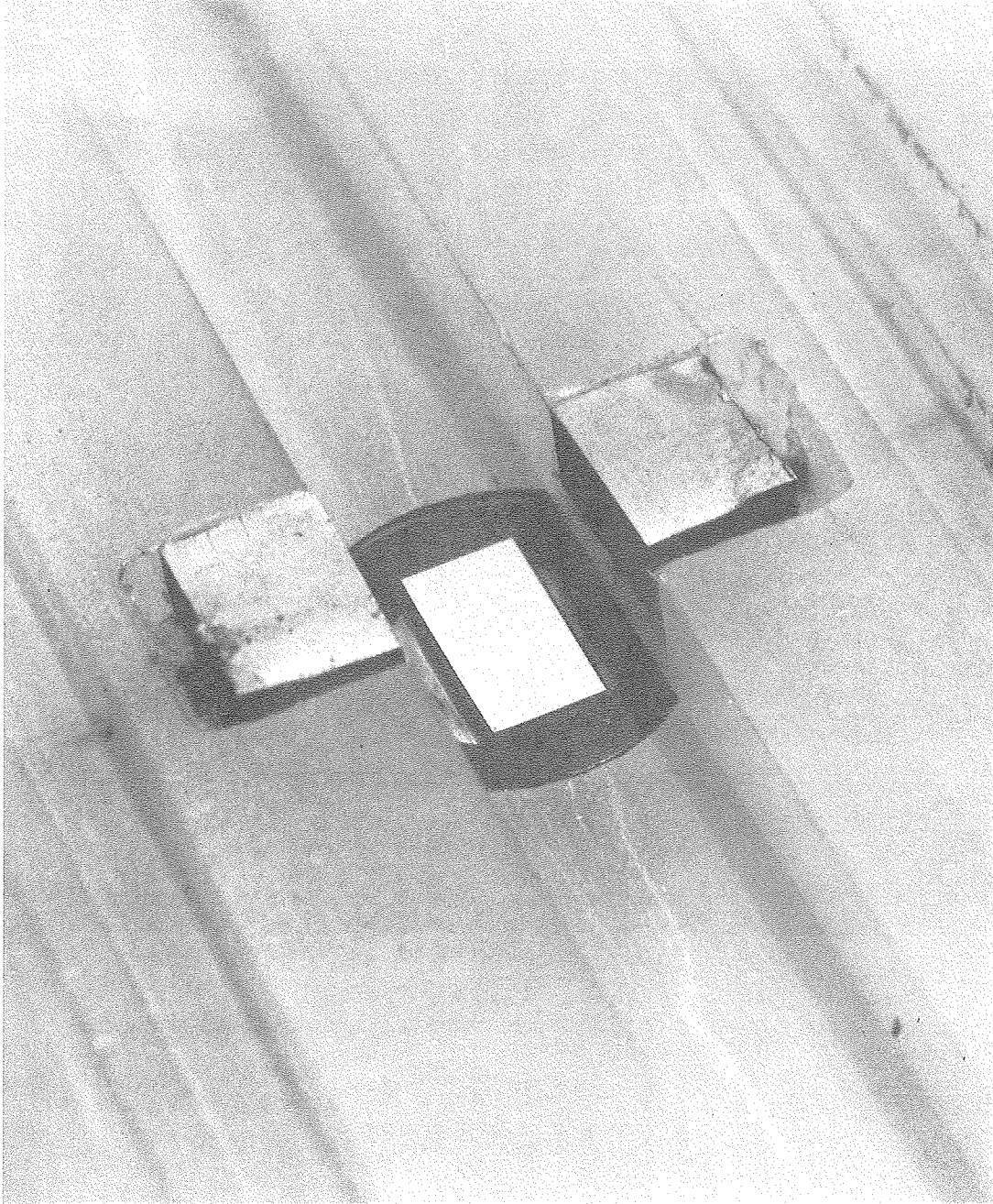
Miscellaneous Materials

- (1) Corning Model 130 pH meter.
- (2) Power Designs Inc. power source model 2005.
- (3) Mettler balance type K7T.



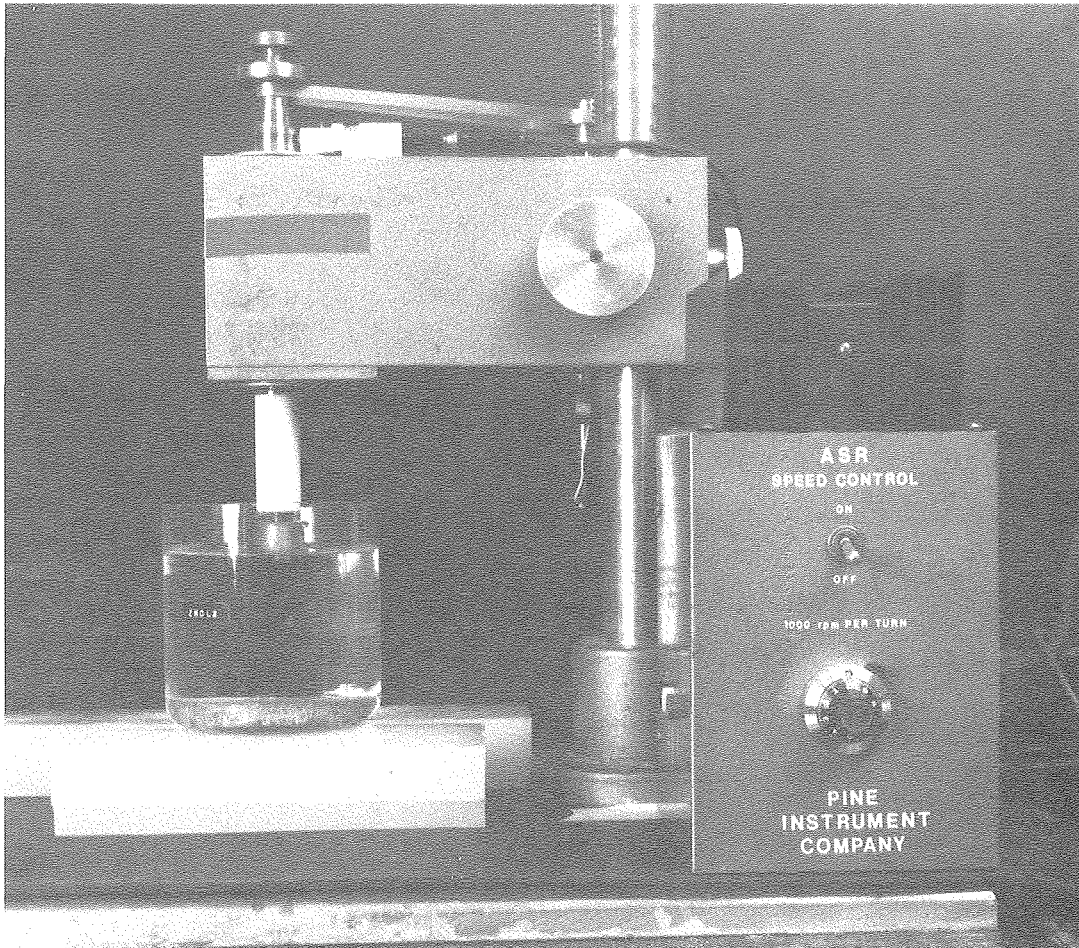
CBB 856-4650

Figure 3.1 - Flow channel cell for zinc electrodeposition
with videomicroscope and illumination device



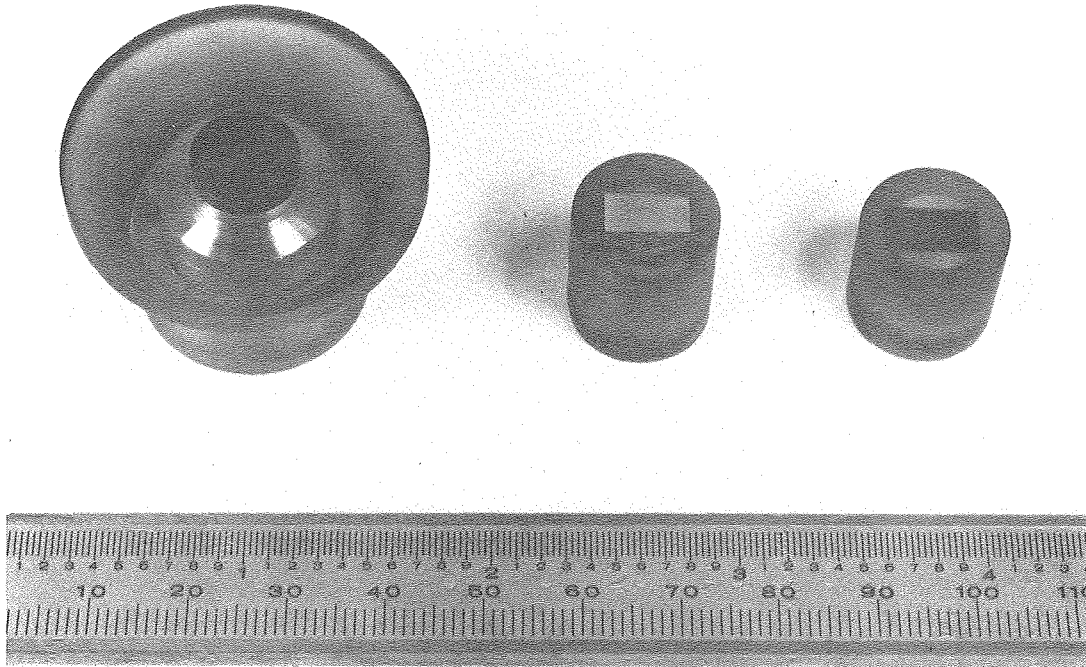
CBB 820-10747

Figure 3.2 - Close view of in-situ flow cell showing cathode and two anodes (from J. Faltemier's thesis)



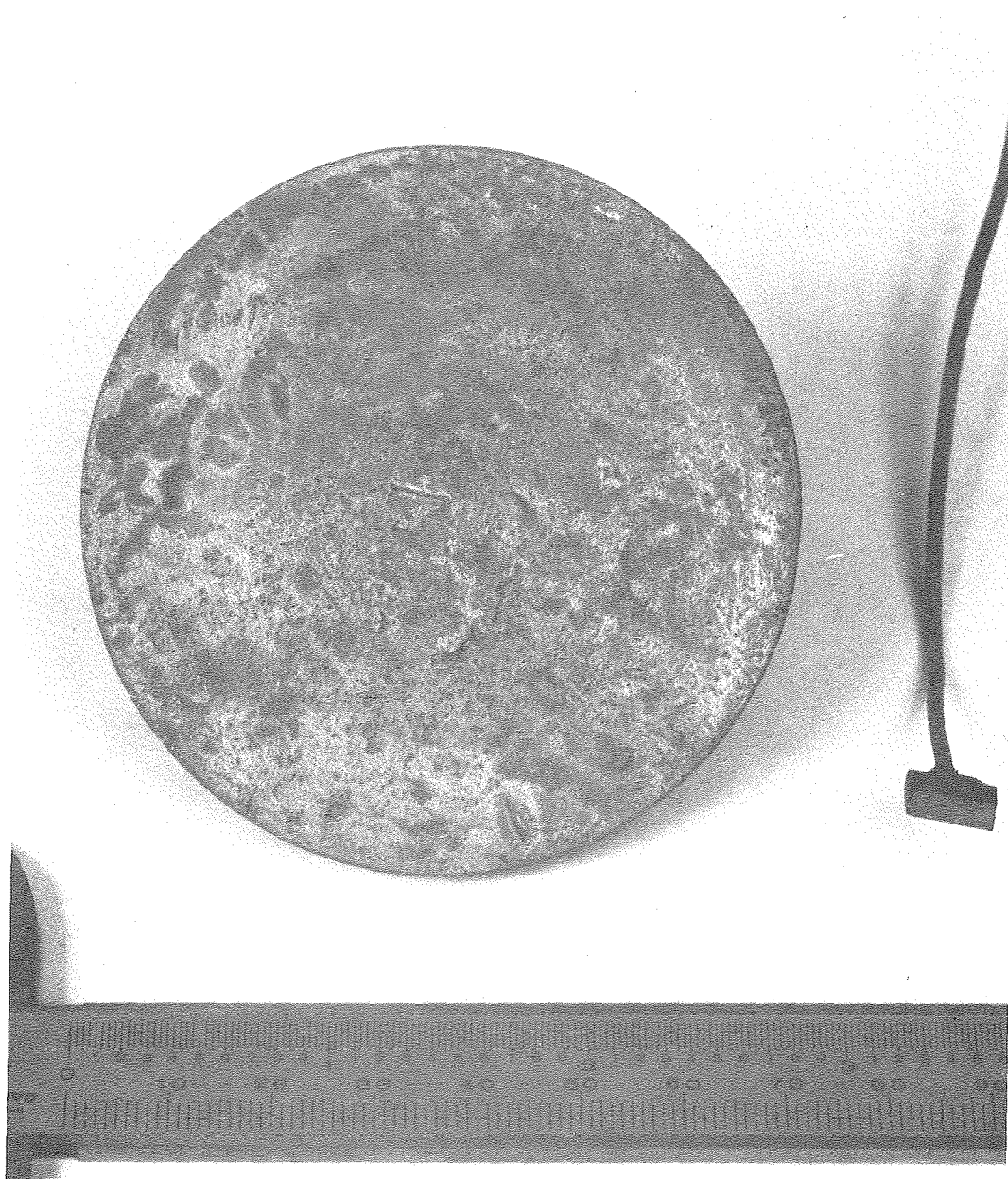
XBB 863-2104

Figure 3.3 - The rotating disk cell



XBB 863-2102

Figure 3.4 - Cathodes used in rotating disk and channel flow cells, (left to right) Union Carbide synthetic graphite (used in rotating disk cell), platinum, Gould synthetic graphite



XBB 863-2103

Figure 3.5 - Anodes used in flow cells, (left to right) zinc anode used in rotating disk cell and zinc anode used in channel flow cell



CBB 856-4652

Figure 3.6 - Equipment for video studies of micromorphology of zinc deposits

Left to right: Video screen showing imaged, developing deposit, the width of the video image corresponds to 0.8 mm on the electrode surface; electrical instrumentation; flow channel for deposition of zinc from acid chloride solution

IV. EXPERIMENTAL PROCEDURES

1. Electrode Preparation

All electrodes were polished with successively finer grit sandpapers, beginning with 180-grit (coarse) and ending with 600-grit (extra fine) silicon carbide sandpaper. The polishing fluid used was water. In between polishing steps, the electrode was ultrasonically cleaned in a bath of distilled water to remove any coarse particles. The electrode was rotated 90 degrees after each polishing step.

The platinum surfaces were further polished on the polishing wheel using 1-micron and 0.25-micron diamond paste. These pastes were mixed with distilled water to produce a foam, which was then applied to the polishing wheel. After the electrodes were polished to a mirror-like finish, they were ultrasonically cleaned, washed with water, acetone, and ethanol and dried using hot air. The electrodes were then stored in a dust-free environment before use.

Before use, the platinum electrodes were preanodized in a solution of 1M KOH and 0.5M NaCl for 15 minutes at 300 mA/cm^2 (52). The synthetic graphite electrodes were soaked in nitric acid for about 24 hours and dried under vacuum. The electrodes were washed again with distilled water and allowed to drain before use.

2. Electrolyte Preparation

The electrolytes were prepared using analytical grade zinc chloride, and potassium chloride. The molarities ranged from 1M to 4M, and the supporting electrolyte concentration was 3M. Concentrated hydrochloric acid was used to acidify the solutions. The electrolytes

were prepared in 4 liter batches and were purified using a zinc cementation technique. This technique involved heating a suspension of electrolyte and zinc particles (30 mesh) to 90°C. Circulation of the mixture was accomplished by natural convection. The solution was kept at 90°C for about 24 hours and was then filtered. Water was added to replace any that had evaporated, and the solutions were acidified using hydrochloric acid.

3. Preparation of Analysis Solutions

The EDTA solution was prepared using dry analytical-grade powder and distilled and deionized water. The EDTA was dried by heating it to 135°C for 2 hours and allowing the dried powder to cool slowly. The cool, dry powder was then weighed, and distilled water was added to make a 0.1M solution. A 0.01M solution was made by dilution of the 0.1M stock solution, and both solutions were standardized against a known zinc solution before use.

The Erio T indicator solution was prepared by adding 100 mg of Erio T indicator powder to 5 ml of absolute alcohol and 15 ml of triethanolamine. The solution was stirred until the Erio T dissolved and was used within 1 week.

4. Details of Operation

The circuit diagram is shown in Fig. 4.1. The cell was sparged with nitrogen for about 15 minutes after which electrolyte flow was started. Constant current was applied once steady state flow conditions were established.

In the channel flow cell, the deposit was observed in-situ which required extra procedures. Before starting the current, the fiber-optic lights and the video equipment were turned on. The video recorder was prepared by placing a tape inside it and setting it to both record and pause. This enabled the experimenter to focus the microscope using the video monitor. The microscope was focused, and the angle of lighting was then adjusted to best reveal the surface. In some experiments, a traveling stage was used; this would also be set to the desired location on the electrode. After everything was set, the traveling stage was turned on, the pause button on the video recorder was released, and electrolysis was started. Generally, the video recorder operated in real time. In certain experiments the recorder was set to pause and recorded at discrete time intervals. The details of the videomicroscopy system are described in Appendix 1.

Zinc was deposited at room temperature with various current densities and over different time intervals. Generally, from 400 to 500 coulombs/cm² were passed, this resulted in a deposit thickness of about 200 microns if densely packed. The deposits were weighed, dissolved and titrated after each experiment; current efficiencies were calculated for both procedures.

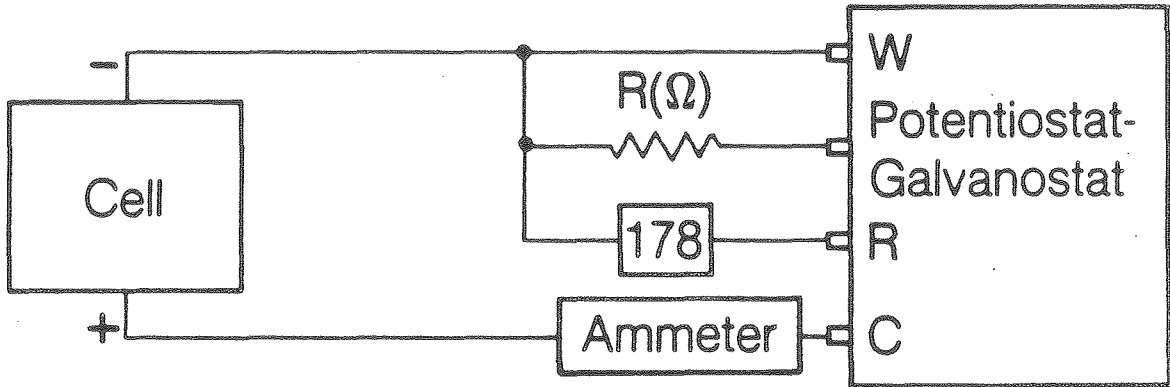
After the experiment was completed, the electrode was washed with distilled water and dried under vacuum for 24 hours. It was then weighed and in certain runs, saved for later examination. The rest of the electrodes were soaked in 10% nitric acid to remove the deposit for analysis by EDTA titration. This procedure involves a complexometric titration in which the zinc forms a more stable complex with EDTA than

with the indicator, Erio T. The color change indicating the endpoint was from purple to blue.

After the electrode deposits were dissolved with nitric acid, the remaining solutions were diluted to 100 ml using distilled and deionized water. Aliquots of 25 ml were taken from each well mixed solution, and 3-5 drops of freshly prepared Erio T indicator were added. The solutions at this point were a light red color; if they were purple, nitric acid was added until the solution turned red. Concentrated ammonium hydroxide was then added until the solution turned purple. The purpose of adding concentrated ammonium hydroxide was to raise the pH high enough so that any zincate complexes would dissociate. The purple solution was then titrated with EDTA until the solution turned blue. The EDTA was standardized in the same manner using a solution of known zinc concentration. The calculations used to find the zinc concentration and the resulting current efficiencies are noted in Appendix 2. Some solutions were also analyzed for zinc and chloride by atomic absorption spectroscopy. The atomic absorption spectroscopy was performed by the College of Chemistry's analytical laboratory and by Anamet Laboratories in Emeryville.

In addition to in-situ photography, selected electrodes were examined at higher magnifications using scanning electron microscopy. The purpose of this work was: (1) to record the microstructure of the electrodeposited zinc (2) to determine flow and concentration effects on the morphology and (3) to determine the effect of intentionally added impurities.

Galvanostatic Operation



XBL 8512-9042

Figure 4.1- Electrical circuit diagram

V. RESULTS AND DISCUSSION

1. The Morphology of Electrodeposited Zinc from Acidic Solutions

The morphology of zinc deposited from acidic solutions ranged from smooth and flat to highly nodular and dendritic. The factors that influenced the appearance of the deposit were the current density, flow rate and zinc concentration.

A. The Nature of the Initial Deposits

The initial stages in the deposition of zinc on platinum were: (1) the covering of zinc on the surface, (2) nucleation, and (3) the growth of nodules. After the passage of several coulombs, the deposit appeared striated, or had fishnet structures or dendrites (13,16,53). On platinum, the covering of the surface by zinc was characterized by a drastic change in reflectivity of the substrate. It is possible that there wasn't a distinct layer of zinc on the platinum substrate; the interface could be an alloy of zinc and platinum. Zinc was found to interact with platinum in studies by Despic and co-workers (54), who used cyclic voltammetry to elucidate the interactions between these two metals. As seen in Fig. 5.1, the platinum surface is first covered by a webbed-like surface upon which a few nuclei form. After passage of several coulombs, the surface becomes covered with nuclei as shown in Fig. 5.2.

The initial stages of deposition on synthetic graphite were studied by Anderson (24). Synthetic graphite is not known to alloy with zinc (54), and no significant changes in the reflectivity of a graphite surface have been observed that would indicate interactions between zinc and graphite.

B. Effect of Current on the Morphology

Naybour (26) studied the morphology of zinc electrodeposited from alkaline solutions of zincate ions supported by potassium hydroxide. He found that as the current density increased, at a constant flow rate, the morphological appearance changed from flat, to bulbous, to dendritic. A progressive roughening of the zinc deposit with increasing current density is shown in Fig. 5.3. At low current densities, the surface is smooth and may show striations. The edges also show the flat morphology and are branched downstream in the direction of flow. As shown in Fig. 5.4, the deposit is fine grained, uniform and crystalline. At high current densities, the deposit, as pictured in Fig. 5.5, becomes more porous and nodular. The edge growths take on the appearance of typical three-dimensional dendrites, which grow toward the anodes, not in the direction of flow. The deposit shows the imprint of hydrogen bubbles.

The work of Fisher and co-workers (55,56) can give some insight into the reasons for the changes in morphology. At low overpotentials and low current densities growth occurs via the formation of two-dimensional nuclei, and continues by the extension of layers. Growth of the electrodeposit at high current densities and high overpotentials occurs by the continuous nucleation and growth of three-dimensional nuclei.

The interfacial concentration, expressed as the percentage of the limiting current, was observed by Kindler (19) to be the main variable affecting changes in morphology. As the interfacial concentration decreased, roughness developed. It is well known that the current

density is higher on the protrusions, and therefore the metal will preferentially deposit in these areas. At low current densities, the concentration of the electroactive species is more uniform, and so deposition occurs in low lying areas as well. At high current densities, low concentration develops of the electroactive species in recesses therefore, protrusions grow preferentially. This phenomena was observed by Rogers and Taylor (18) as well as others.

C. Effect of Flow Rate on the Morphology

As observed by Naybour (26), increasing flow rate produces a flatter striated deposit. The effect of the Reynolds' number on the appearance of the deposit is shown in Fig. 5.6. The electrodeposit obtained at $Re = 1000$ exhibits signs of zinc depletion on the downstream portion of the electrode as well as edge growths that are not influenced by the electrolyte flow. At $Re = 4000$, the deposit is striated and the edge growths incline toward the flow direction. Flattening occurs because the surface concentration increases, due to increased reactant supply at high flow rates, and deposition occurs more evenly on all parts of the surface.

D. Effect of Zinc Concentration on the Morphology

In Fig. 5.7, the effect of concentration on the appearance of the deposit at both low and high current densities is exhibited. No differences are discernible between deposits obtained at high current densities from 2 or 3M zinc chloride (photos 5.7b and d). In contrast, low current density deposits from 2M zinc chloride solution are flatter, but the morphology becomes striated when 3M zinc chloride is used. In 1M

solution deposits are not striated when current density is above 30 mA/cm². The interfacial concentration, which depends on the bulk concentration, has a definite role in determining the region in which striations will form.

E. Effect of Hydrogen Ion Concentration on the Morphology

Some researchers have proposed that the formation of hydrogen encourages the formation of striations (35,47). Three mechanisms have been suggested: (1) striations form downstream of hydrogen bubbles, (2) hydrogen bubbles block areas on the surface where protrusions may grow, causing ridges to evolve in which hydrogen bubbles occupy the valleys between ridges and (3) hydrogen ion reduction blocks sites on the surface preventing zinc deposition in these areas on the surface. From our in-situ experiments, striations were observed to form without the existence of any bubbles on the surface or on the electrode edges. Experiments were conducted at current densities where striations were observed, to examine whether increasing hydrogen concentration could influence the formation of striae. As shown in Fig. 5.8, increasing the hydrogen concentration had no effect on the morphology at low current densities; all three of the deposits have a similar number of comparable striations.

Hydrogen gas evolution, however, can affect the morphology of electrodeposited zinc at low pH (< 0.6) and at high current densities. As demonstrated in Fig. 5.9a and b, bubbles can block areas of the zinc surface to further deposition. Gas bubbles can travel along the surface and create valleys as shown in Fig. 5.9c. Even on a striated electrode, bubbles can alter the shape of a striation as illustrated in Fig. 5.9d.

F. Effect of Impurities on the Morphology

In the course of this investigation, the effect of several impurities on the deposit appearance were examined using both macrophotography and scanning electron microscopy. The impurity content of the deposit was determined by atomic absorption spectroscopy. In Fig. 5.10, the effect of nickel is seen. Addition of 10 ppm nickel chloride to the electrolyte was observed to promote both hydrogen evolution and roughness development in the form of dendrites. The nickel content of the deposit was less than 0.02%, (seen in Table 5.1).

Addition of 40 ppm FeCl_3 ions had effects similar to the addition of nickel chloride, but the deposit was not as rough. The effect of iron contamination on the deposit appearance is shown in Fig. 5.11. Ferric ions also promote hydrogen evolution; hydrogen bubble development may have contributed to the surface roughening process. The percentage of iron in the deposit was less than 0.03% (shown in Table 5.1).

Scanning electron micrographs of the effect of ferric ions on the deposit structure is shown in Fig. 5.12. No effect on the morphology was observed for iron concentration levels of less than 10 ppm; higher levels caused the deposit to become less oriented and layerlike.

The effect of cadmium on the quality of the deposit is illustrated in Fig. 5.13. 10 ppm of cadmium is sufficient to roughen the deposit and striations are not observed. A contamination level of 30 ppm further roughens the deposit. 40 ppm cadmium appears to improve the deposit relative to the 30 ppm addition. Foulkes and co-workers (49) have suggested that the development of surface roughness is caused by enhancement of hydrogen evolution achieved with low cadmium

contaminations. Measurements of the overpotential for hydrogen evolution revealed that the overpotential first decreased and then increased with increasing cadmium concentration. At cadmium contaminations of 40 ppm, these researchers proposed that cadmium was incorporated into the deposit and refined the grain size. In the present study, the cadmium co-deposition level ranged from 1-2%, this level didn't increase upon further increase in the concentration of cadmium.

Differences in the structure of the cadmium contaminated deposits are shown in Fig. 5.14. Substantial cadmium contamination is shown to completely destroy the crystalline appearance of the deposit, which also shows evidence of gas evolution. No refinement of the grains is evident when the deposit obtained at a contamination level of 40 ppm is compared to one obtained at 10 ppm contamination.

G. Effect of Substrate on the Deposit Morphology

Two different substrates were investigated in the present study: synthetic graphite, composed of grains of graphite encased in resin, and platinum, a crystalline metal (fcc). In thick deposits, one would not expect to see differences in the morphology on a microscopic scale, that is, zinc layers would be formed on top of a zinc substrate. However, macroscopic features, such as striations, formed as a result of the initial deposition of zinc on a foreign substrate may exist on one substrate and not on the other. So, although the microscopic structure of the deposit might be the same, the macroscopic appearance of the deposit may be different.

As shown in Fig. 5.15, the structure of zinc deposited from different substrates, as expected, was the same; crystalline with well defined grains.

The macroscopic appearance of the deposits, depicted in Fig. 5.16, shows differences in the appearance and the extent of striation. In contrast to the deposit obtained on platinum, the deposit morphology (at the identical deposition conditions) on graphite is striated. The edge growths on platinum are large and are beginning to look similar to those obtained using higher average current densities. In addition, dendritic growths in several areas of the electrode occur. Both deposits show evidence of hydrogen evolution in the downstream area and dendritic growth on the edges of the electrode. Unlike the deposit obtained from the platinum substrate, most of the dendritic growth on synthetic graphite originates from the propagation of striations. The appearance of striae may be a reflection of the higher activity of the platinum electrode toward zinc deposition.

H. The Appearance of Striations

Striations have been observed to occur in the deposition of different metals (19,28) on various substrates in both alkaline and acidic electrolytes, over a wide range of flow rates and current densities. In the case of zinc, striations have been observed on zinc, platinum, graphite loaded polymers and synthetic graphite substrates. Ridges have been obtained in channel flow cells, rotating disk systems and using electrodes with no leading edges, such as the rotating cylinder (23,13,24,21,37). Deposition current densities resulting in a striated morphology have been below 100 mA/cm^2 (23,13,24,21).

There appear to be several conditions that determine whether striations will form. The interfacial concentration, as expressed by the percentage of the limiting current, is the primary criterion. This factor is interlinked with the activity of the substrate toward zinc deposition. Together, these two parameters determine the zinc nucleation density on the surface. Flow rate is another important variable, since without flow or movement of the electrode, no striations will form. Electrolyte flow influences the interfacial concentration and also contributes to the development of the hydrodynamic conditions for striations to form. The magnitude of the Reynolds' number may determine the upper limit of current density (for a given concentration) at which striations will still develop (see Fig. 5.6 where raising the flow rate at the identical deposition conditions produced striae). Faltemier (13) observed a limit of current density below which striations will not form.

In Fig. 5.17, the development of a striation is shown as a function of time or coulombs passed. First, protrusions appear on the surface (Fig. 5.17a). With advancing time, the protrusions gradually join parallel to the direction of flow; this propagation is described by Fig. 5.17b, where some protrusions have joined into striae while others are oriented in the direction of flow. As the thickness of the deposit increases, the formation of the basic pattern of grooves is completed and the deposit grows evenly, resulting in the formation of (what some authors call) ridges. The formation of striations is not related to the presence of sanding marks on the substrate (see Fig. 1.7a where both preferred nucleation in the grooves resulting from sanding and stria-

tions are evident.). It does not appear that the formation of ridges is separate from the formation of striations; some authors have suggested that the formation of ridges and striae are different phenomena (37).

I. The Propagation of Striations

Striations have been observed to propagate both upstream and downstream (13). Using videomicrography, the propagation of striations was observed "in-situ". The goal of this research was to define the mechanism of propagation of striae and to understand the physical situation that leads to the growth of protrusions into ridges. In Fig. 5.18 the development of a striation is shown over time. The enhancement of growth of a protrusion occurs primarily in the downstream direction, however, as shown in Fig. 5.19, enhanced growth also can occur in the upstream direction. The mechanism of the formation of striations, once the nodules are oriented in the direction of flow, involves the enhanced growth of existing, large protrusions, as visualized in Fig. 5.20.

Several mechanisms have been proposed to explain the development of striations. Jaksic (21) proposed that striations formed as a result of roll cells forming in the grooves of a roughening deposit. He stated that propagation of striations occurred due to a mechanism that caused the enhanced growth of a upstream protrusion, resulting in a "tail" which eventually joins a protrusion downstream, and that striations formed in a periodic manner. Observations in the present study indicate, however, that: (1) striations do not necessarily merge periodically, and (2) striae are also formed at Reynolds numbers at which Taylor vortices are not known to form.

Tsuda and Faltemeier (13,23) proposed that protrusions evolve into striations due to a mechanism that involved the formation of well mixed regions behind upstream protrusions which causes enhanced crystal growth in these locations. There are several facets of this theory that do not seem to agree with the present results. Carlson (20) observed no effect of the wake on the growth of protrusions less than 0.1 mm in height. In addition, no wake effects were observed at less than 90% of the limiting current. Our experiments were all performed well below 90% of the limiting current. Carlson (20) did not observe enhanced growth directly downstream from protrusions; it was stated that the area up to 2 diameters behind the protrusion was a region of low agitation. Naybour (26) observed that as increased mixing occurred, the deposit became flatter, that is, all nuclei grew at about the same rate. Anderson (24) found that the surface density of nuclei was of the order of 1000 nodules/mm²-mV, so it would be expected that a substantial number of smaller nuclei would exist between two large protrusions. This would imply that propagation occurs by the mechanism shown in Fig. 5.21. The growth of small nodules was not observed to be enhanced, rather they were consumed by larger nodules which grew at a significantly enhanced rate.

What is the physical situation that leads to the formation of striations? Carlson (20) stated that low agitation occurs in the area behind a protrusion, and it is well known that in flow around a sphere there is a stagnation point directly downstream and parallel to the direction of flow. Fischl (58) visualized flow around protrusions using hydrogen bubbles and found that there were areas parallel to the direc-

tion of flow in which, although there was circulation, there was less interaction with the bulk flow. Therefore depletion regions could be formed due to the lack of supply of the zinc reactant. The formation of depletion regions would lower the interfacial concentration at the surface, and the limiting current density. The growth of high current density regions would continue at the expense of low current density regions.

How would a surface comprised of several million protrusions act in the face of flow? It could be expected that a surface densely covered by protrusions would act in an analogous manner to a surface covered by pits. Alkire (59) studied the flow pattern in a pit, and found that in a sufficiently large pit, recirculating patterns would form, allowing corrosion products to build up. Such a recirculating pattern is shown in Fig. 5.22. Similarly, in zinc deposition, the region behind a protrusion could contain a recirculating pattern provided the protrusion is large enough. The concept of a critical size agrees with the work of Tsuda (23), who originally proposed this hypothesis. The critical size was observed to decrease with increasing flow rate and increasing current density in this study.

When the supply of reacting ion to protruding surface elements is significantly better than it is to recesses, and the average current density is high, the rate of growth of protrusions is especially fast compared to the recesses. This growth pattern has been observed by Rogers and Taylor for dendrites growing in zincate solutions (81) and is confirmed in Fig. 5.23 where the protrusion that has reached the critical size grows, while smaller protrusions do not grow (note that the

width plotted in this figure is actually the difference in width from a reference point). Bockris and co-workers (32) established that a dendrite growing under mass transport control will have a constant rate of growth with time. Moshtev and Zlatilova (39) confirmed the applicability of the Diggle, Despic and Bockris model for protrusions growing in alkaline solutions. As seen in Fig. 5.24, the growth downstream of the upstream protrusion diagrammed in Fig. 5.18 has a linear dependence with time.

The existence of recirculating regions in close proximity to the electrode can explain apparently anomalous results concerning the development of striae. The growth of protrusions on the upstream side is one example. Protrusions can be close enough so that both the upstream and downstream protrusion benefit from enhanced growth in the recirculating region. If the current density is higher on the downstream protrusion than on the upstream protrusion, then the downstream protrusion will grow at a faster rate toward the upstream protrusion, than the latter does downstream. Therefore, the striation will propagate upstream.

Striations have not been observed to form at high current densities nor do they form when pulsed current is used. In both of these situations, the density of nucleation is enhanced, and therefore less space between emerging nodules exists. As shown by Anderson (24) and by Tsuda (23), the average size of nodules decreases with increasing current density for the same number of coulombs passed. Alkire (59) indicated, that no recirculating regions develop in small pits. At higher limits of current density, the density of nodules is so large that no large

pits ever form, that is, the protrusions coalesce both parallel and perpendicular to the flow direction before they grow to the critical size at which recirculating flow patterns form. As a consequence, the densely spaced nodules on the surface grow at about the same rate, and a flat surface results.

In summary, the important parameters in the formation of striations are the interfacial concentration of the reactant, the protrusion density, and the average protrusion height. Of minor importance is the magnitude of the flow rate, which will influence the diffusion layer thickness and therefore, the critical height at which recirculating patterns form. Striations will form at any current density in which the growth rate of protrusions is such that they will reach a critical height at which recirculating flow patterns form before they coalesce parallel to the flow direction with other protrusions of similar size.

2. Current Efficiency in the Electrodeposition of Zinc

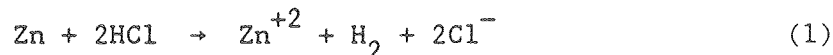
A. Shape of the Current Efficiency Curves

The variation of current efficiency with current density was similar for all combinations of zinc concentration, pH, flow rate and substrate. For low current densities, the current efficiency increased with increasing current, until a plateau near 100% current efficiency was achieved. Between 25 and 150 mA/cm², the current efficiency was 95-100%, independent of the current density. Above 150 mA/cm² the current efficiency decreased rapidly with increasing current density. A typical curve showing the variation of current efficiency with current density is shown in Fig. 5.25. The high current density portion of the

curve, above 150 mA/cm², is above the effective limiting current density. The consecutive reaction is hydrogen evolution. It is interesting to note that if one ignores the effects of complexing the limiting current density is near 700 mA/cm².

The apparent independence of the current efficiency with increasing current in the range of average current densities from 25-150 mA/cm² is the result of the fast kinetics of the zinc discharge reaction. In this region, the electrodeposition of zinc is not clearly mass transport limited. The evolution of hydrogen, the thermodynamically preferred reaction, is kinetically limited. Other researchers (46,60,61) have also reported that the current efficiency is independent of current in this region, in both acidic and alkaline electrolytes.

Up to 25 mA/cm², the current efficiency increased with current density. This result was consistently observed under all conditions of flow rate and concentration. One can identify several reasons for the increase in current efficiency with current density. It is possible that the decrease in current efficiency is due to dissolution of the deposit by one of the following reactions:



or in chlorine evolving cells



Reaction 2 has been identified as the major source of inefficiency in the zinc/chloride battery, (35). In our cell the dissolution of zinc was the anodic reaction, and therefore no chlorine was present. The dissolution of zinc in hydrochloric acid, according to Equation 1, (used

in the electrolyte to adjust the pH) is plausible, and is supported by the observation that the current efficiency decreased slightly with increasing coulombs passed (Fig. 5.26). A corrosion experiment was performed, and it was found that the deposit dissolved at a rate of 1.1 mg/hr-cm² in a flow cell (Re = 4000, pH = 1.4) corresponding to a dissolution current density of 9.3×10^{-4} mm/cm². Dissolution of the deposit is clearly not the only factor in the increase of current efficiency with increasing current density.

An explanation of the direct relationship between current efficiency and current density at low current densities was advanced by Epelboin and co-workers (60), who noted that the current efficiency increased with current density in a sulfate system. According to these authors, zinc adsorbs on the surface in preference to hydrogen. With increasing current density, zinc displaces hydrogen already on the surface, preventing the thermodynamically favored hydrogen reaction. The displacement of hydrogen ions by zinc leads to an increase of current efficiency.

B. Accuracy of the Current Efficiency Measurements

An important component of any current efficiency measurement is the error involved in taking the measurement. Both random and systematic errors need to be considered. The random error in the weight measurements is 0.01 mg or 0.01%, for the EDTA titration it is less than 0.1%. The random error is about 1% for zinc concentrations determined by atomic absorption spectroscopy.

Many authors have neglected consideration of systematic errors in their measurements of the current efficiency (41,46,62). To evaluate the systematic errors in this study, two independent methods for determining the amount of zinc deposited were used: weight measurements and EDTA titration. As shown in Fig. 5.27, the current efficiencies measured by titration and by weight of the deposit were generally in good agreement.

A possible source of discrepancy between the two types of measurements is that the weight measurements were affected by oxidation of the deposit. On removal from the cell, many of the deposits turned color from a light to a dark grey. Calculations indicate, though, that a large percentage of the deposit would have to be oxidized to produce noticeable error in the determination of current efficiency.

The current efficiency figures obtained could also have been erroneously low if parts of the deposit had been lost in transit. Precautions were taken to ensure that this did not occur, so transfer losses cannot be considered a source of error in these measurements.

A larger problem is the occlusion of salts in the deposit. SEM and in situ micrographs indicate that the deposit may have a small porosity. Other researchers (63,34,41) have produced evidence that deposits obtained from zinc solutions are not densely packed. To estimate the extent of occluded salts, the chloride concentration of the zinc deposit was measured by atomic absorption spectroscopy. The zinc associated with the chloride was obtained by assuming that the proportion of zinc to chlorine in the occluded salts is the same as the proportion of zinc to chlorine in the bulk solution. The total correction for occluded

salts was approximately 3% for weight measurements and about 2% for titration results.

Both the titration and the weight results could have been affected by the codeposition of impurities. As the solutions were purified before use, it is not believed that this was a problem.

It is believed that the total accuracy of the weight measurements is 3% for the weight and the atomic absorption spectroscopy measurements, and 1.5% for the titration measurements. The reproducibility of these measurements is within $\pm 2\%$.

C. The Effect of Zinc Concentration on the Current Efficiency

The effect of the zinc ion concentration on the current efficiency is shown in Figs. 5.28 and 5.29. In Fig. 5.28 the current efficiency increases for increasing zinc ion concentration, from 1-3M. This is the expected result since there is a greater concentration of the electroactive species in the 3M solution.

In Fig. 5.29, the effect of current density on the current efficiency for 2 and 3M zinc chloride solutions is compared. Over the entire pH range investigated the current efficiency is the same for current densities between 30 and 160 mA/cm². For current densities under 30 mA/cm², the current efficiency for 3M zinc chloride was observed to be smaller than that for 2M zinc chloride. In the 3M solutions zinc is more complexed than in 2M solution. Because there is less zinc available to displace adsorbed hydrogen on the surface the reduction of hydrogen ion may have occurred. The inflection point where the current efficiency becomes a decreasing function of the current density

does not appear to have shifted in proportion to the change in concentration. Two reasons could have accounted for the lack of change in the limiting current density: (1) Due to complexing in the solution, the concentration of the electroactive species increased less than did the apparent concentration, and (2) Since more zinc is complexed in anionic form, the effective transference number of all zinc ionic species is more negative (39,64).

D. The Effect of Hydrogen Ion Concentration on the Current Efficiency

Figure 5.30 shows the effect of hydrogen ion concentration on the current efficiency for a 1M zinc chloride solution supported by potassium chloride. As expected, the current efficiency increases with decreasing hydrogen ion concentration. The current efficiency is below 100% which indicates that some hydrogen evolution is taking place. Little change is seen in the current efficiency in the range of 25-175 mA/cm². This result is in agreement with the conclusions of Begum and co-workers (46).

Figure 5.31 shows the effect of hydrogen ion concentration for a 3M zinc chloride solution supported by potassium chloride. A measurement was inadvertently omitted at 10 mA/cm² for the solution at pH = 0.6. At low currents, the current efficiency decreases with increasing pH, but increases with current density. In this region zinc displaces adsorbed hydrogen ions. More protons in the solution results in more hydrogen adsorbed on the surface, and a therefore lower percentage of hydrogen ions is displaced by zinc. Consequently, the current efficiency decreases.

A more interesting effect is shown at higher current densities. The current efficiency is higher in a low pH solution than it is at a higher pH. The opposite trend would be expected. It is possible that adding acid to a fully-complexed solution reduces the amount of the basic zinc complexes in the solution. The existence of hydrohalozinc complexes advanced by Selman and co-workers (37,35) tends to support the hypothesis that acid interacts with basic complexes. Jorne and Ho (64) measured the transference number of zinc in solutions of varying zinc and hydrogen ion concentration. It was found that the transference number of zinc increased with increasing acidity of the solution, indicating a smaller proportion of anodic complexes. Mackinnon and co-workers (65) and Selman (37) both noted a refinement in the deposit structure with the addition of acid. The effect of adding acid to the solution could be to increase the concentration of the electroactive species and consequently, the current efficiency.

E. The Effect of Flow Rate on the Current Efficiency

Increasing the flow rate is well known to affect the limiting current due to a thinning of the mass transport layer. Larger flow rates increase the interfacial concentration which should enhance the current efficiency. The effect of the flow rate on the current efficiency is shown in Fig. 5.32. The curves exhibit the same basic shape but are shifted relative to each other. At low currents the current efficiency decreases with increasing Reynolds number. This is possibly due to an increase of the rate of chemical dissolution (66) of zinc by the reaction:



Transport of the acid to the surface is enhanced by the increasing the flow rate, therefore the deposit is chemically dissolved more rapidly.

At higher current densities, the current efficiency increases with flow rate. The reason for this is that the transport of zinc ions to the cathode increases with flow rate, resulting in a higher interfacial concentration of the zinc ion available for discharge. In laminar flow, the effective limiting current, measured by determining the high current density inflection point of the current efficiency curve, was found to be proportional to the 1/3 power of the Reynolds number, in general agreement with published correlations. The diffusion coefficient calculated from the effective limiting current is approximately 3×10^{-6} cm²/s, in agreement with the results of Selman (16,37).

F. The Effect of Substrate on the Current Efficiency

The availability of sites on the surface would be expected to influence the current efficiency. The fraction of available sites will be different depending on the substrate. To evaluate this effect, two substrates were evaluated; synthetic graphite, manufactured by Gould, and not known to interact with zinc, and platinum, known to alloy with zinc (54,67,68). As shown in Fig. 5.33, the platinum substrate gave consistently lower current efficiencies than synthetic graphite, although the general shape of the current efficiency curves were similar. Anderson (24) determined the densities of nodules for zinc deposited from 1M zinc chloride solution. He found that there were fewer nodules found on platinum than on synthetic graphite. Fewer sites

available for zinc nucleation could result in a lower current efficiency. Another possible reason for lower current efficiency on platinum could be that this substrate has a lower overpotential for hydrogen evolution than synthetic graphite.

G. The Effect of Impurities on the Current Efficiency

The influence of added cadmium, iron and nickel chlorides on the current efficiency, and on the nature of the deposit, has been a subject of numerous investigations in the past (40,41,51,62,65). Only a modest effort was devoted to this problem area in the present investigation. The effect of increasing concentrations of Cd^{++} , Fe^{+++} , and Ni^{++} on the current efficiency is depicted in Fig. 5.34. Ni^{++} promotes hydrogen evolution and leads, as well, to rough deposits and dendrite formation. Curiously, the nickel content of the deposits did not exceed 0.02%. Iron had a similar, somewhat smaller, effect to nickel, although the deposit was not as degraded (see Fig. 5.12). Again, iron codeposition promotes hydrogen evolution (41), which may contribute to the development of roughness. The iron content of the deposit did not exceed 0.03%.

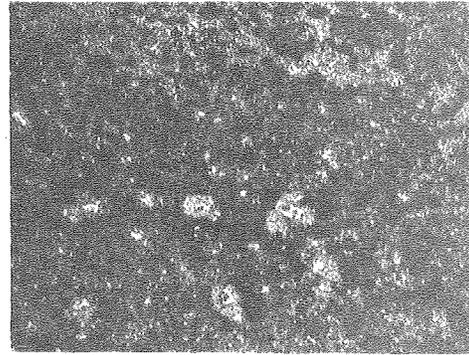
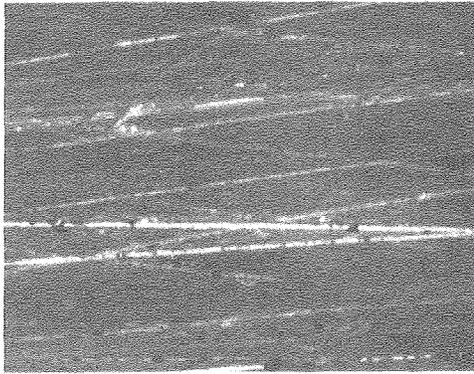
The most surprising behavior was demonstrated by cadmium, which decreased the current efficiency at low concentrations in the electrolyte (10 ppm), presumably because of the lowering of the overpotential of hydrogen evolution (49). At higher concentrations (20 and 40 ppm) the current efficiency of zinc deposition improves. Paralleling this improvement, the inclusion of small concentrations of cadmium leads to grain refining in the deposit. In contrast to iron and nickel, cadmium readily codeposits with zinc (41,49).

Table 5.1. Co-Deposition of Impurities with Zinc.

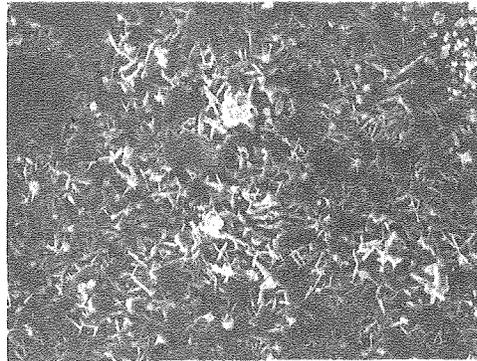
Electrolyte Concentration g/l	Impurity (% Deposited)		
	Nickel	Cadmium	Ferric
10	0	0.78	0.02
20	0.005	1.06	0.02
30	0.008	1.7	0.025
40	0.02	1.07	0.022

Sensitivity: 5 ppb, accuracy $\pm 10\%$.

Figure 5.1 - Structure of the initial deposit of zinc on platinum



(a) before deposition 8.19 μm (b) after deposition 100 μm



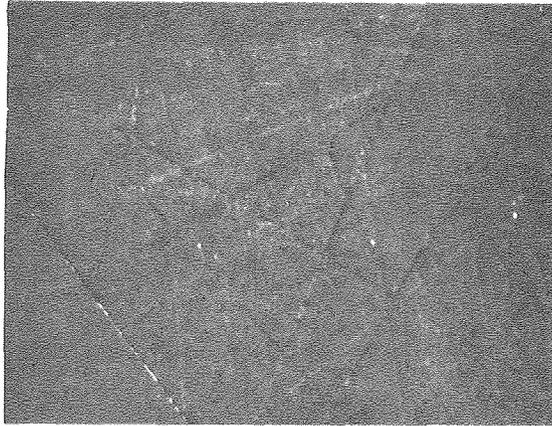
(c) after deposition 14.3 μm

1M zinc chloride pH=5.2

Re= 9000 1 min of deposition

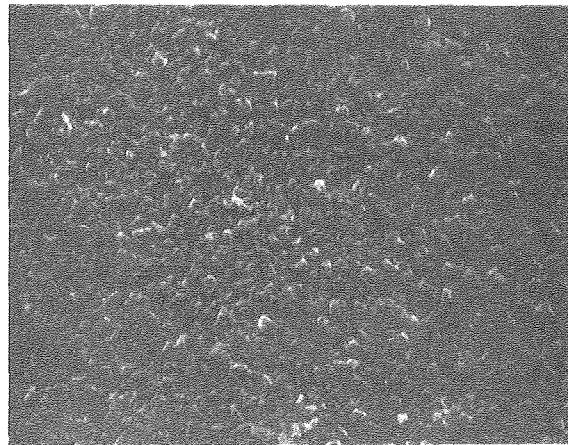
platinum substrate, 31 mA/cm²

Structure of the initial deposit of zinc on platinum



(a) before deposition

14.2 μm



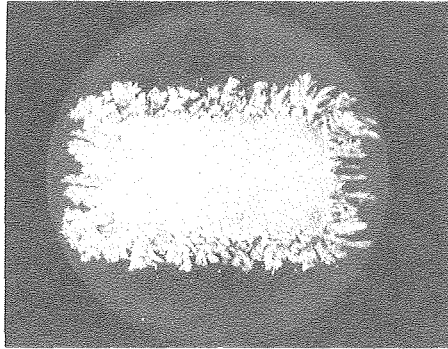
(b) after deposition

1M zinc chloride, pH = 5.2,
platinum substrate, 100 mA/cm²
Re = 9000 3 min of deposition

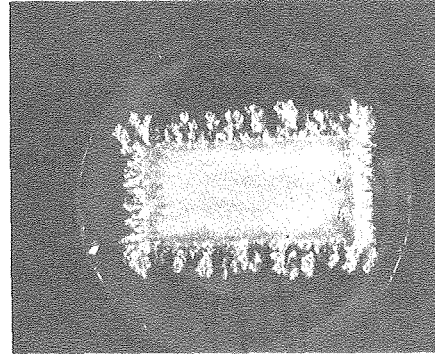
XBB 865-3588

Figure 5.2

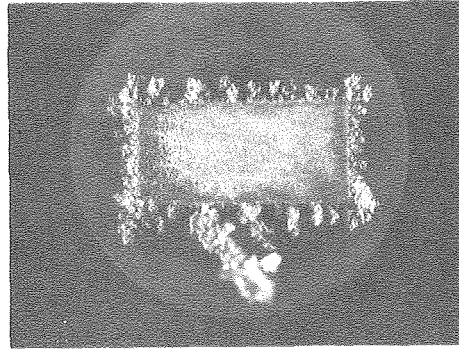
Effect of the current density on the deposit appearance



(a) 28.6 mA/cm^2



(b) 142.8 mA/cm^2



(c) 286 mA/cm^2

3M zinc chloride, 3M potassium chloride, $pH = 1.5$

$Re = 4000$, synthetic graphite substrate

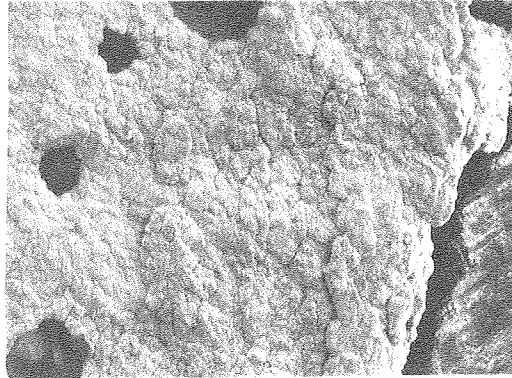
$500 \text{ coulombs/cm}^2$ deposited,

electrode size $1.0 \text{ cm} \times 0.5 \text{ cm}$

XBB 865-3600

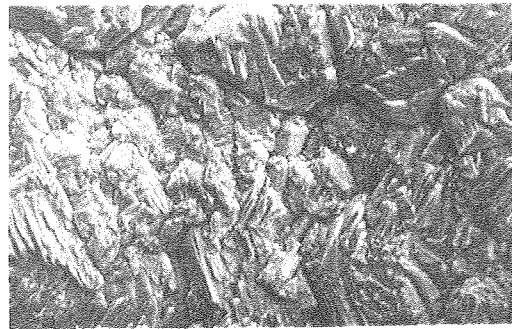
Figure 5.3

Appearance of the deposits at low current densities



73.0 μm

(a)



9.8 μm

(b)

1M zinc chloride, 3M KCl, pH=1

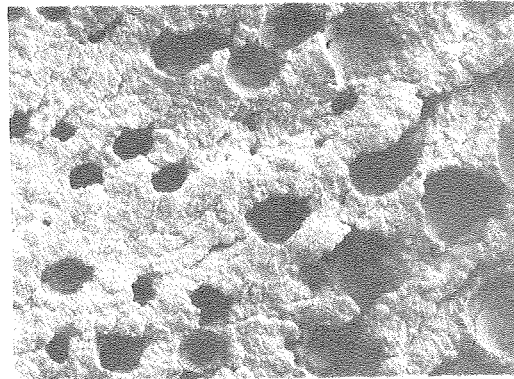
zinc deposited on synthetic graphite

9.9 mA/cm^2 $\text{Re}=1022$, 500 $\text{coulombs}/\text{cm}^2$ deposited

XBB 865-3601

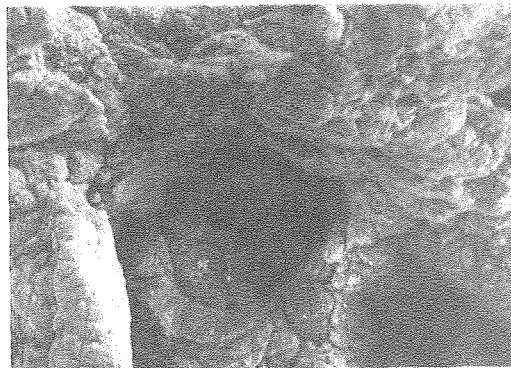
Figure 5.4

Appearance of the deposits at high current densities



(a)

143.0 μm



(b)

28.6 μm

1M zinc chloride, 3M KCl, pH=1

zinc deposited on synthetic graphite

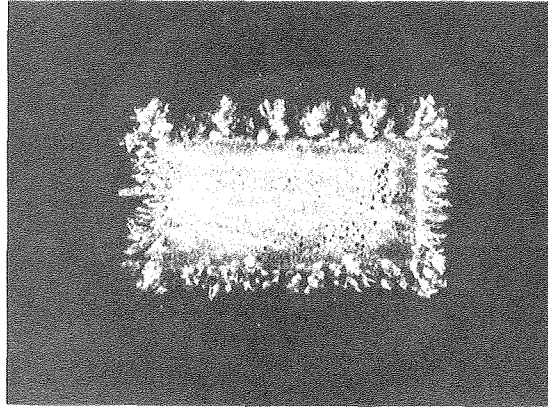
107 mA/cm² Re=1022,

500 coulombs/cm² deposited

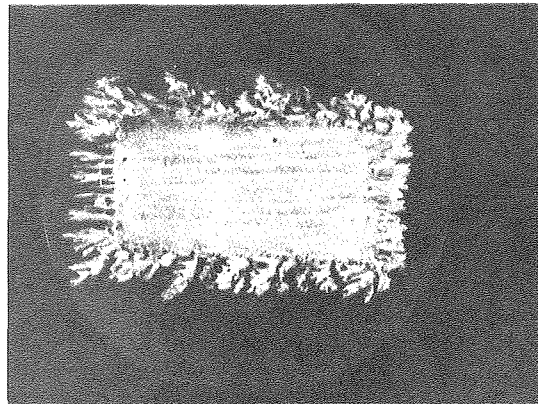
XBB 865-3602

Figure 5.5

Effect of flow rate on the deposit appearance



(a)



(b)

3M zinc chloride, 3M KCl, pH = 1.5

47.6 mA/cm², 500 coulombs/cm²

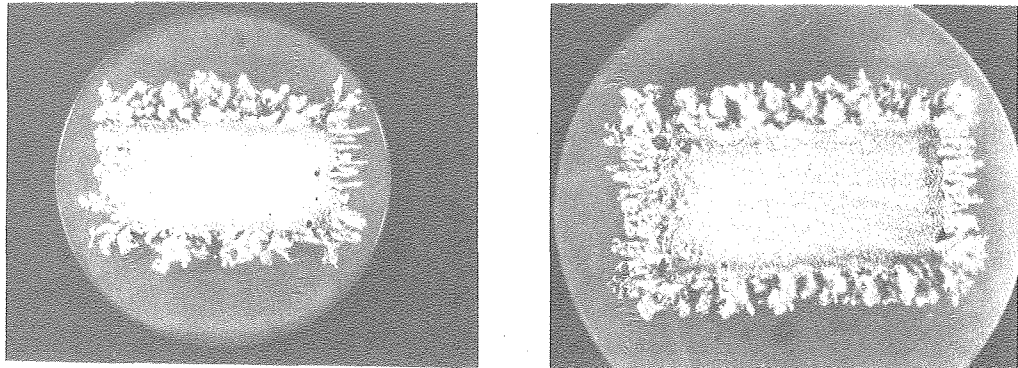
(a) Re = 1000

(b) Re = 4000

XBB 865-3603

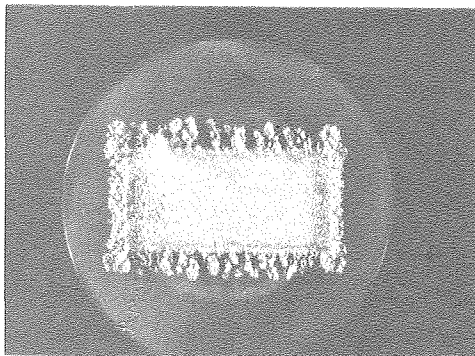
Figure 5.6

Effect of zinc chloride concentration on the deposit appearance,

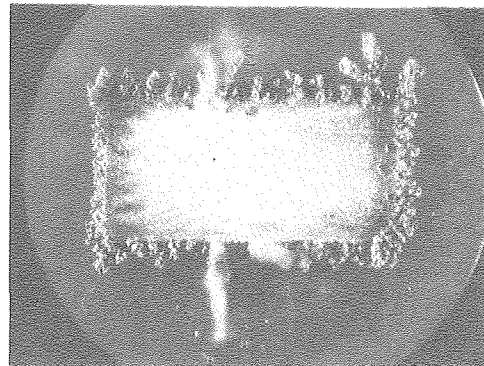


(a)

(c)



(b)



(d)

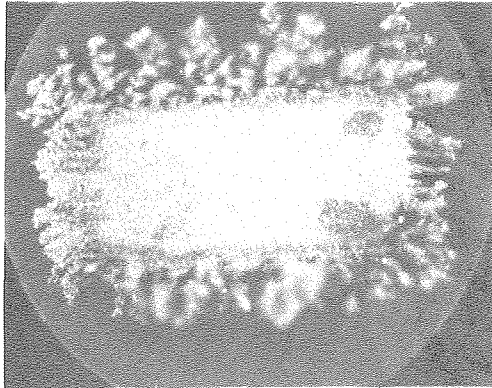
synthetic graphite substrate, $Re=1000$, $pH=3$
 $500 \text{ coulombs/cm}^2$ deposited,

- (a) 2M zinc chloride, 3M KCl, 35.03 mA/cm^2
- (b) 2M zinc chloride, 3M KCl, 140.4 mA/cm^2
- (c) 3M zinc chloride, 3M KCl, 46.1 mA/cm^2
- (d) 3M zinc chloride, 3M KCl, 142.6 mA/cm^2

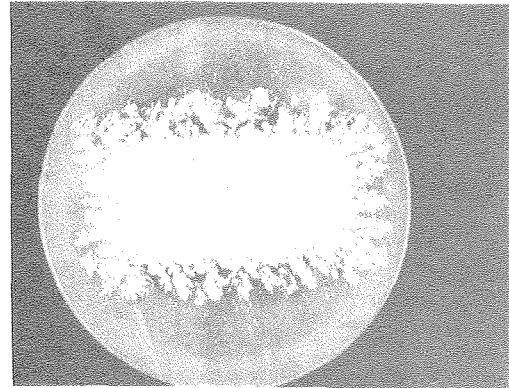
XBB 865-3598

Figure 5.7

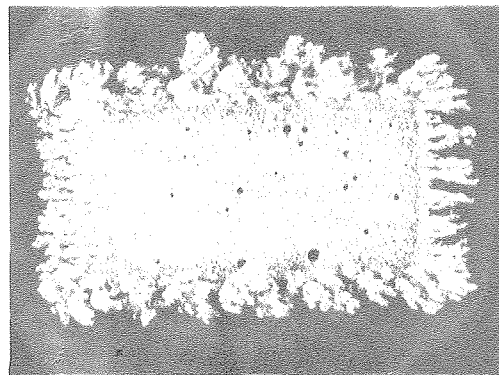
Appearance of the deposit at different pH



(a)



(b)



(c)

3M zinc chloride, 3M KCl

Re=1000 28.6 mA/cm² 500 coulombs/cm²

synthetic graphite surface

(a) pH=3

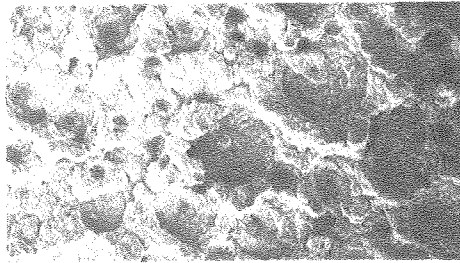
(b) pH= 1.5

(c) pH= 0.6

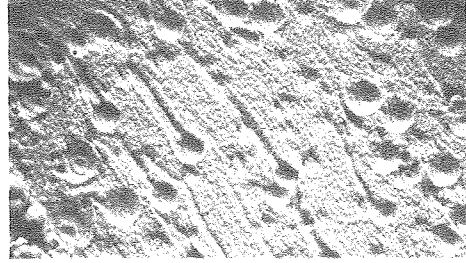
XBB 865-3597

Figure 5.8

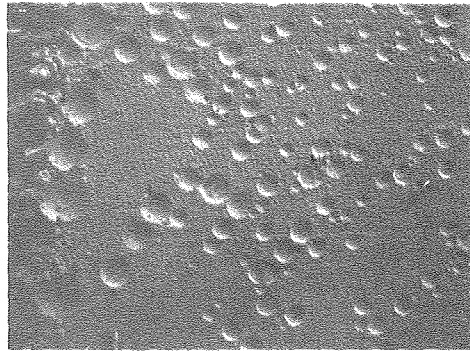
Imprint of hydrogen bubbles on zinc deposited on a synthetic graphite surface



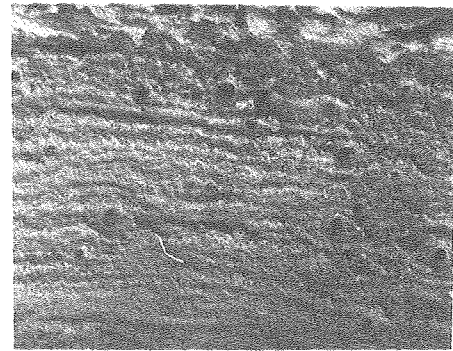
(a) $200\ \mu\text{m}$



(c) $625\ \mu\text{m}$



(b) $333\ \mu\text{m}$



(d) $555\ \mu\text{m}$

(a) $1\text{M ZnCl}_2 + 3\text{M KCl}$, $51\ \text{mA}/\text{cm}^2$, $\text{Re}=1022$, $\text{pH}=1$, 10 minutes

(b) $1\text{M ZnCl}_2 + 3\text{M KCl}$ $200\ \text{mA}/\text{cm}^2$, $\text{Re}=3118$, $\text{pH}=1$, 10 min

(c) $1\text{M ZnCl}_2 + 3\text{M KCl}$, $\text{pH}=1$, $178\ \text{mA}/\text{cm}^2$, $\text{Re}=1022$, 10 min

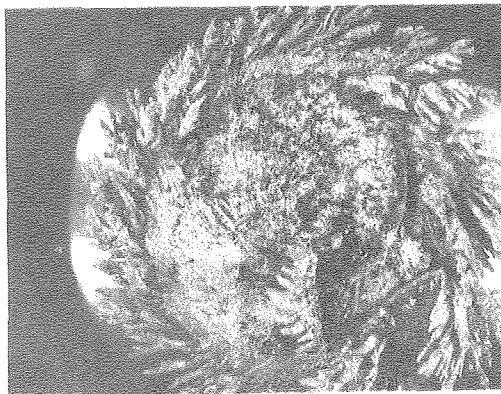
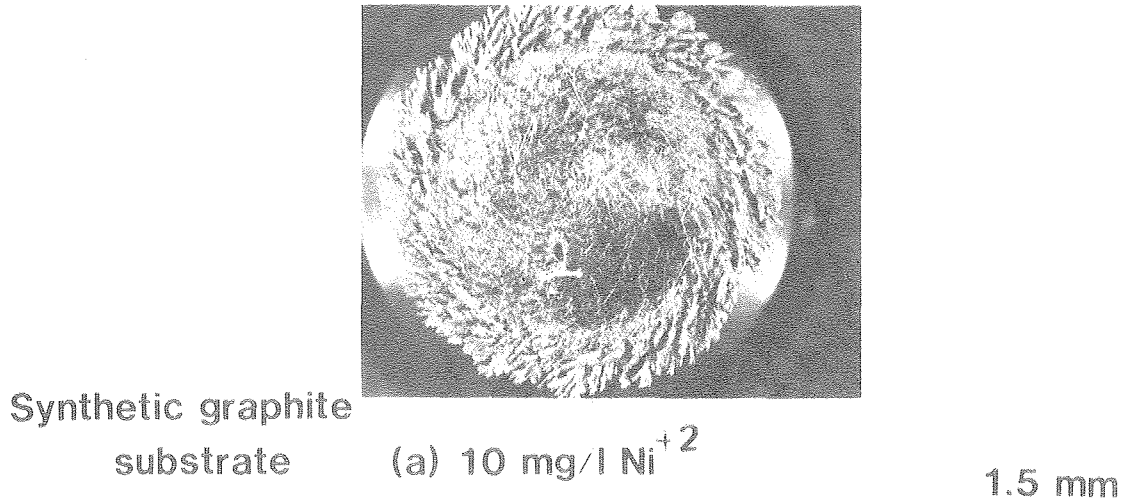
(d) $3\text{M ZnCl}_2 + 3\text{M KCl}$, $\text{pH}=0.6$, $28.6\ \text{mA}/\text{cm}^2$, $\text{Re}=1000$,

$500\ \text{coulombs}/\text{cm}^2$

XBB 865-3596

Figure 5.9

Effect of Nickel contamination on the appearance of the deposit



(b) 40 mg/l Ni⁺²

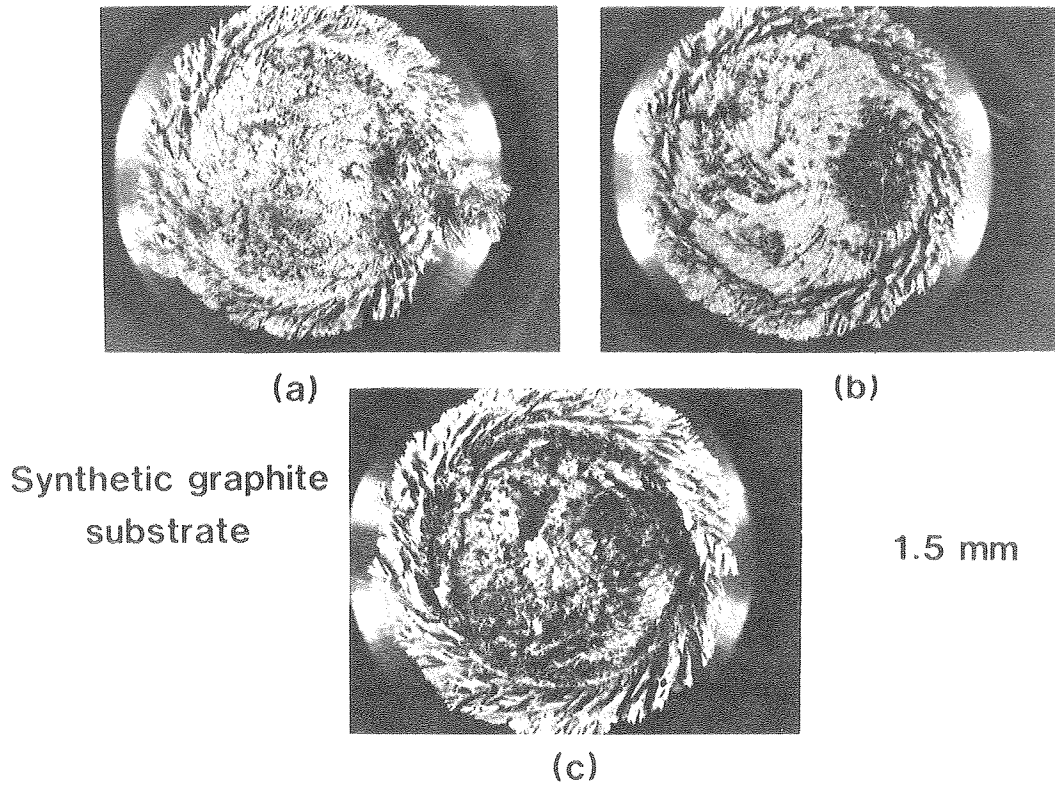
3M ZnCl₂ 3M KCl pH=0.6 1600 rpm

28.6 mA/cm² 500 coulombs/cm² deposited

XBB 865-3594

Figure 5.10

Effect of Iron contamination on the appearance of the deposit



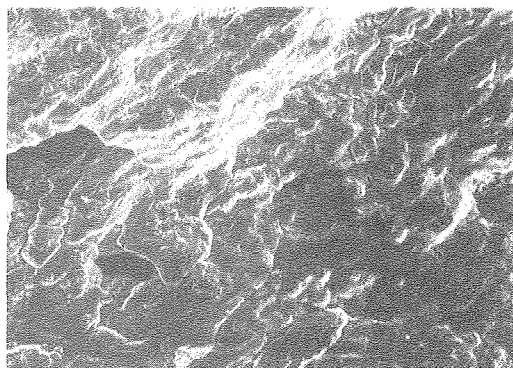
$3\text{M ZnCl}_2 + 3\text{M KCl}$ pH=0.6 28.6 mA/cm^2 1600 rpm
500 coulombs/cm² deposited

- (a) 20 mg/l Fe⁺³
- (b) 30 mg/l Fe⁺³
- (c) 40 mg/l Fe⁺³

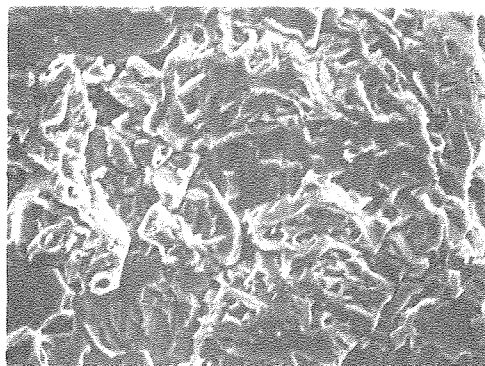
XBB 865-3595

Figure 5.11

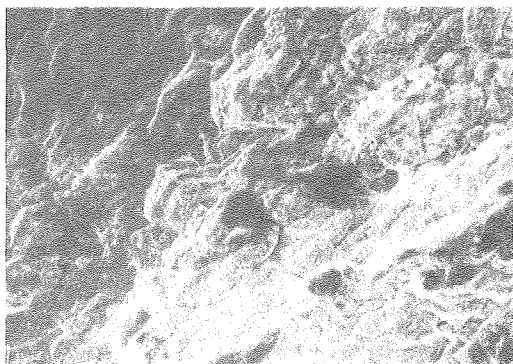
Effect of Iron contamination on the structure of the deposit



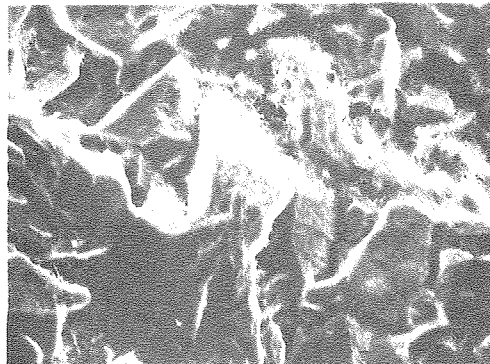
(a) 0 mg/l Fe^{+3}



(c) 20 mg/l Fe^{+3}



(b) 10 mg/l Fe^{+3}



(d) 30 mg/l Fe^{+3}

synthetic graphite substrate

3M $ZnCl_2$ + 3M KCl pH=0.6 1600 rpm

28.6 mA/cm² 500 coulombs/cm² deposited

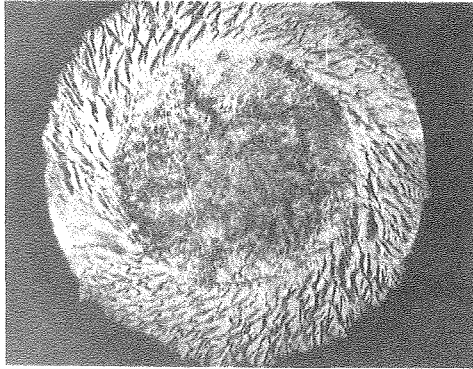
(a) (b) --- 18.1 μm

(c) (d) --- 6.2 μm

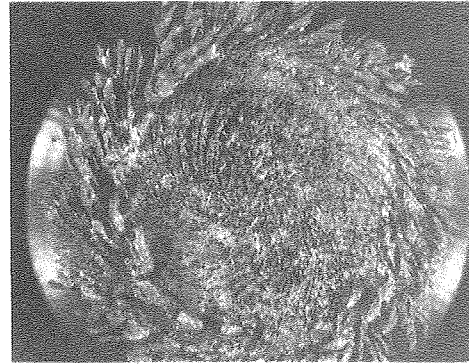
XBB 865-3630

Figure 5.12

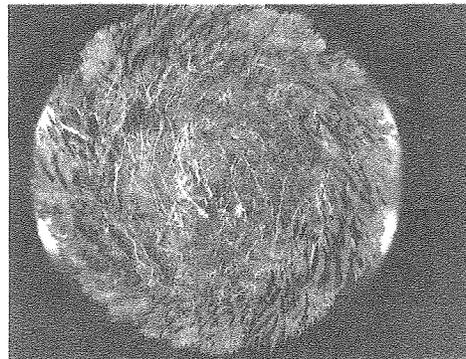
Effect of Cadmium contamination on the appearance of the deposit



(a) 10 mg/l Cd^{+2}



(b) 30 mg/l Cd^{+2}



(c) 40 mg/l Cd^{+2}

1.5 mm

Synthetic graphite substrate

3M ZnCl_2 + 3M KCl pH=0.6

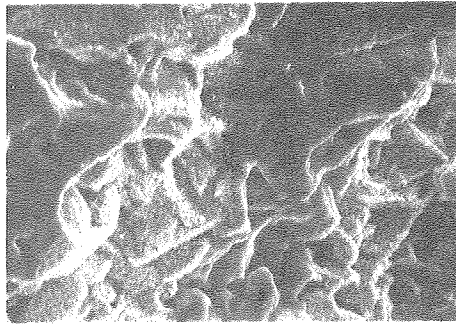
28.6 mA/cm^2 1600 rpm

500 coulombs/ cm^2 deposited

XBB 865-3604

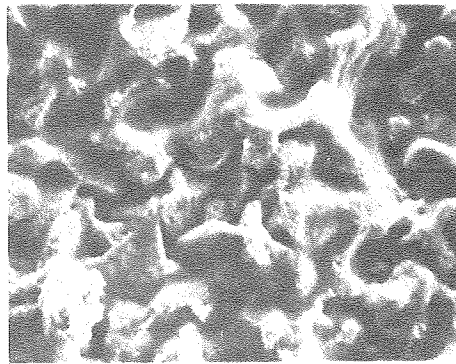
Figure 5.13

Effect of Cadmium contamination on the structure of the deposit



(a) 10 mg/l Cd⁺²

8.47 μm



(b) 40 mg/l Cd⁺²

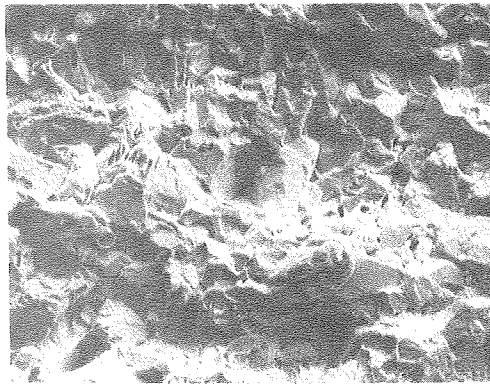
Synthetic graphite substrate

**3M ZnCl₂ 3M KCl pH=0.6 1600 rpm,
28.6 mA/cm² 500 coulombs/cm² deposited**

XBB 865-3605

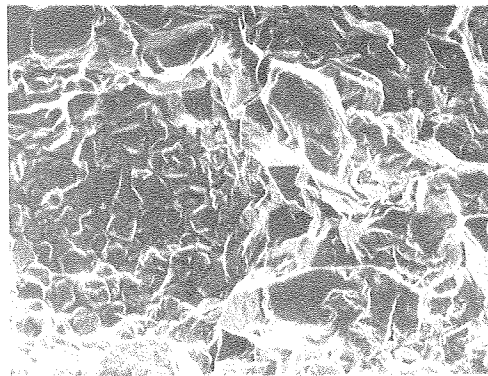
Figure 5.14

Effect of substrate on the structure of the deposit



synthetic graphite
surface

(a)



platinum surface

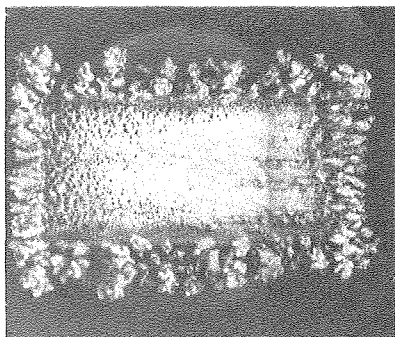
(b)

$3\text{M ZnCl}_2 + 3\text{M KCl}$ $\text{pH}=0.6$
 28.6 mA/cm^2 $\text{Re} = 1000$
 $500 \text{ coulombs/cm}^2$ deposited
— = $17 \mu\text{m}$

XBB 865-3606

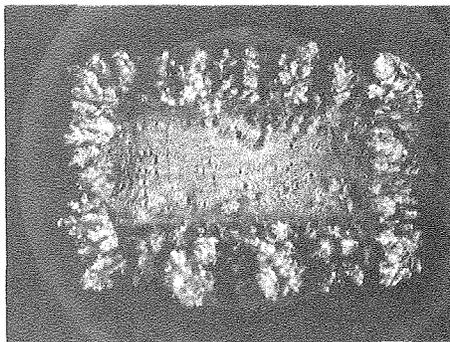
Figure 5.15

Effect of substrate on the appearance of the deposit



synthetic graphite
surface

(a)



platinum
surface

(b)

$3M ZnCl_2 + 3M KCl$ pH=0.6 Re = 1000

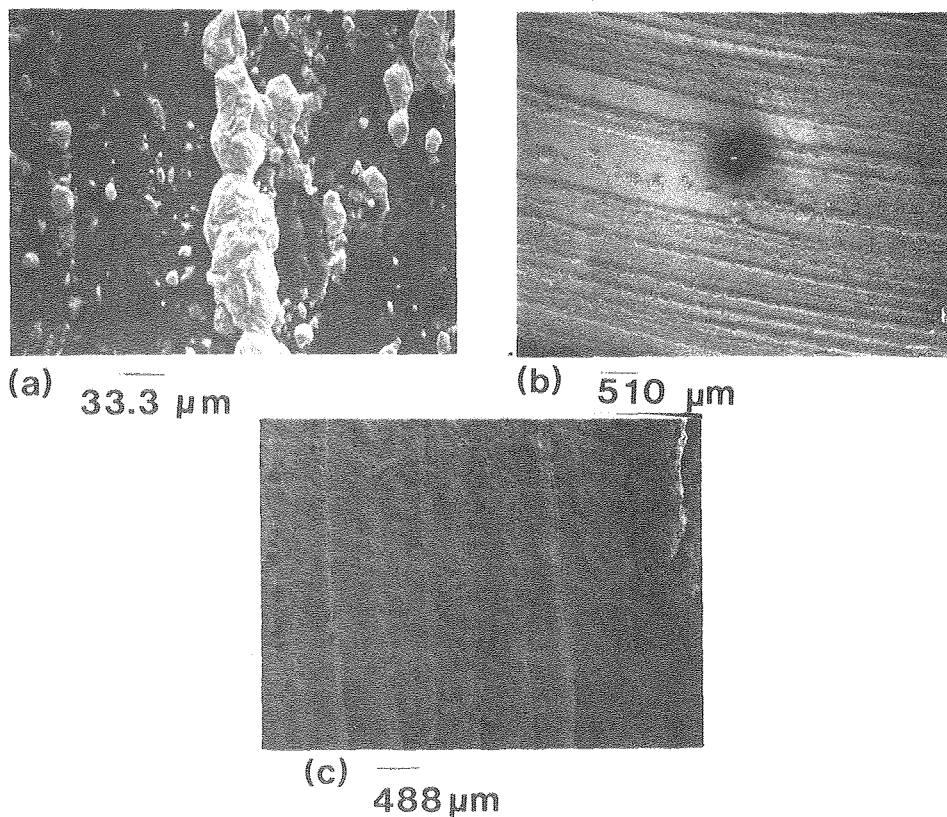
23.9 mA/cm² 500 coulombs/cm² deposited

electrode dimensions 1 cm X 0.5 cm

XBB 865-3607

Figure 5.16

Appearance of striations with increasing time



1M ZnCl₂ + 3M KCl

(a) 6 coulombs/cm² passed, 10 mA/cm² Re=3115 pH=1

(b) Platinum substrate 30 mA/cm² Re=9000
108 coulombs/cm² passed pH=5.2

(c) 500 coulombs/cm² passed 25.5 mA/cm² Re=1022
Ph=1

XBB 865-3587

Figure 5.17

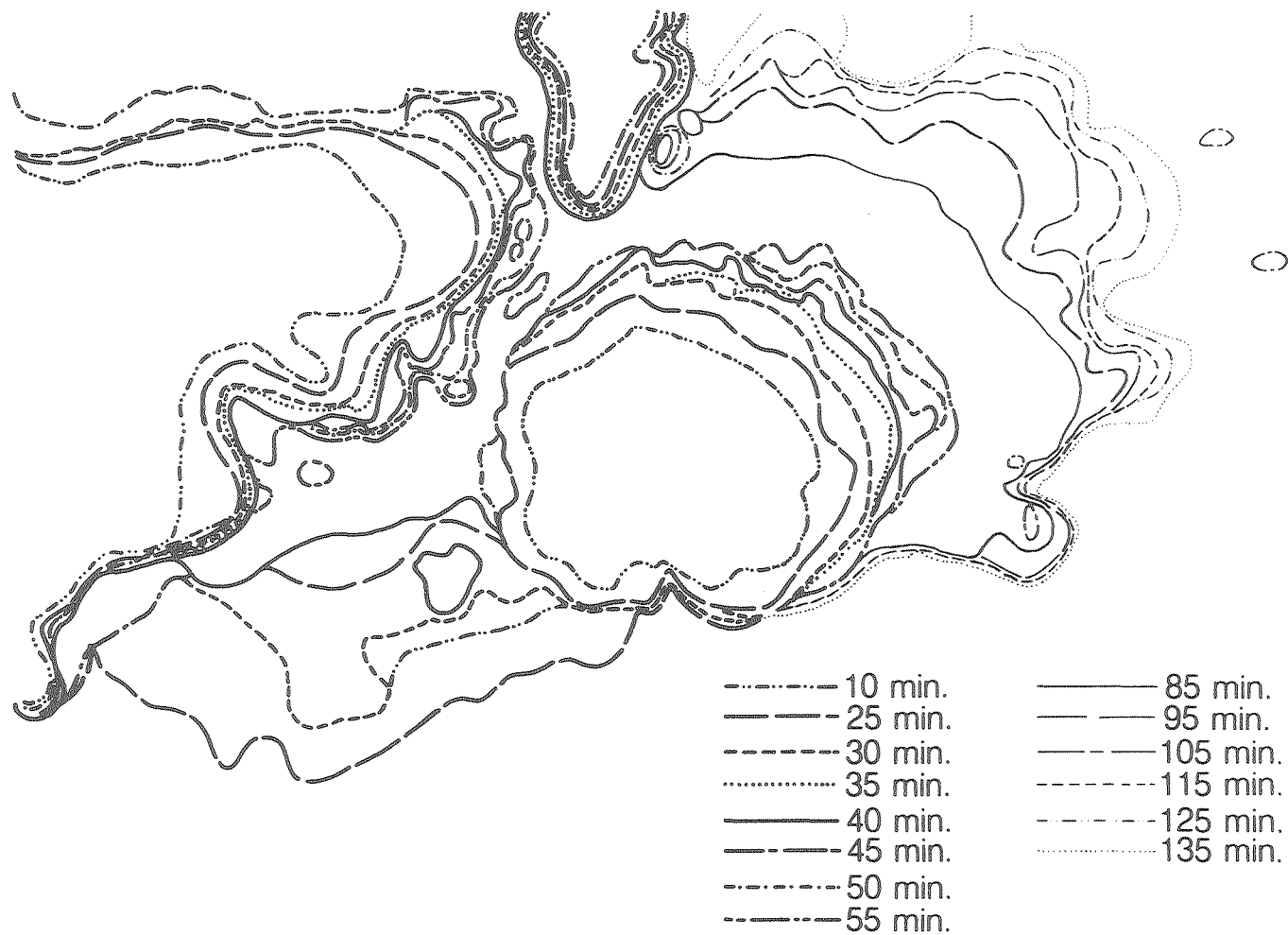


Figure 5.18- Progression of a striation downstream
(flow direction is from left to right)

XBL 863-11097

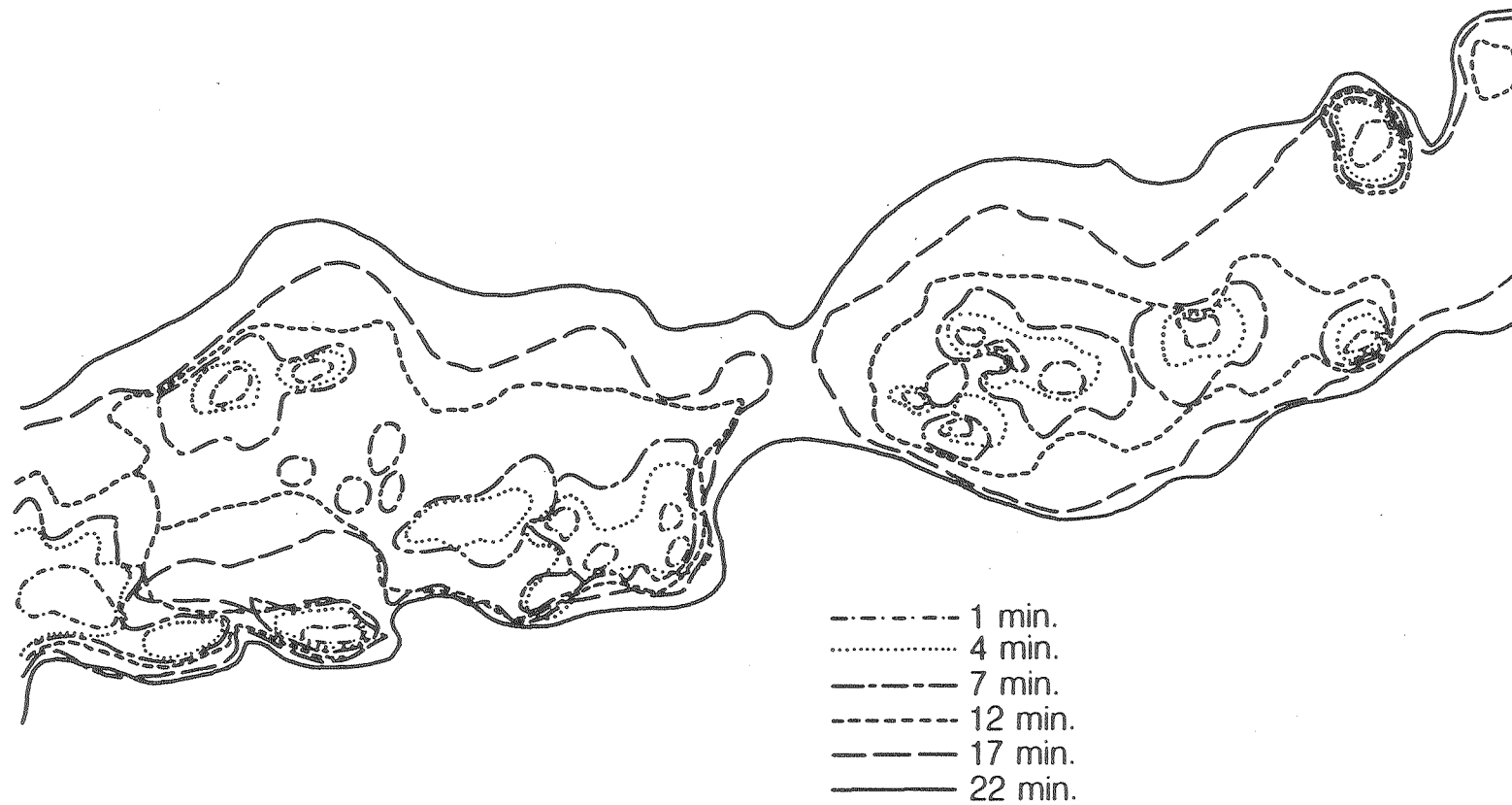
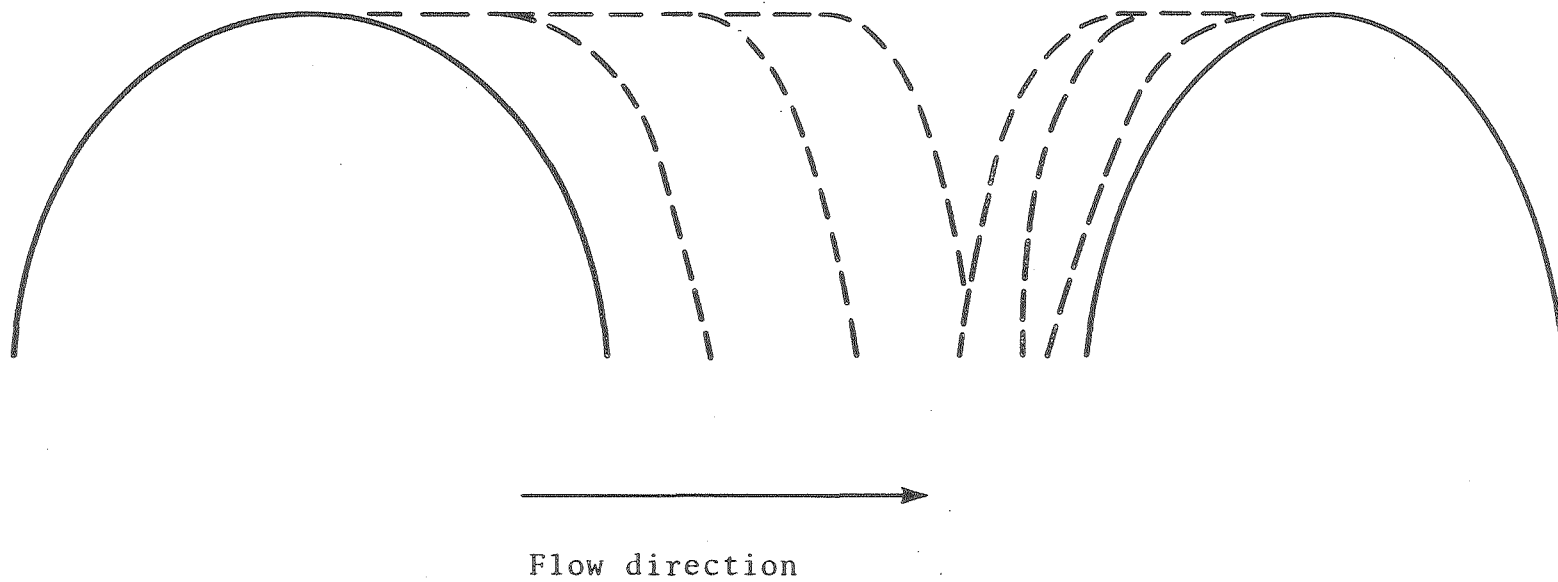


Figure 5.19- Propagation of a striation
(flow direction is from left to right)

XBL 863-11098



XBL 863-11102

Figure 5.20- Mechanism of striation propagation

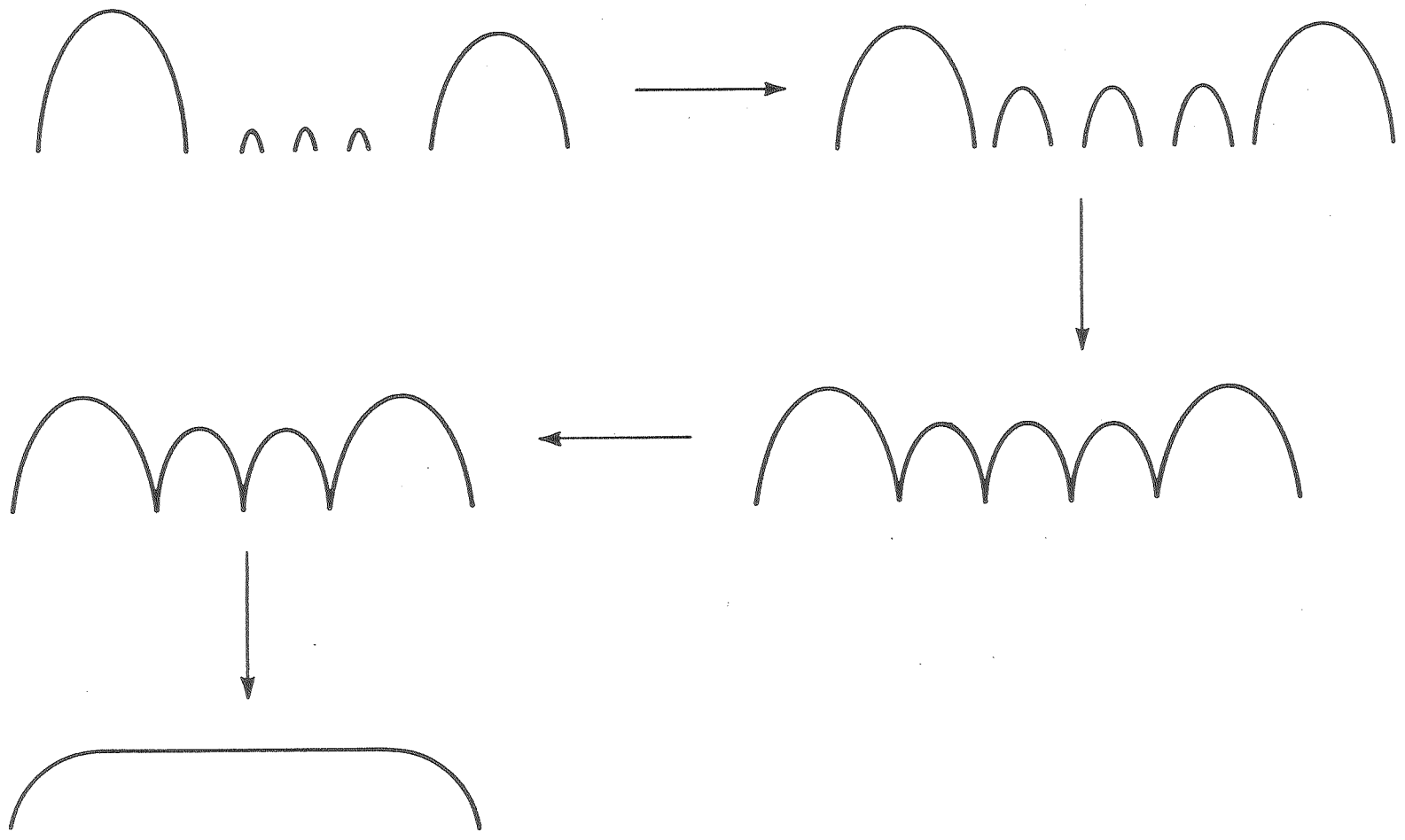
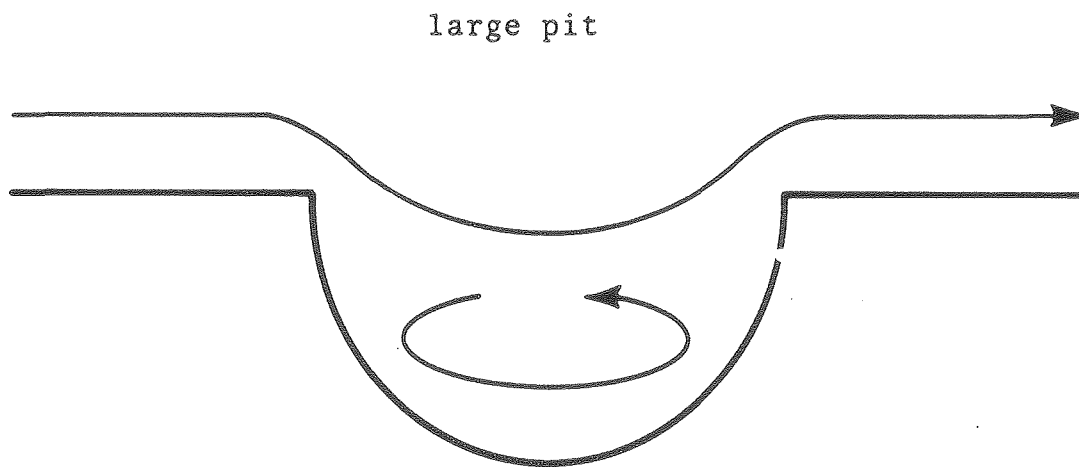
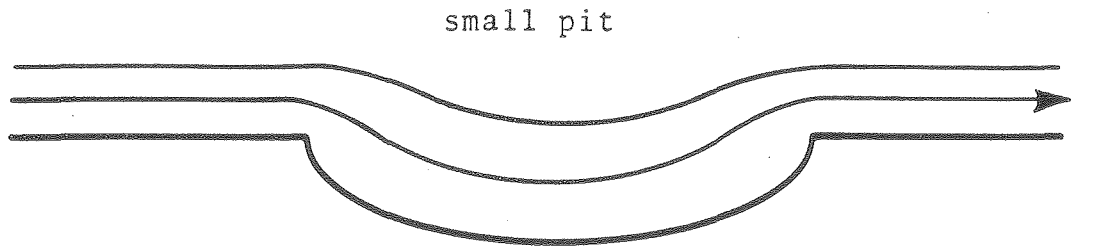


Figure 5.21- Method of striation propagation proposed by Faltmier and Tsuda (13, 23) (flow is from left to right)



XBL863-11100

Figure 5.23- Recirculating flow patterns visualized by Alkire(59) (flow is in the direction of the arrows)

Growth of protrusions over time

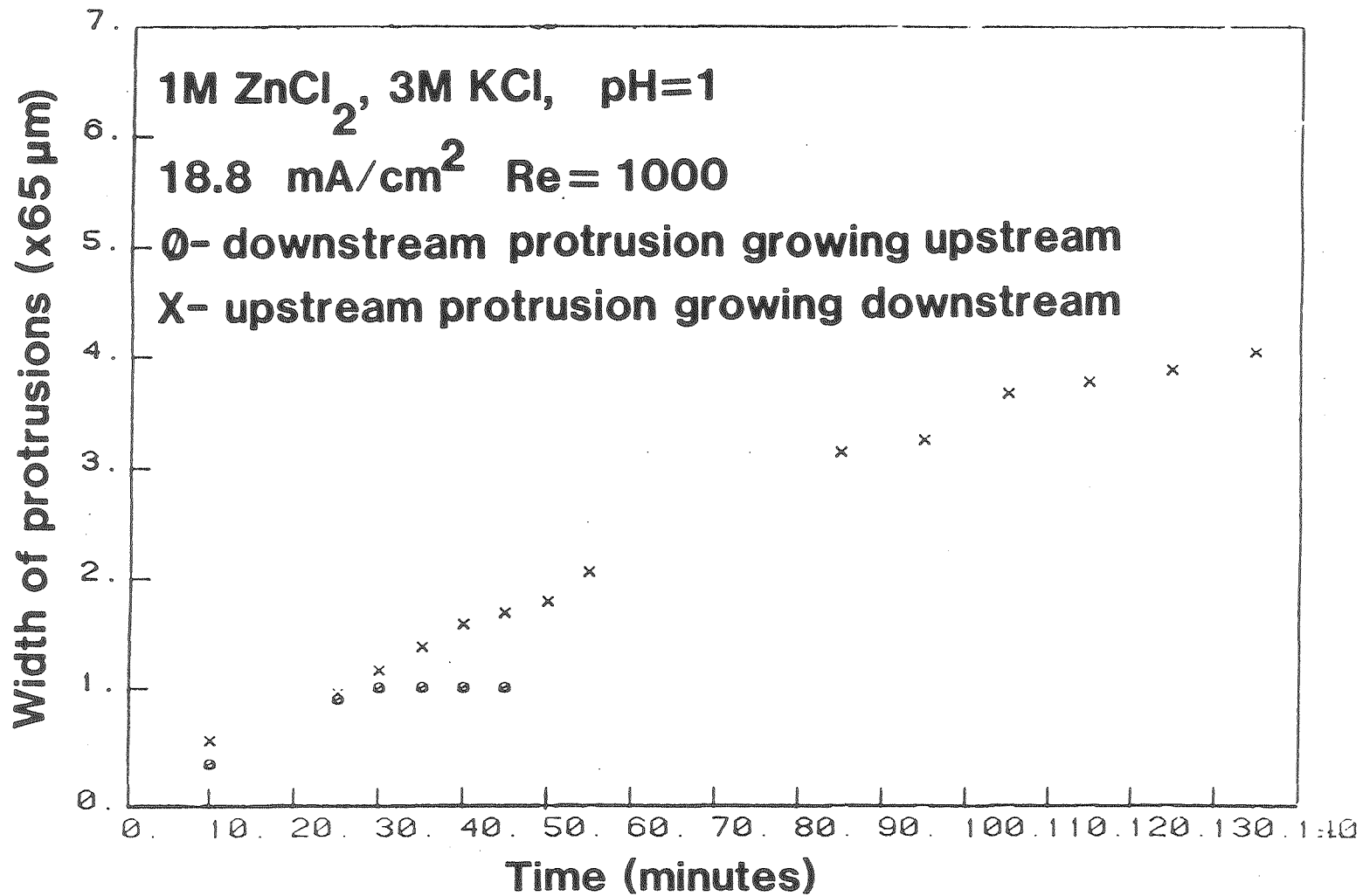


Figure 5.23

XBL 865-1911

Growth of protrusions over time

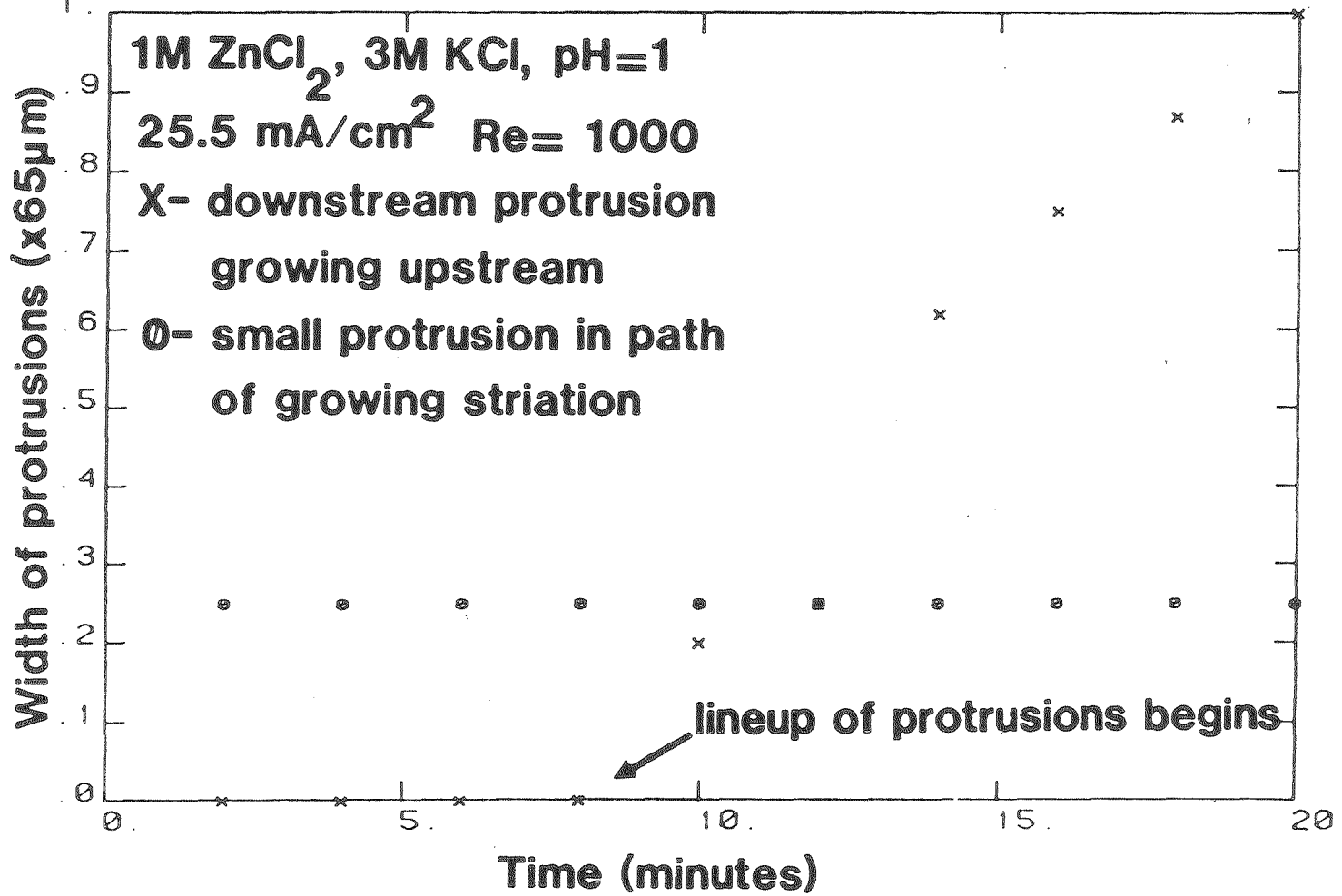


Figure 5.24

Effect of current on the current efficiency

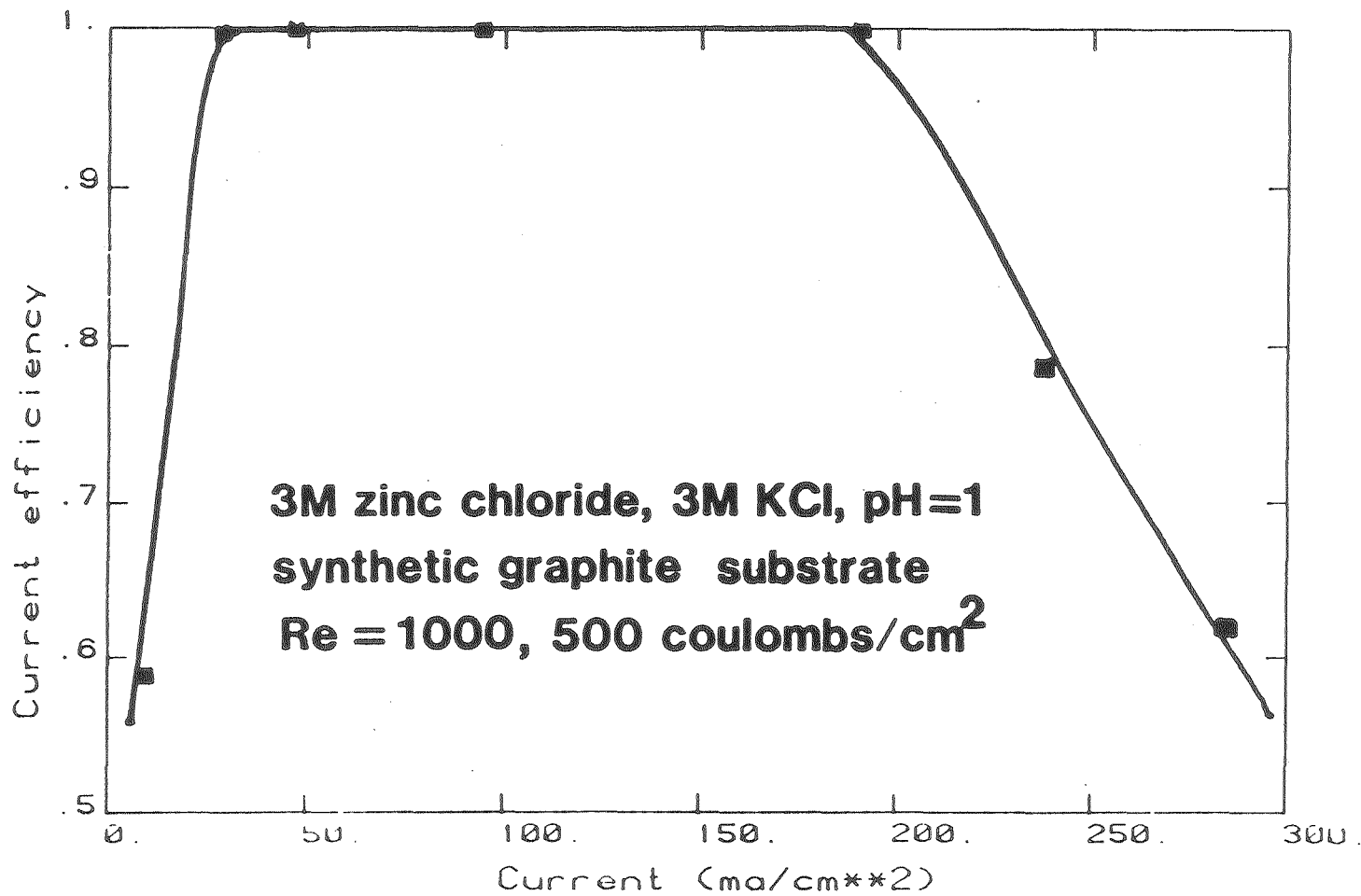


Figure 5.25

XBL 865-1847

Effect of the number of coulombs passed on current efficiency

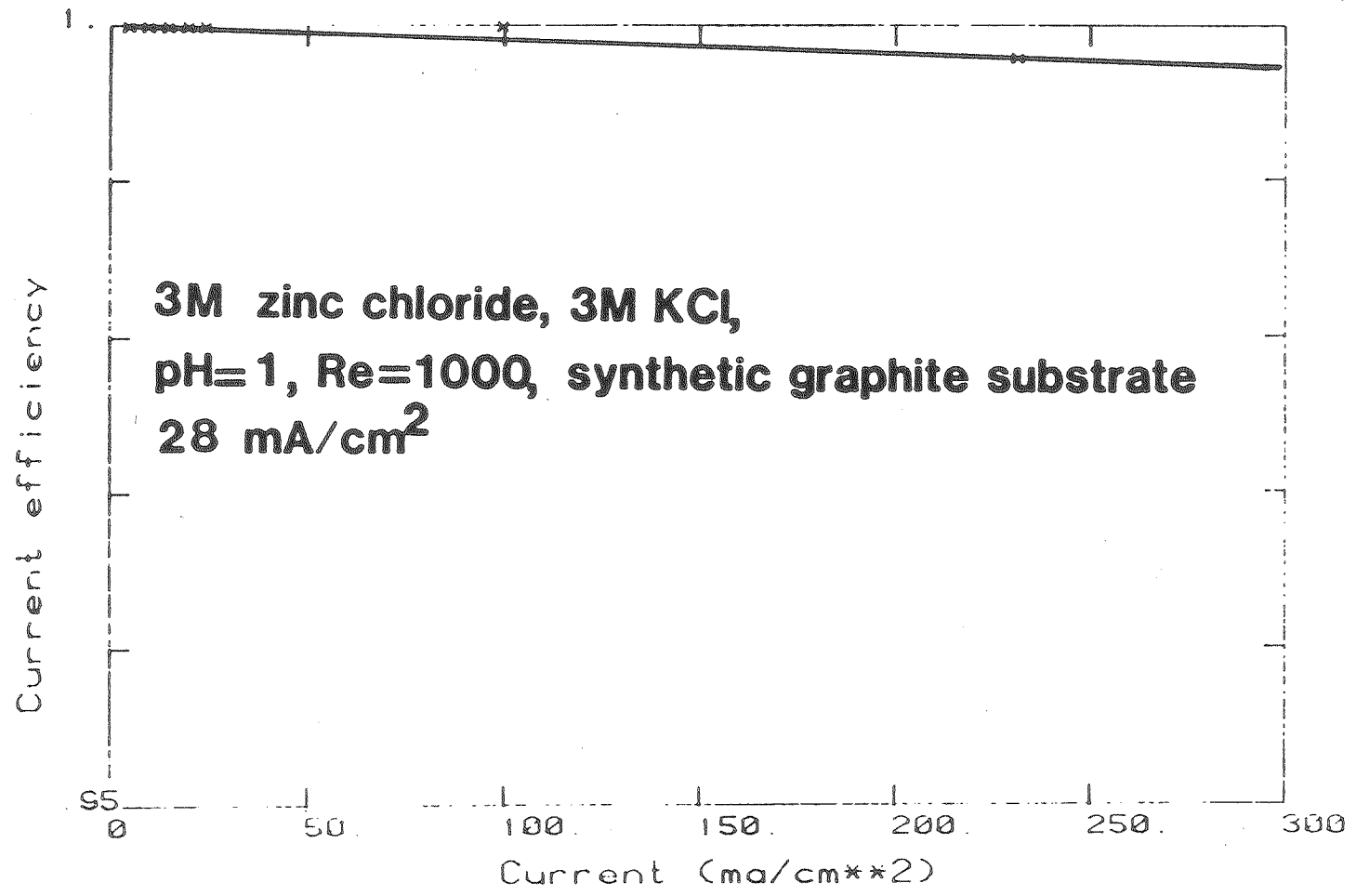


Figure 5.26

XBL 865-1846

Effect of current on the current efficiency

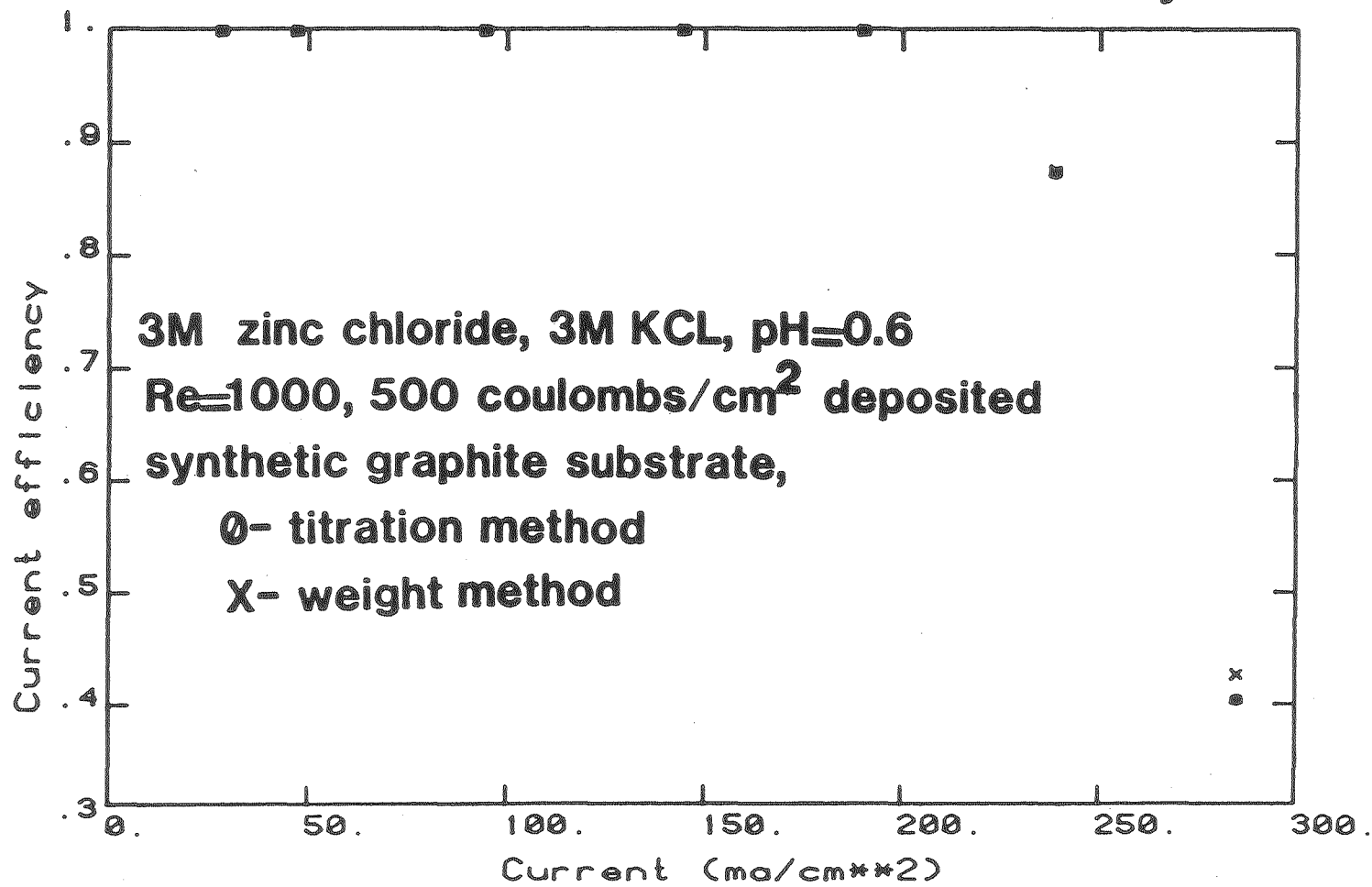


Figure 5.27

XBL 865-1845

Effect of $ZnCl_2$ concentration on Current Efficiency

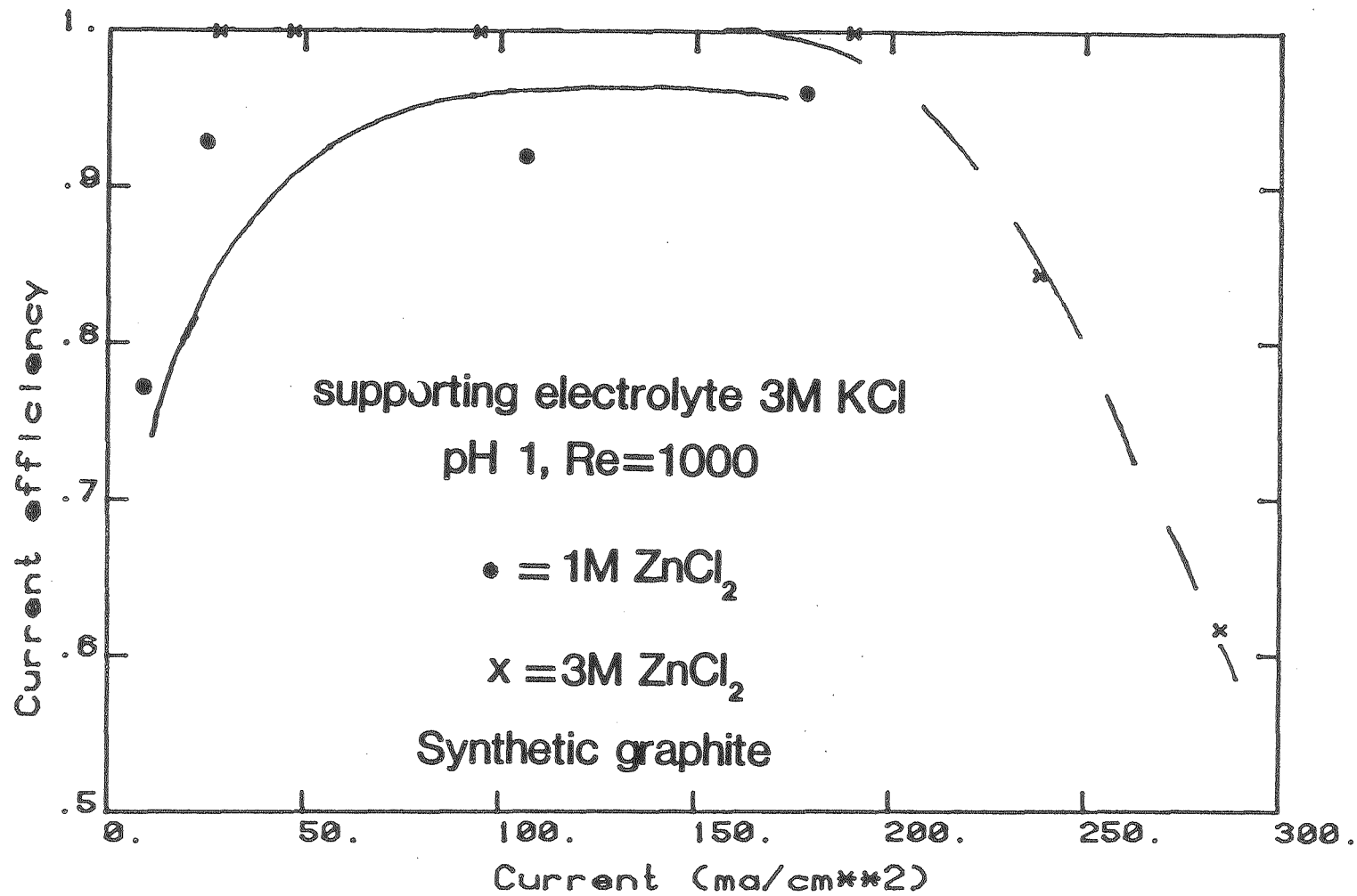


Figure 5.28

XBL 865-1826

Effect of $ZnCl_2$ concentration on Current Efficiency

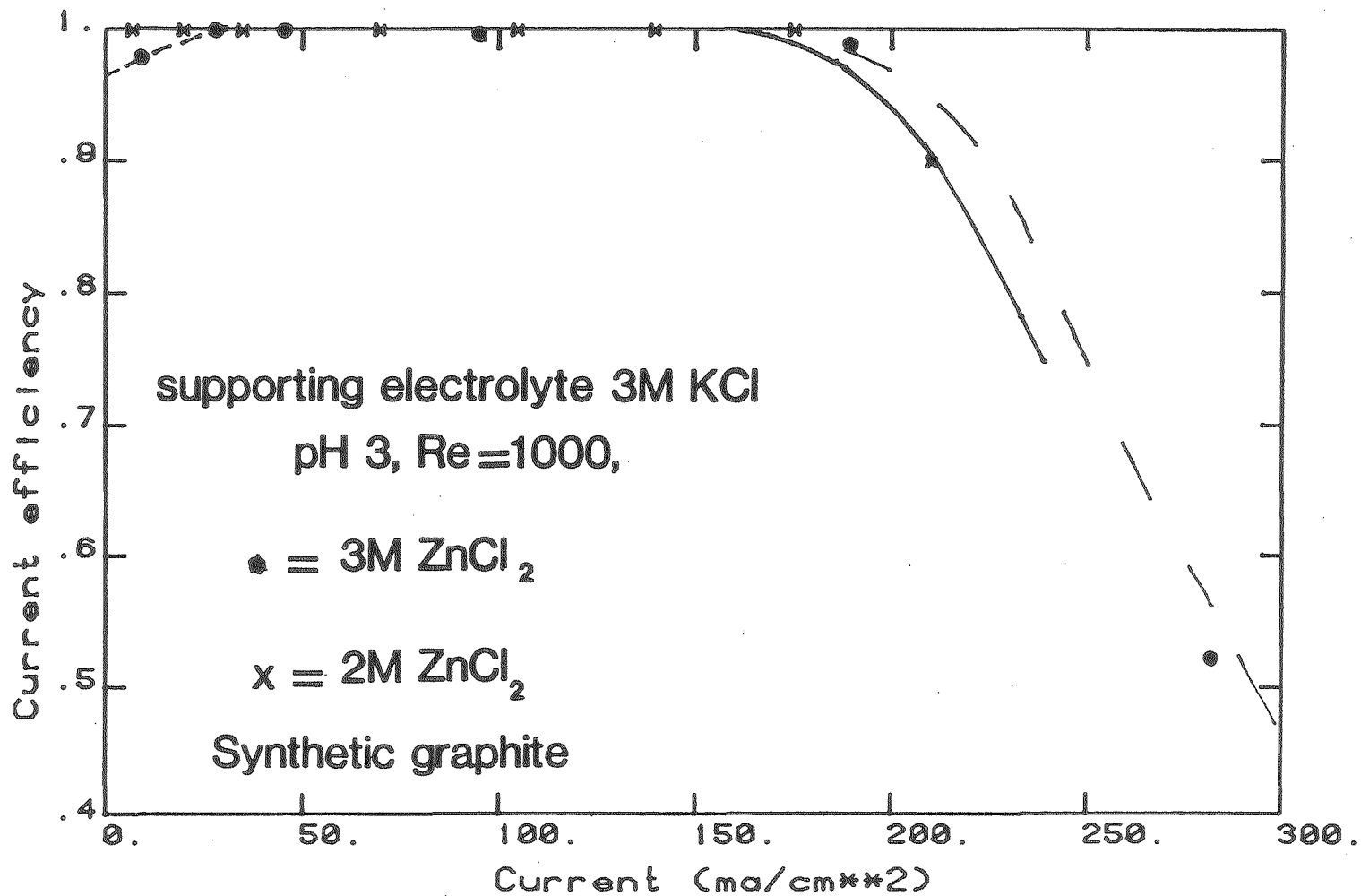


Figure 5.29

XBL 865-1827

Effect of pH on Current Efficiency

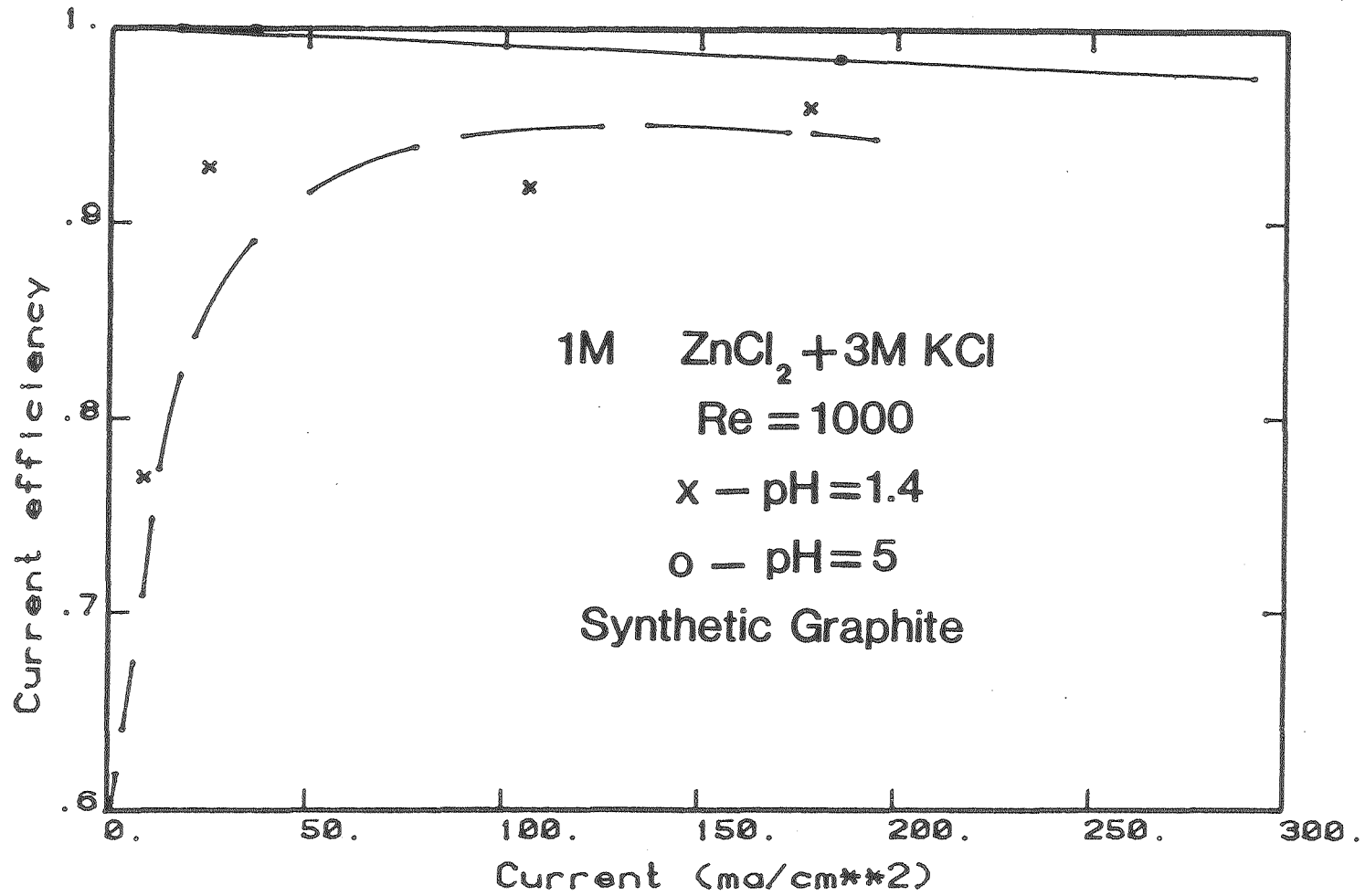


Figure 5.30

XBL 865-1909

Effect of pH on Current Efficiency

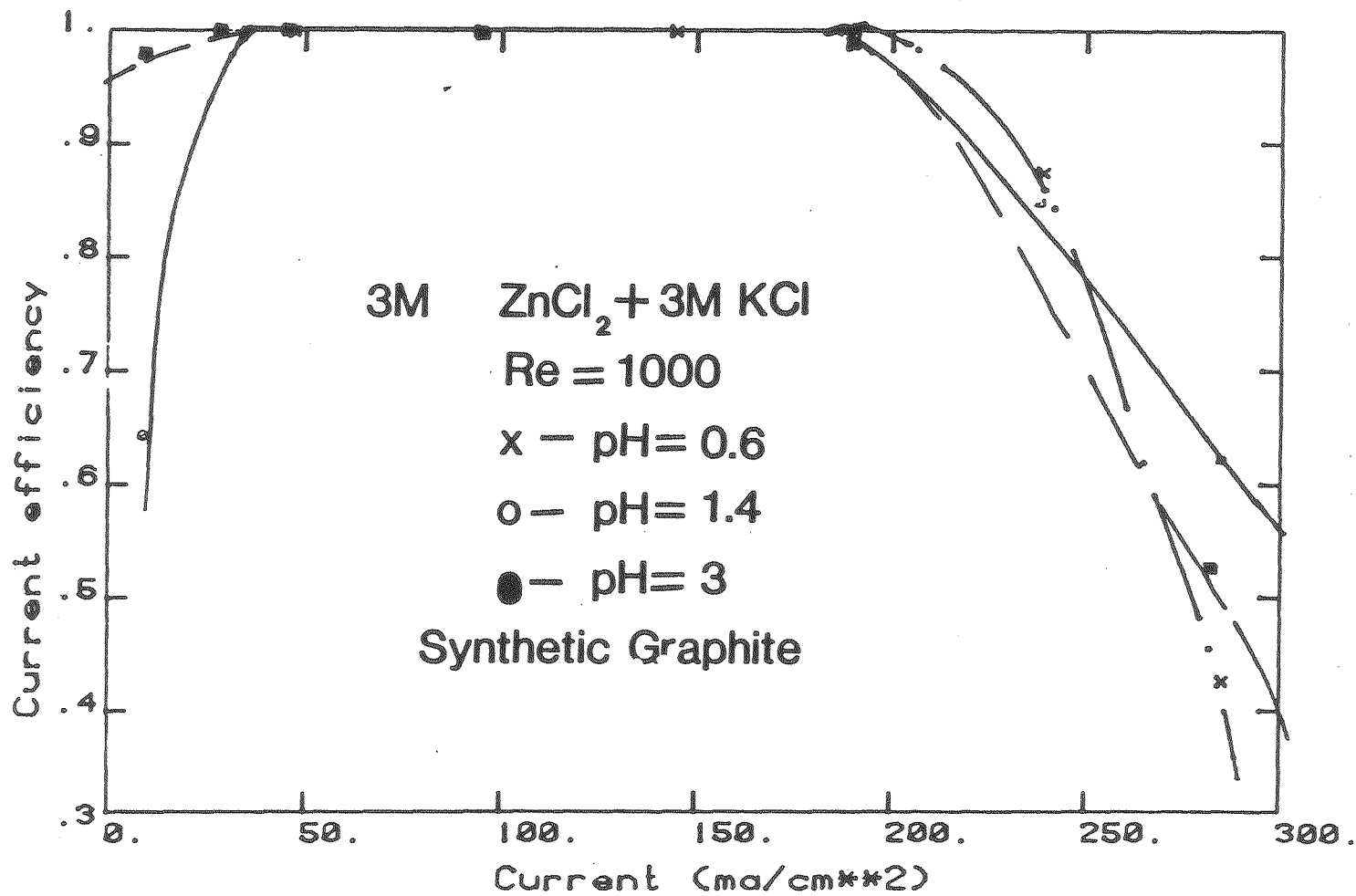


Figure 5.31

XBL 865-1912

Effect of Reynolds number on Current Efficiency

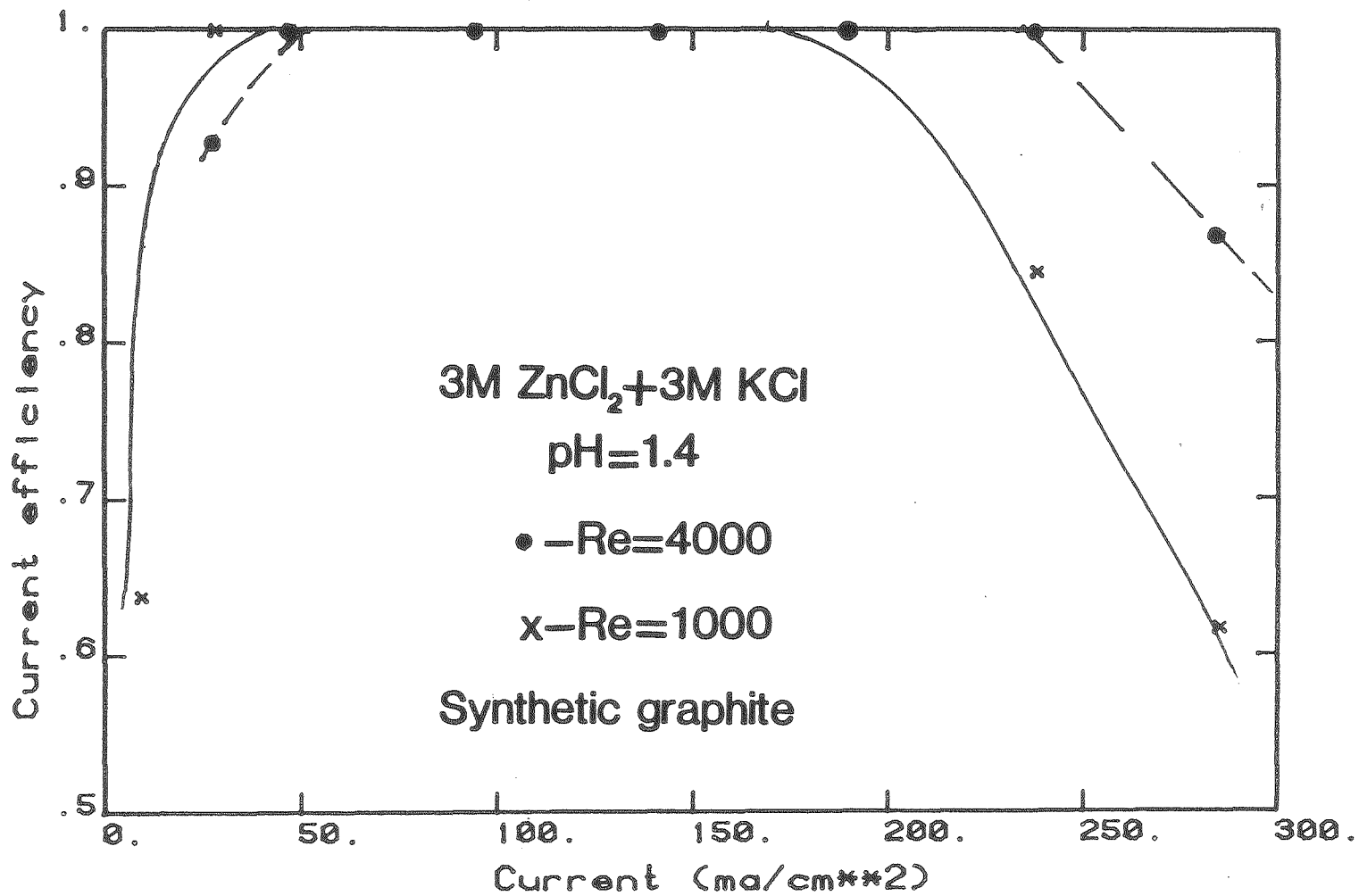


Figure 5.32

XBL 865-1828

Effect of Substrate on Current Efficiency

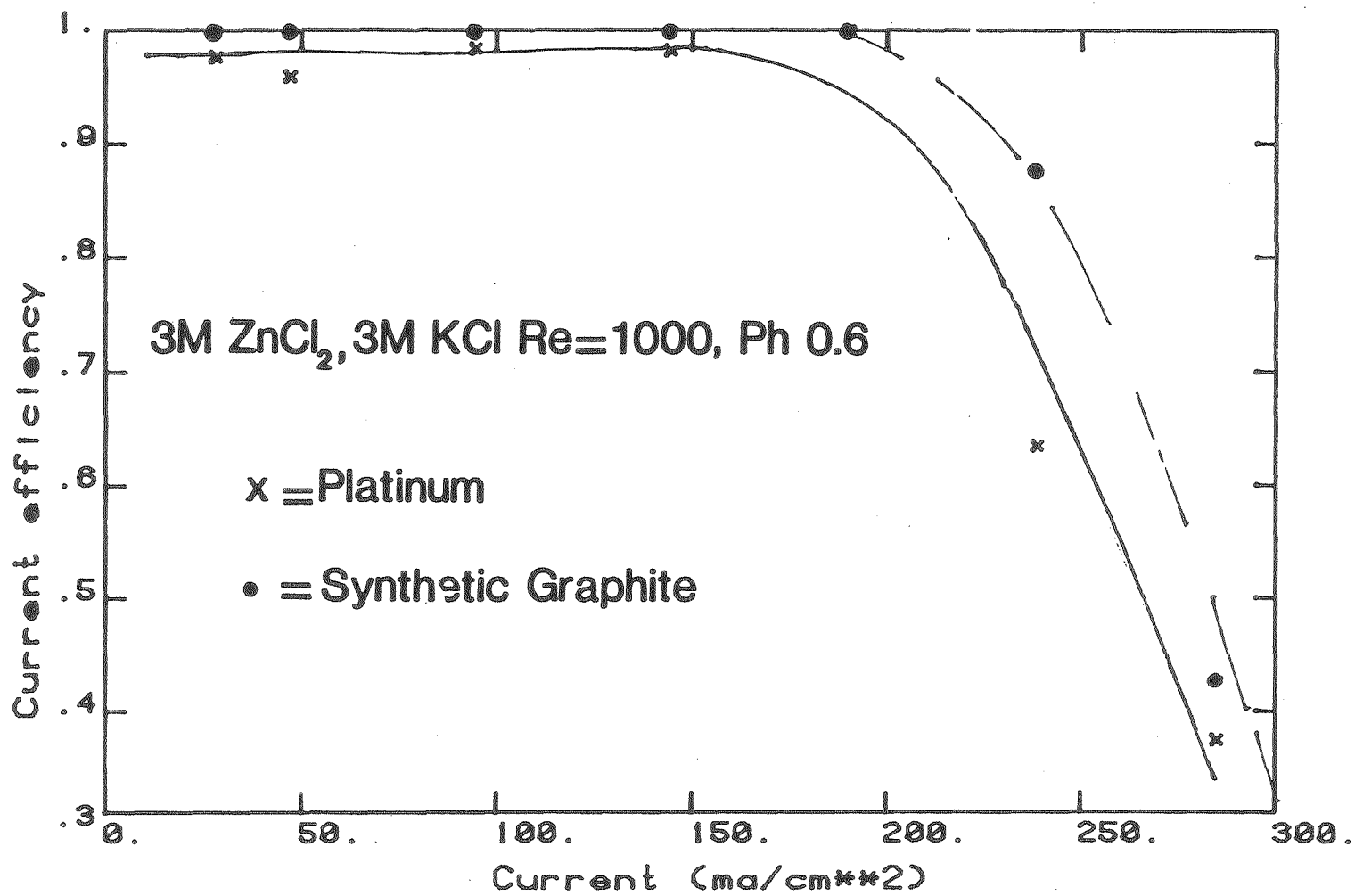


Figure 5.33

XBL 865-1829

Effect of impurities on the current efficiency

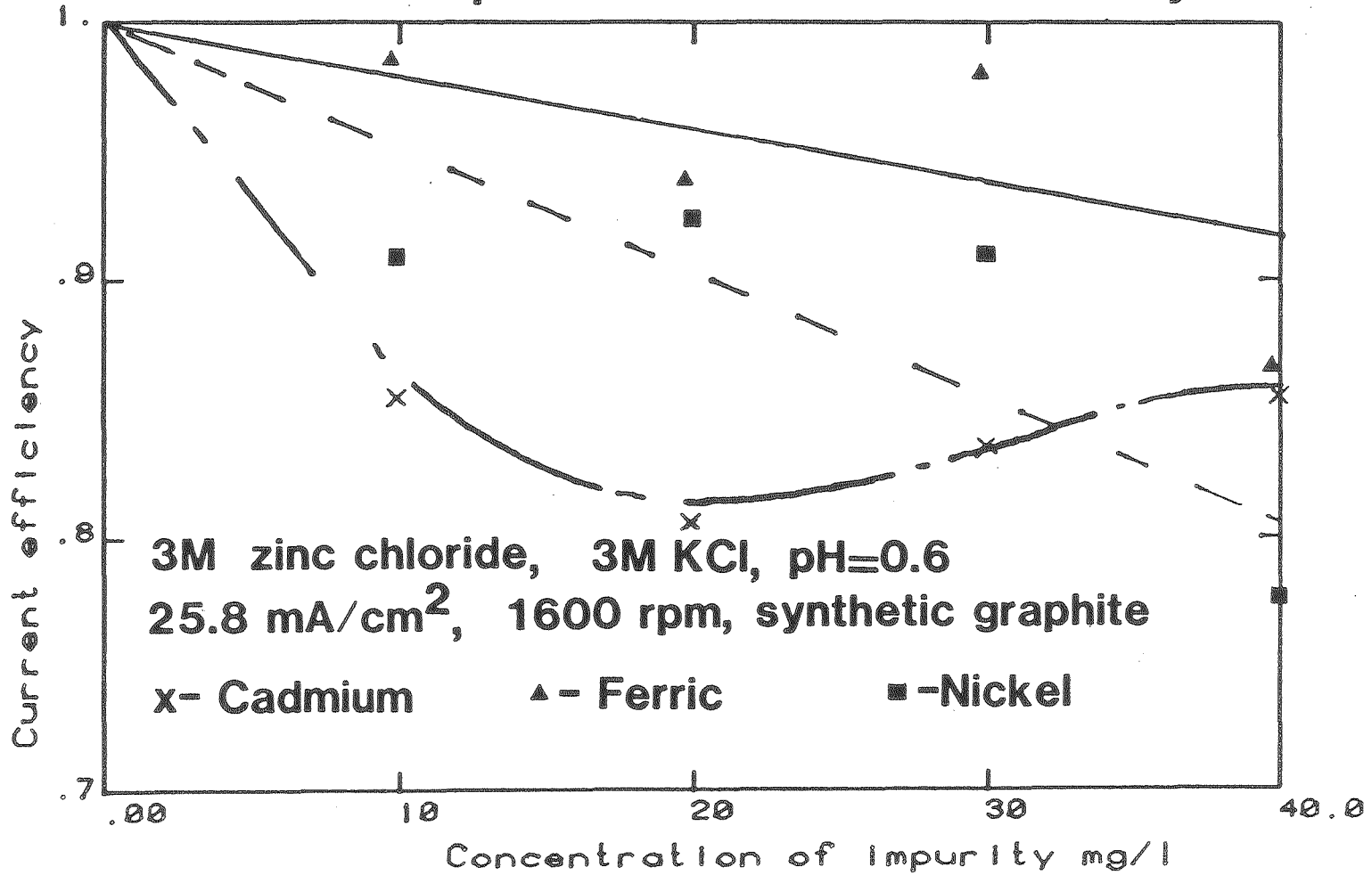


Figure 5.34

XBL 865-1910

VI. SUMMARY AND CONCLUSIONS

The preceding investigation examined the current efficiency, and the morphology of zinc electrodeposited from chloride solutions, with or without added potassium chloride.

Six experimental variables were investigated to alter the conditions of deposition. Two variables, the zinc concentration and the flow rate, were altered to influence the limiting current density. The current density was changed to produce different fractions of the limiting current density. The pH was lowered from 3-0.6 to examine the effect of hydrogen ion concentration on the morphology and the current efficiency. Two substrates were employed, synthetic graphite and platinum, to examine the effect of the surface activity on the progress of zinc deposition. Three metallic impurity ions, nickel, cadmium and ferric, were added to study the effects of impurities on the morphology and current efficiency.

A) The portion of the total current devoted to zinc deposition was determined by studying the current efficiency for zinc deposition, through both EDTA complexometric titration and weight measurements. The results may be summarized as follows:

- (1) The current efficiency is in the range of 98- 100% for current densities between 25 and 140 mA/cm².
- (2) A current efficiency vs time curve will be parabola-shaped because of hydrogen evolution at high current densities, and both chemical attack of the deposit and preferential hydrogen evolution on the substrate, at low current densities.

- (3) The current efficiency decreases rapidly at high current densities due to hydrogen evolution. The decrease in current efficiency may be used to determine the effective limiting current for concentrated zinc chloride solutions.
- (4) For laminar flow, current density at which the current efficiency begins to decrease is proportional to the 0.3 power of the flow rate.
- (5) The activity of the substrate toward zinc deposition, which determines the number of sites available for zinc deposition, affects the current efficiency.
- (6) The current efficiency decreases with increasing hydrogen ion concentration.
- (7) The current efficiency increases with increasing zinc concentration in the range of 65 to 195 g/l.
- (8) The current efficiency decreases with increasing concentrations of iron and even more so with nickel impurities.
- (9) The current efficiency decreases with increasing concentrations of cadmium impurities up to 20 mg/l. At higher cadmium concentrations the current efficiency improves, probably because of higher overpotential of cadmium containing deposits toward hydrogen evolution.

B) Using videomicroscopy, macrophotography and scanning electron microscopy, the morphology of electrodeposited zinc was investigated. Videomicroscopy was used to record the progress of deposition in-situ. Some experiments involved simultaneous observation of several areas on the electrode; these observations were accomplished by using a traveling stage with the videomicroscopy system. The visual magnification used in the in-situ microscopy ranged from 56x to 400x. Some surfaces were examined after deposition was completed using scanning electron microscopy and macrophotography. The following conclusions can be made.

- (1) At first, zinc covers the surface; this initial deposition may involve alloying with the substrate.
- (2) Small nuclei grow and coalesce to form larger, randomly placed nuclei; it is unclear whether this coalescence is affected by hydrodynamic flow.
- (3) Upon further growth larger nuclei line up parallel to the direction of flow; this orienting starts upstream and progresses downstream. This orientation occurs due to enhanced growth in the areas of large downstream protrusions that lie in the wake of large upstream protrusions.
- (4) The protrusions join by a mechanism involving growth parallel to the direction of flow of the highest current density regions. The growth of areas of the protrusions parallel to flow is under mass transport control.
- (5) After the striation is fully formed, growth occurs over the entire electrode. This results in ridges after long times.

- (6) The most important variable in determining whether striations will form is the interfacial concentration of the reactant. This variable determines the number density of nuclei.
- (7) A variable of secondary importance is the flow rate. Striations will form at any flow rate and interfacial concentration in which the protrusion growth rate is such that a critical height is reached at which flow effects can occur before the protrusion joins with other large protrusions both parallel and perpendicular to the direction of flow.
- (8) Hydrogen bubble evolution has no role in the formation of striations, although bubble evolution can prevent striations from joining and may change the shape of striations.
- (9) Raising the current density causes the deposit to become more nodular and porous.
- (10) At a constant current density, increasing the flow rate causes a more rapid development of grooved patterns.
- (11) Raising the zinc concentration has little effect on the deposit appearance in the range of 2-3M; the lack of change in the deposit appearance may be due to complexing effects.
- (12) In spite of declining current efficiency, lowering the pH from 3-0.6 had no effect on the deposit appearance.
- (13) Nickel promotes the formation of tree-like dendritic growths in the deposit.
- (14) Iron both facilitates the formation of dendrites and destroys the crystalline appearance of the surface.

- (15) Cadmium promotes roughness at low concentrations and refines the surface structure at high concentrations.
- (16) Upon continued deposition, the substrate has little effect on the appearance of the deposit, although the substrate's activity toward zinc deposition determines the initial number density of nuclei, which determines whether striae will form.

APPENDIX 1

Description of the Video Microscopy System

A major part of this project involved photography through the microscope using a video camera. A photograph of the system is shown in Fig. A.1 and a schematic of the apparatus is shown in Fig. A.2. Every microscope has an eyepoint, which, by definition, is the point in space where the eye looks through the microscope. At this point, the product of magnification of the objective and the eyepiece is the total magnification. The magnification increases as one moves away from this point, and vignetting increases (69). So, for best results, one should put the video camera as close as possible to the eyepoint, in effect making the camera an electric eye. The recommended camera configuration is shown in Fig. A.3.

The role of the camera is far different from that in conventional photography. The camera's only role in photomicrography is as a holder for the film, or in the application in this study, as a sensor for the videotape machine. In fact, satisfactory images have been made without additional lenses (69). The camera is only a holder for the sensing medium, in order to allow as much light as possible to strike the sensing medium, the optimum aperture opening for the camera lens should be wide open, or the lowest f-number. The aperture of the camera does not affect the depth of field of the microscope image, and closing the aperture only vignettes the image.

Studies have shown that the microscopist's eyes focus at infinity when looking at a focused microscope image (69). Therefore, the camera

should be focused at infinity when used in photomicrography. This ensures that the image is in focus at the sensing plane. All focusing is done through the microscope, using the coarse and then the fine focusing knobs. In this application, focusing was done using the microscope, and the resulting image was observed on the video monitor.

Photomicroscopy requires both sufficient illumination of the surface and proper exposure. Many applications of photomicroscopy have the drawback that there is not enough light, and so the photographs are of poor quality, since the lighting cannot reveal all of the details of the surface. In this study, a fiber-optic light source was used to provide maximum illumination. This light source was adjusted to give the best quality picture.

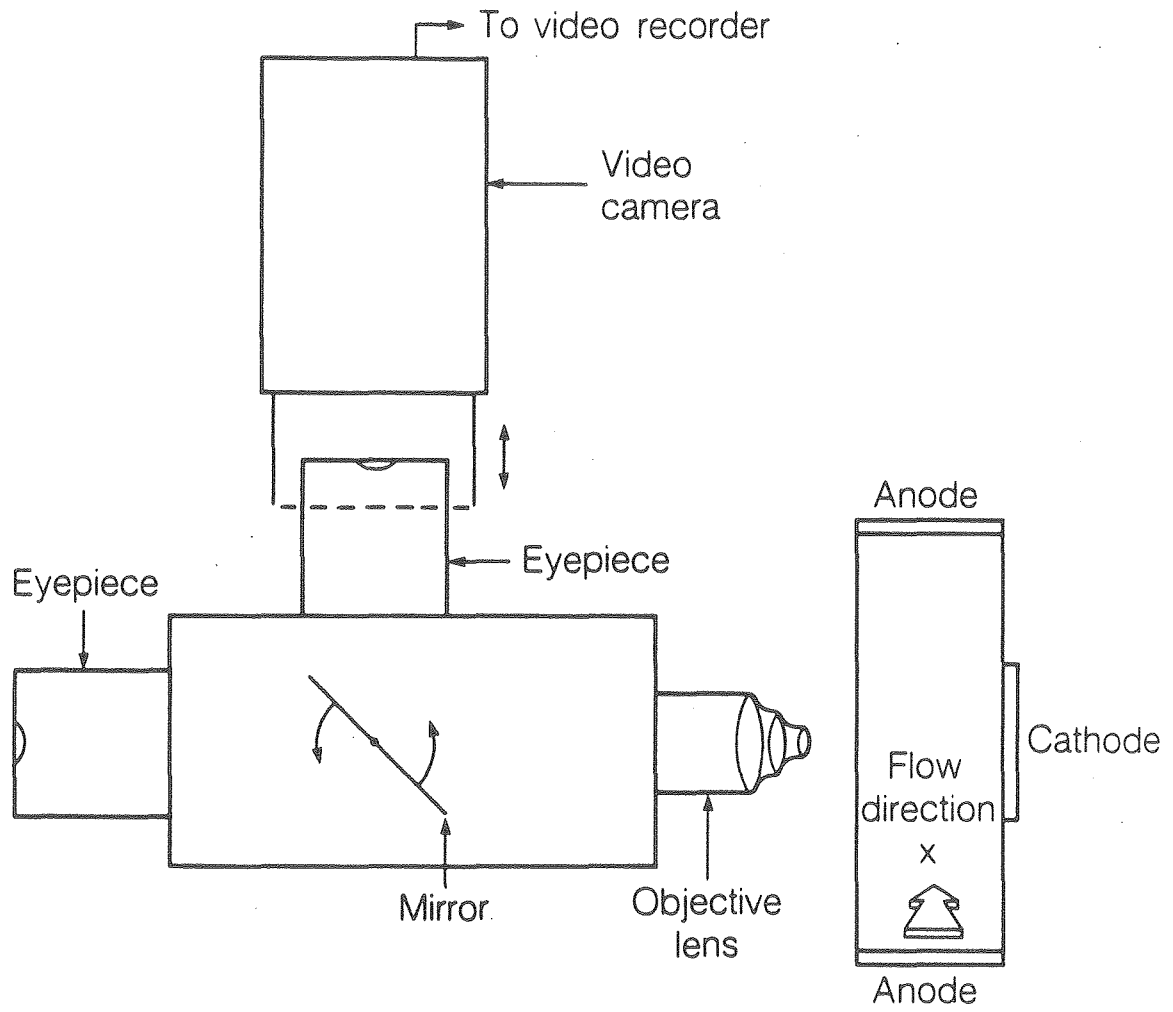
Because the electrode could only be approached to within 10 mm, this study required retrofocusing lenses. The lens used in this application was a long-focusing Leitz lens with a working distance of 13 mm. The nominal magnification of the lens was 32 \times , and N.A. was 0.3. Objective lenses are typically corrected for a specific cover-glass thickness which is much thinner than the minimum 1/8" thickness of acrylic sheet. Therefore, some degradation of the image was unavoidable in the existing setup.



CBB 856-4652

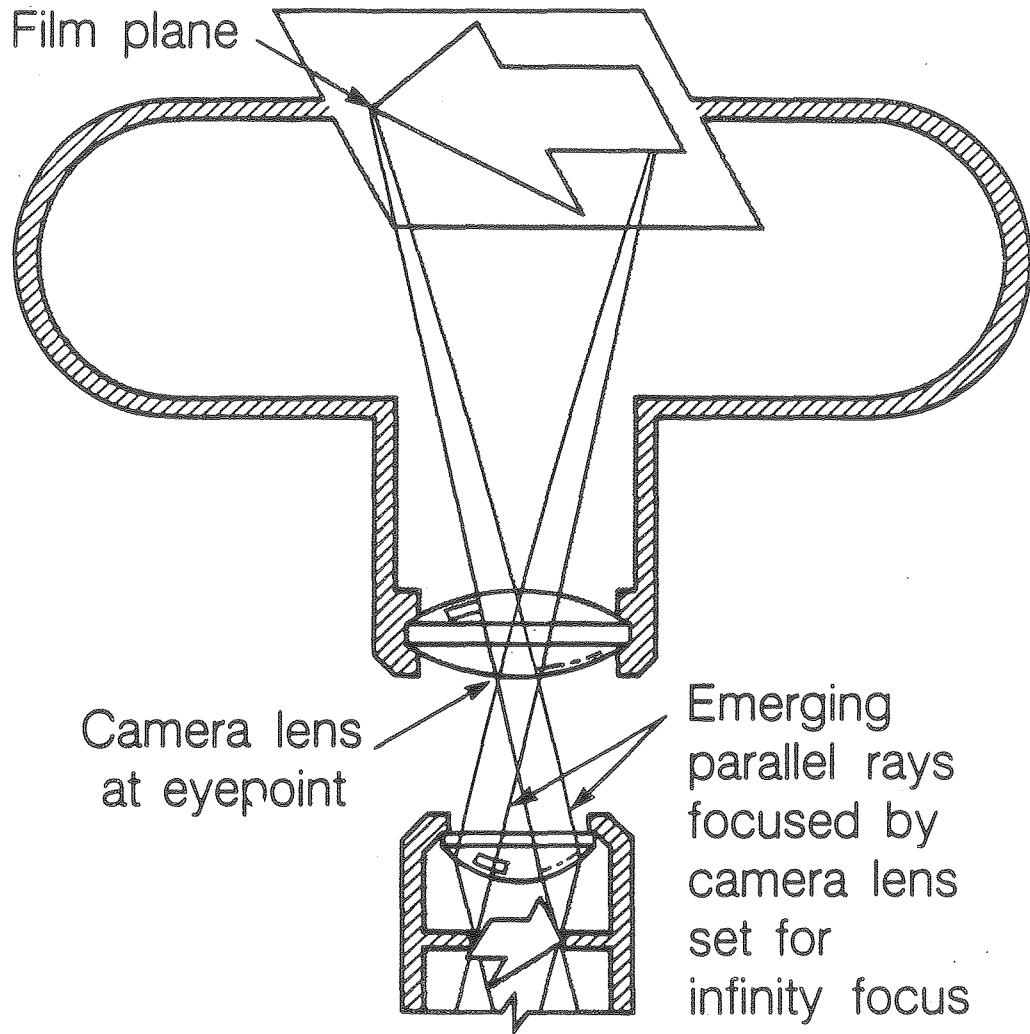
Figure A-1- Apparatus setup showing video and electrical systems

Schematic of Videomicroscopy System



XBL 8512-9041

Figure A-2



XBL 8512-9043

Figure A-3- Recommended camera and microscope configuration (69)

APPENDIX 2

Calculation of Current Efficiency

The deposited zinc was determined by EDTA titration and direct weighing. In both cases calculation of the current efficiency was the same:

Weight deposited for 100% efficiency:

$$I \text{ (mA)} \times 10^{-3} \times t(\text{sec}) = \text{coulombs passed} \quad (\text{A-1})$$

$$\text{Coulombs} \times \text{A.W.}/2 \times 10^5 = \text{weight deposited (g)} \quad (\text{A-2})$$

When the direct-weighing method was used, the weight deposited was found by subtracting the weight of the deposit free electrode from that with deposit. This weight was compared to the weight for 100% efficiency by using the formula:

$$\begin{aligned} & (\text{actual weight/weight for 100\% efficiency}) \\ & \times 100\% = \text{current efficiency (\%)} \quad (\text{A-3}) \end{aligned}$$

When the EDTA-titration procedure was used, the zinc composition was determined by the following formulas:

$$\begin{aligned} & \text{average endpoint} \times \text{concentration of EDTA (M)}/1000 \text{ ml} = \\ & \text{moles of EDTA in aliquot ;} \quad (\text{A-4}) \end{aligned}$$

$$\text{moles of EDTA in aliquot} = \text{moles of zinc in aliquot} ; \quad (\text{A-5})$$

$$\begin{aligned} \text{moles of zinc in aliquot} \times 100/\text{aliquot size} \\ = \text{total moles in sample} ; \quad (\text{A-6}) \end{aligned}$$

$$\begin{aligned} \text{total moles of zinc in sample} \times 65.38 \\ = \text{grams of zinc in sample} . \quad (\text{A-7}) \end{aligned}$$

Then, Equation A-3 was used to determine the current efficiency.

REFERENCES

1. Cotton, F.A. and G. Wilkinson, Advanced Inorganic Chemistry, 4th edition, Chapter 18, Wiley, NY (1980).
2. Meyerstein, D. and W.A. Mulac, Inorg. Chem. 9, 1762 (1970).
3. Symons, M.C.R. and R.S. Eachus, J.A.C.S., 92, 3080 (1970).
4. Kerridge, D.H. and S.A. Tariq, J.A.C.S., 92, 1122 (1970).
5. McBreen, J. and E. Cairns, The Zinc Electrode, in Advances in Electrochemistry and Electrochemical Engineering, H. Gerisher and C.W. Tobias, eds., Volume 11, John Wiley and Sons, NY, 1978.
6. Bard, A.J. ed., Encyclopedia of the Electrochemistry of the Elements, Vol. 5, Marcel Dekker, NY, 1976.
7. Kirk, R.E. and D. Othmer, eds., Encyclopedia of Chemical Technology, 3rd edition, Wiley Interscience, NY, 1978.
8. Hendrikx, J., The zinc electrode: its behavior in the nickel oxide zinc accumulator, PhD thesis, Technological University Eindhoven, Netherlands, May (1984).
9. Mantell, C.L., Electrochemical Engineering, 4th edition, McGraw-Hill Inc., NY (1960).
10. Bockris, J. O'M., ed., Comprehensive Treatise of Electrochemistry, vol. 2, Electrochemical Processes, Plenum Press, NY (1981).
11. Jorne, J., Flow Batteries, American Scientist 71 (5), 507-513 (1983).
12. Putt, R.A. and A. Attia, Development of zinc bromide batteries for stationary energy storage, EPRI report EM-2497, July (1982).

13. Faltemeier, J. and C.W. Tobias, The effect of hydrodynamic flow on the morphology of electrodeposited zinc, PhD Thesis, University of California, Berkeley, LBL report no. 16485, August (1983).
14. Jorne, J., Flow distribution in the zinc chloride battery, JES, 129, 2251-2253 (1982).
15. Butler, P.C., D.W. Miller and C.E. Robinson, Final battery evaluation report: ERC zinc bromine battery, Sandia National Laboratory report no. 84-0799, March (1984).
16. Roughness evolution and dendritic growth in zinc electrodeposition from halide electrolytes, EPRI report 2937, March (1983).
17. Selman, J.R. and W.S. Hsie, Dendritic zinc deposition from flowing acidic solutions, LBL report no. 19757, March (1985).
18. Rogers, G.T. and K.J. Taylor, A rotating disc electrode study of the electrodeposition of zinc from alkaline zincate solutions, J. Electroanal. Chem. 167, 251-264 (1984).
19. Kindler, A. and C.W. Tobias, The morphology of electrodeposited copper, PhD thesis, University of California, Berkeley, LBL report no. 12838, November (1981).
20. Carlson, E.J., Electrodeposition around protruding surface imperfections in turbulent flow, MS Thesis, University of California, Berkeley, LBL report no. 3175, January (1975).
21. Jaksic, M., Hydrodynamic effects on the electrodeposition of zinc, I. Flat plate electrode, to be published.

22. Rajenbah, D., J. Faltemeier, C.W. Tobias, Mass transfer limiting currents of zinc deposition in acidic zinc chloride and zinc sulfate solutions, LBL report no. 15338, October (1983).
23. Tsuda, T. and Charles W. Tobias, The influence of lead ions on the macromorphology of electrodeposited zinc, MS thesis, University of California, Berkeley, LBL report no. 13057, September (1981).
24. Anderson, R. and C.W. Tobias, Studies on zinc nodules electrodeposited from acid electrolytes, MS thesis, University of California, Berkeley, LBL report no. 18646, December (1984).
25. Wranglen, G., Dendrites and growth layers in the electrocrystallization of metals, *Electrochim. Acta*, 2, 130-146 (1960).
26. Naybour, R.D., The effect of electrolyte flow on the morphology of zinc electrodeposited from aqueous alkaline solution containing zincate ions, *JES*, 116, 520 (1969).
27. Levich, V.G., Physiochemical Hydrodynamics, Prentice-Hall, Inc., Englewood Cliffs, NJ, 1962.
28. Rogers, G.T. and K.J. Taylor, Effect of small protrusions on mass transport to a rotating disk electrode, *Nature*, 200, 1062 (1963).
29. Kim, J.T. and J. Jorne, The kinetics and mass transfer of zinc electrode in acidic zinc chloride solution, *JES*, 127, 8 (1980).
30. McBreen, J. and E. Gannon, Electrodeposition of zinc on glassy carbon from zinc chloride and zinc bromide electrolytes, *JES* 130 (8), 1667 (1983).

31. McBreen, J., in Extended Abstracts: Seventh Battery and Electrochemical Contractors Conference, November 18-21, 1985, Crystal City, Virginia.
32. Diggle, J.W., A.R. Despic, and J. O'M. Bockris, The mechanism of the dendritic electrocrystallization of zinc, JES 116, 1503-1514 (1969).
33. Moshtev, R.V. and P. Zlatilova, Kinetics of growth of zinc dendrite precursors in zincate solutions, J. Appl. Electrochem. 8, 213-222 (1978).
34. Adcock, P.A., A.R. Ault, and O.M.G. Newman, The importance of cathode zinc morphology as an indicator of industrial electrowinning performance, J. Appl. Electrochem. 15, 865-878 (1985).
35. Zinc deposition from zinc halide electrolytes, EPRI report no. 2393, May (1982).
36. Landau, U., Surface morphology of electrodeposits, presented to the Rolle-Mo. Conference, June (1983).
37. Hsie, W.S., Dendritic zinc deposition from flowing acidic solutions, PhD thesis, Illinois Institute of Technology, December (1985).
38. Popov, K.I. and N.V. Krstajic, The mechanism of spongy electrodeposits formation on inert substrate at low overpotentials, J. Appl. Electrochem. 13, 775-782 (1982).
39. Thomas, B.K. and D.J. Fray, Electrolysis of zinc chloride solutions at high current densities, Trans. Instn. Min. Metall. (Section C: Mineral Process. Extr. Metall.) 91, C105 (1982).

40. Thomas, B.K. and D.J. Fray, The effect of additives on the morphology of zinc electrodeposited from a zinc chloride electrolyte at high current densities. *J. Appl. Electrochem.* 11, 677-683 (1981).
41. Mackinnon, D.J., J.M. Brannen and R.M. Morrison, Zinc electrowinning from aqueous chloride electrolyte, *J. Appl. Electrochem.* 12, 39-53 (1982).
42. Mackinnon, D.J., J.M. Brannen and R.C. Kerby, The effect of cadmium on zinc deposit structures obtained from high purity industrial acid sulphate electrolyte, *J. Appl. Electrochem.* 9, 71-79 (1979).
43. Kalinovski, E.A. and V.V. Stender, *Ukr. Khim. Zh.* 23, 384 (1957).
44. Nikivorov, A.F. and V.V. Stender, *Vestn. Akad. Nauk. Kaz. SSR* 10, 42 (1958).
45. Nikivorov, A.F. and V.V. Stender, *Ukr. Khim. Zh.*, 25, 18 (1959).
46. Begum, S., P.V. Vasudeva Rao, and H.V.K. Udupa, Deposition of zinc from zinc chloride solution, in *Memoirs, 1982 Central Electrochemical Research Institute, Karakudi, India.*
47. Rogers, G.T. and K.J. Taylor, A rotating disc electrode study of the electrodeposition of zinc from alkaling zincate solutions, *J. Electroanal. Chem.*, 167, 251-264 (1984).
48. Gay, A.J. and F. Bergsma, The influence of nitrate ion on the morphology on zinc electrodeposits, *Electrochim. Acta.*, 23, 1067-1072 (1978).
49. Foulkes, F.R., J.W. Smith, R. Kalia and D.W. Kirk, Effects of cadmium impurities on the electrowinning of zinc, *JES*, 128, 2307

- (1981).
50. Fratesi, R., G. Roventi, M. Maja, and N. Penazzi, Effect of nickel impurities on zinc electrodeposition, *J. Appl. Electrochem.* 10, 765-774 (1980).
 51. Mackinnon, D.J., J. Brannen and R.C. Kerby, The effect of lead on zinc deposit structures obtained from high purity synthetic and industrial acid sulphate electrolytes, *J. Appl. Electrochem.* 9, 55-70 (1979).
 52. Richardson, J.H., Optical Microscopy for the Material Sciences, Marcel Dekker, Inc., NY (1971).
 53. Bockris, J. O'M., Z. Nagy and D. Drazic, On the morphology of zinc electrodeposition from alkaline solutions, *JES*, 120, 30 (1973).
 54. Despic, A.R. and M.G. Pavlovic. Deposition of zinc on foreign substrates, *Electrochim. Acta*, 27, 1539-1549 (1982).
 55. Fischer, H., Electrocrystallization of metals under ideal and real conditions, *Angew. Chem. Internat. Edit.*, 8, 108 (1969).
 56. Fischer, H., The nucleation dependent growth layer—a structure element in electrocrystallization, presented at the 56th Annual Convention, American Electroplaters Society, Detroit, Michigan, June 16, 1969.
 57. Cachet, C., U. Stroder and R. Wiart, The kinetics of zinc electrode in alkaline zincate electrolytes. *Electrochim. Acta* 27, 903-908 (1982).

58. Fischl, D.S., R.H. Muller and C.W. Tobias, Effects of small flow obstacles on the limiting current and pressure drop in a square duct, MS thesis, University of California, Berkeley, LBL report no. 16422, August (1983).
59. Alkire, R.C., D.B. Reiser and R.L. Sani, Effect of fluid flow in removal of dissolution products from small cavities, JES, 131, 2795-2800 (1984).
60. Epelboin, I., M. Kasouri, and R. Wiart, On a model for electrocrystallization involving an autocatalytic step, JES 122, 1207 (1975).
61. Foller, P.C., Zinc/Air batteries, to be published.
62. Mackinnon, D.J. and P.L. Fenn, The effect of germanium on zinc electrowinning from industrial acid sulphate electrolyte, J. Appl. Electrochem. 14, 467-474 (1984).
63. Kralik, D. and J. Jorne, Hydrogen evolution and zinc nodular growth in the zinc chloride battery, JES, 127, 2335-2340 (1980).
64. Jorne, J. and W.T. Ho, Transference numbers of zinc chloride battery electrolytes, JES, 129, 907 (1982).
65. Mackinnon, D.J., J.M. Brannen and V.I. Lakshmanan, Zinc deposit structures obtained from synthetic zinc chloride electrolyte, J. Appl. Electrochem. 9, 603-613 (1979).
66. Oren, Y. and U. Landau, Growth of zinc dendrites in acidic zinc chloride solutions, E. Acta 27, 739-748 (1982).
67. Milchev, A., Role of the substrate state in electrochemical nucleation, Electrochim. Acta, 28, 947-953 (1983).

68. Chu, M.G., J. McBreen and G. Adzic, Substrate effects on zinc deposition from zincate solutions: 1. Deposition on Cu, Au, Cd and Zn, JES, 128, 2281 (1981).
69. Photography through the microscope, 7th edition, Eastman Kodak Co. (1980).
70. Kuhn, A.T., Industrial electrochemical processes, Elsevier, NY (1971).
71. Mason, C.W., Handbook of Chemical Microscopy, Volume 1, 4th edition, John Wiley and Sons, NY (1983).
72. McBreen, J. and E. Gannon, Morphology of zinc electrodes, Quarterly Status report number 2, Department of Energy and Environment, Brookhaven National Laboratory, March (1982).
73. Jaksic, M.M., Impurity effects on the macromorphology of electrodeposited zinc: 1. Theoretical considerations and a review of existing knowledge, Surface Technology, 24, 193-217 (1985).
74. Extended abstracts: Seventh Battery and Electrochemical Contractors' Conference, November 18-21, 1985, Crystal City, Virginia.
75. Wark, I.W., The electrodeposition of zinc from acidified zinc sulphate solution, J. Appl. Electrochem. 9, 721-730 (1979).
76. Armstrong, R.D. and S.J. Churchouse, Dendritic growth of cadmium in relation to the Ni-Cd cell, Electrochim. Acta 28, 185-190 (1983).
77. Barnard, R., G.S. Edwards, J. Holloway, and F.L. Tye, Studies concerning the growth of cadmium dendrites: III. Morphology in acidic media, J. Appl. Electrochem. 13, 765-773 (1983).

78. Barnard, R., J. Holloway, C.F. Randell, and F.L. Tye, Studies concerning the growth of cadmium dendrites: III. Theoretical treatment, *J. Appl. Electrochem.*, 14, 187-196 (1984).
79. Epelboin, I., M. Kasouri, E. Lejay and R. Wiart, A study of the elementary steps of electron transfer during the electrocrystallization of zinc, *Electrochim. Acta*, 20, 603-605 (1975).
80. Gerisher, H., Mechanism of electrolytic deposition and dissolution of metals, *Anal. Chem.* 3, 33-39 (1959).
81. Thomas, B.K. and D.J. Fray, The conductivity of aqueous zinc chloride solutions, *J. Appl. Electrochem.* 12, 1-5 (1982).
82. Popov, K.I., D.N. Keca and M.D. Andjelic, Electrodeposition of zinc on copper from alkaline zincate solutions, *J. Appl. Electrochem.* 9, 19-23 (1978).

This report was done with support from the Department of Energy. Any conclusions or opinions expressed in this report represent solely those of the author(s) and not necessarily those of The Regents of the University of California, the Lawrence Berkeley Laboratory or the Department of Energy.

Reference to a company or product name does not imply approval or recommendation of the product by the University of California or the U.S. Department of Energy to the exclusion of others that may be suitable.

*LAWRENCE BERKELEY LABORATORY
TECHNICAL INFORMATION DEPARTMENT
UNIVERSITY OF CALIFORNIA
BERKELEY, CALIFORNIA 94720*